

Drivers of plant nutrient acquisition and allocation strategies and their influence
on plant responses to environmental change

by

Evan A. Perkowski, B.S.

A Dissertation

In

Biological Sciences

Submitted to the Graduate Faculty
of Texas Tech University in
Partial Fulfillment of
the Requirements for
the Degree of

Doctor of Philosophy

Approved

Dr. Nicholas G. Smith
Chair of Committee

Dr. Aimée T. Classen

Dr. Natasja van Gestel

Dr. Lindsey C. Slaughter

Dr. Dylan W. Schwilk

Dr. Mark Sheridan
Dean of the Graduate School

May 2023

Copyright 2023, Evan A. Perkowski

Acknowledgements

Placeholder for text

Table of Contents

Acknowledgements	ii
Abstract	vi
List of Tables	vii
List of Figures	viii
1. Introduction	1
2. Structural carbon costs to acquire nitrogen are determined by nitrogen and light availability in two species with different nitrogen acquisition strategies	2
2.1 Introduction	2
2.2 Methods	6
2.2.1 <i>Experiment setup</i>	6
2.2.2 <i>Plant measurements and calculations</i>	7
2.2.3 <i>Statistical analyses</i>	8
2.3 Results	10
2.3.1 <i>Carbon costs to acquire nitrogen</i>	10
2.3.2 <i>Whole plant nitrogen biomass</i>	13
2.3.3 <i>Root carbon biomass</i>	15
2.3.4 <i>Root nodule biomass</i>	17
2.4 Discussion	21
3. Soil nitrogen availability modifies leaf nitrogen economies in mature temperate deciduous forests: a direct test of photosynthetic least-cost theory	29
3.1 Introduction	29
3.2 Methods	33
3.2.1 <i>Study site description</i>	33
3.2.2 <i>Experimental design</i>	34
3.2.3 <i>Leaf gas exchange and trait measurements</i>	34
3.2.4 <i>A_{net}/C_i curve-fitting and parameter estimation</i>	37

3.2.5 <i>Proportion of leaf nitrogen allocated to photosynthesis and structure</i>	39
3.2.6 <i>Tradeoffs between nitrogen and water use</i>	40
3.2.7 <i>Soil nitrogen availability and pH</i>	41
3.2.8 <i>Statistical analyses</i>	43
3.3 Results	45
3.3.1 <i>Leaf N content</i>	45
3.3.2 <i>Net photosynthesis and leaf biochemistry</i>	48
3.3.3 <i>Leaf N allocation</i>	51
3.3.4 <i>Tradeoffs between nitrogen and water use</i>	54
3.4 Discussion	57
3.4.1 <i>Soil nitrogen availability modifies tradeoffs between nitrogen and water use</i>	58
3.4.2 <i>Soil pH did not modify tradeoffs between nitrogen and water usage</i>	60
3.4.3 <i>Species identity explains a large amount of variation in leaf and whole plant traits</i>	61
3.4.4 <i>Implications for photosynthetic least-cost theory model development</i>	62
3.4.5 <i>Conclusions</i>	64
4. The relative cost of resource use for photosynthesis drives variance in leaf nitrogen content across climate and soil resource availability gradients	65
4.1 Introduction	65
4.2 Methods	67
4.2.1 <i>textit{Site descriptions and sampling methodology}</i>	67
4.2.2 <i>Leaf trait measurements</i>	67
4.3 Results	73
4.4 Discussion	73

5. Optimal resource investment to photosynthetic capacity maximizes nutrient allocation to whole plant growth under elevated CO₂	74
5.1 Introduction	74
5.2 Methods	79
5.2.1 <i>Seed treatments and experimental design</i>	79
5.2.2 <i>Growth chamber conditions</i>	80
5.2.3 <i>Leaf gas exchange measurements</i>	82
5.2.4 <i>Leaf trait measurements</i>	83
5.2.5 <i>A/C_i curve fitting and parameter estimation</i>	85
5.2.6 Stomatal limitation	85
5.2.7 <i>Proportion of leaf nitrogen allocated to photosynthesis and structure</i>	86
5.2.8 <i>Whole plant traits</i>	88
5.2.9 <i>Statistical analyses</i>	89
5.3 Results	91
5.4 Discussion	91
6. Conclusions	92
References	93

Abstract

List of Tables

2.1 Analysis of variance results exploring species-specific effects of light availability, nitrogen fertilization, and their interactions on carbon costs to acquire nitrogen, whole-plant nitrogen biomass, and root carbon biomass	11
2.2 Analysis of variance results exploring effects of light availability, nitrogen fertilization, and their interactions on <i>G. max</i> root nodule biomass and the ratio of root nodule biomass to root biomass*	18
2.3 Slopes of the regression line describing the relationship between each dependent variable and nitrogen fertilization at each light level*	19
3.1 Effects of soil N availability, soil pH, and species on leaf N content per unit leaf area (N_{area}), leaf N content per unit leaf mass (N_{mass}), and leaf mass per unit leaf area (M_{area})	46
3.2 Effects of soil N availability, soil pH, species, and N_{area} on leaf biochemistry	49
3.3 Effects of soil N availability, soil pH, and species on the proportion of leaf nitrogen content allocated to photosynthesis, Rubisco, bioenergetics, and structure	52
3.4 Effects of soil N availability, soil pH, species, and N_{area} on tradeoffs between nitrogen and water use	55

List of Figures

2.1 Relationships between soil nitrogen fertilization and light availability on carbon costs to acquire nitrogen in <i>G. hirsutum</i> and <i>G. max</i>	12
2.2 Relationships between soil nitrogen fertilization and light availability on whole-plant nitrogen biomass in <i>G. hirsutum</i> and <i>G. max</i>	14
2.3 Relationships between soil nitrogen fertilization and light availability on root carbon biomass in <i>G. hirsutum</i> and <i>G. max</i>	16
2.4 Effects of shade cover and nitrogen fertilization on root nodule biomass and the ratio of root nodule biomass to root biomass in <i>G. max</i>	20
3.1 Effects of soil N availability and species on leaf N content per unit leaf area, leaf nitrogen content per unit leaf biomass, and leaf mass per leaf area	47
3.2 Effects of soil N availability, species, and leaf N content leaf biochemistry	50
3.3 Effects of soil N availability, species, and leaf N content on the fraction of leaf nitrogen allocated to photosynthesis and structure	53
3.4 Effects of soil N availability, species, and leaf N content on tradeoffs between nitrogen and water use	56

4.1 Maps that detail site locations along 2006-2020 mean annual precipitation (panel A) and mean annual temperature (panel B) gradients in Texas, USA.	72
--	----

1 Chapter 1
2 Introduction

3 Chapter 2

4 Structural carbon costs to acquire nitrogen are determined by
5 nitrogen and light availability in two species with different nitrogen
6 acquisition strategies

7 2.1 Introduction

8 Carbon and nitrogen cycles are tightly coupled in terrestrial ecosystems.
9 This tight coupling influences photosynthesis (Walker et al. 2014; Rogers et al.
10 2017), net primary productivity (LeBauer and Treseder 2008; Thomas et al. 2013),
11 decomposition (Cornwell et al. 2008; Bonan et al. 2013; Sulman et al. 2019), and
12 plant resource competition (Gill and Finzi 2016; Xu-Ri and Prentice 2017). Ter-
13 restrial biosphere models are beginning to include connected carbon and nitrogen
14 cycles to improve the realism of their simulations (Fisher et al. 2010; Brzostek
15 et al. 2014; Wieder et al. 2015; Shi et al. 2016; Zhu et al. 2019). Simula-
16 tions from these models indicate that coupling carbon and nitrogen cycles can
17 drastically influence future biosphere-atmosphere feedbacks under global change,
18 such as elevated carbon dioxide or nitrogen deposition (Thornton et al. 2007;
19 Goll et al. 2012; Wieder et al. 2015; Wieder et al. 2019). Nonetheless, there
20 are still limitations in our quantitative understanding of connected carbon and
21 nitrogen dynamics (Thomas et al. 2015; Meyerholt et al. 2016; Rogers et al.
22 2017; Exbrayat et al. 2018; Shi et al. 2019), forcing models to make potentially
23 unreliable assumptions.

24 Plant nitrogen acquisition is a process in terrestrial ecosystems by which
25 carbon and nitrogen are tightly coupled (Vitousek and Howarth 1991; Delaire
26 et al. 2005; Brzostek et al. 2014). Plants must allocate photosynthetically de-

27 rived carbon belowground to produce and maintain root systems or exchange with
28 symbiotic soil microbes in order to acquire nitrogen (Högberg et al. 2008; Hög-
29 berg et al. 2010). Thus, plants have an inherent carbon cost associated with
30 acquiring nitrogen, which can include both direct energetic costs associated with
31 nitrogen acquisition and indirect costs associated with building structures that
32 support nitrogen acquisition (Gutschick 1981; Rastetter et al. 2001; Vitousek
33 et al. 2002; Menge et al. 2008). Model simulations (Fisher et al. 2010; Brzostek
34 et al. 2014; Shi et al. 2016; Allen et al. 2020) and meta-analyses (Terrer et al.
35 2018) suggest that these carbon costs vary between species, particularly those
36 with different nitrogen acquisition strategies. For example, simulations using iter-
37 ations of the Fixation and Uptake of Nitrogen (FUN) model indicate that species
38 that acquire nitrogen from non-symbiotic active uptake pathways (e.g. mass flow)
39 generally have larger carbon costs to acquire nitrogen than species that acquire
40 nitrogen through symbiotic associations with nitrogen-fixing bacteria (Brzostek
41 et al. 2014; Allen et al. 2020).

42 Carbon costs to acquire nitrogen likely vary in response to changes in soil
43 nitrogen availability. For example, if the primary mode of nitrogen acquisition
44 is through non-symbiotic active uptake, then nitrogen availability could decrease
45 carbon costs to acquire nitrogen as a result of increased per-root nitrogen up-
46 take (Franklin et al. 2009; Wang et al. 2018). However, if the primary mode of
47 nitrogen acquisition is through symbiotic active uptake, then nitrogen availabil-
48 ity may incur additional carbon costs to acquire nitrogen if it causes microbial
49 symbionts to shift toward parasitism along the parasitism–mutualism continuum
50 (Johnson et al. 1997; Hoek et al. 2016; Friel and Friesen 2019) or if it reduces

51 the nitrogen acquisition capacity of a microbial symbiont (van Diepen et al. 2007;
52 Soudzilovskaia et al. 2015; Muñoz et al. 2016). Species may respond to shifts in
53 soil nitrogen availability by switching their primary mode of nitrogen acquisition
54 to a strategy with lower carbon costs to acquire nitrogen in order to maximize
55 the magnitude of nitrogen acquired from a belowground carbon investment and
56 outcompete other individuals for soil resources (Rastetter et al. 2001; Menge et al.
57 2008).

58 Environmental conditions that affect demand to acquire nitrogen to sup-
59 port new and existing tissues could also be a source of variance in plant carbon
60 costs to acquire nitrogen. For example, an increase in plant nitrogen demand could
61 increase carbon costs to acquire nitrogen if this increases the carbon that must be
62 allocated belowground to acquire a proportional amount of nitrogen (Kulmatiski
63 et al. 2017; Noyce et al. 2019). This could be driven by a temporary state of
64 diminishing return associated with investing carbon toward building and main-
65 taining structures that are necessary to support enhanced nitrogen uptake, such
66 as fine roots (Matamala and Schlesinger 2000; Norby et al. 2004; Arndal et al.
67 2018), mycorrhizal hyphae (Saleh et al. 2020), or root nodules (Parvin et al. 2020).
68 Alternatively, if the environmental factor that increases plant nitrogen demand
69 causes nitrogen to become more limiting in the system (e.g. atmospheric CO₂;
70 Luo et al. (2004), LeBauer and Treseder (2008), Vitousek et al. (2010), Liang
71 et al. (2016)), species might switch their primary mode of nitrogen acquisition to
72 a strategy with lower relative carbon costs to acquire nitrogen in order to gain a
73 competitive advantage over species with either different or more limited modes of
74 nitrogen acquisition (Ainsworth and Long 2005; Taylor and Menge 2018).

75 Using a plant economics approach, we examined the influence of plant
76 nitrogen demand and soil nitrogen availability on plant carbon costs to acquire
77 nitrogen. This was done by growing a species capable of forming associations
78 with nitrogen-fixing bacteria (*Glycine max* L. (Merr)) and a species not capable
79 of forming these associations (*Gossypium hirsutum* L.) under four levels of light
80 availability (plant nitrogen demand proxy) and four levels of soil nitrogen fertil-
81 ization (soil nitrogen availability proxy) in a full-factorial, controlled greenhouse
82 experiment. We used this experimental set-up to test the following hypotheses:

- 83 1. An increase in plant nitrogen demand due to increasing light availability will
84 increase carbon costs to acquire nitrogen through a proportionally larger
85 increase in belowground carbon than whole-plant nitrogen acquisition. This
86 will be the result of an increased investment of carbon toward belowground
87 structures that support enhanced nitrogen uptake, but at a lower nitrogen
88 return.
- 89 2. An increase in soil nitrogen availability will decrease carbon costs to acquire
90 nitrogen as a result of increased per root nitrogen uptake in *G. hirsutum*.
91 However, soil nitrogen availability will not affect carbon costs to acquire
92 nitrogen in *G. max* because of the already high return of nitrogen supplied
93 through nitrogen fixation.

94 2.2 Methods

95 2.2.1 *Experiment setup*

96 *Gossypium hirsutum* and *G. max* were planted in individual 3 liter pots
97 (NS-300; Nursery Supplies, Orange, CA, USA) containing a 3:1 mix of unfertil-
98 ized potting mix (Sungro Sunshine Mix #2, Agawam, MA, USA) to native soil
99 extracted from an agricultural field most recently planted with *G. max* at the
100 USDA-ARS Laboratory in Lubbock, TX, USA (33.59°N, -101.90°W). The field
101 soil was classified as Amarillo fine sandy loam (75% sand, 10% silt, 15% clay).
102 Upon planting, all *G. max* pots were inoculated with *Bradyrhizobium japonicum*
103 (Verdesian N-Dure™ Soybean, Cary, NC, USA) to stimulate root nodulation. In-
104 dividuals of both species were grown under similar, unshaded, ambient greenhouse
105 conditions for 2 weeks to germinate and begin vegetative growth. Three blocks
106 were set up in the greenhouse, each containing four light treatments created us-
107 ing shade cloth that reduced incoming radiation by either 0 (full sun), 30, 50,
108 or 80%. Two weeks post-germination, individuals were randomly placed in the
109 four light treatments in each block. Individuals received one of four nitrogen fer-
110 tilization doses as 100ml of a modified Hoagland solution (Hoagland and Arnon
111 1950) equivalent to either 0, 70, 210, or 630 ppm N twice per week within each
112 light treatment. Nitrogen fertilization doses were received as topical agents to
113 the soil surface. Each Hoagland solution was modified to keep concentrations of
114 other macro- and micronutrients equivalent (Supplementary Table S1). Plants
115 were routinely well watered to eliminate water stress.

116 2.2.2 *Plant measurements and calculations*

117 Each individual was harvested after 5 weeks of treatment, and biomass
118 was separated by organ type (leaves, stems, and roots). Nodules on *G. max*
119 roots were also harvested. With the exception of the 0% shade cover and 630
120 ppm N treatment combination, all treatment combinations in both species had
121 lower average dry biomass:pot volume ratios than the 1:1 ratio recommended by
122 Poorter et al. (2012) to minimize the likelihood of pot volume-induced growth
123 limitation (Supplementary Tables S2, S3; Supplementary Fig. S1). All harvested
124 material was dried, weighed, and ground by organ type. Carbon and nitrogen
125 content (g g^{-1}) was determined by subsampling from ground and homogenized
126 biomass of each organ type using an elemental analyzer (Costech 4010; Costech,
127 Inc., Valencia, CA, USA). We scaled these values to total leaf, stem, and root
128 carbon and nitrogen biomass (g) by multiplying dry biomass of each organ type
129 by carbon or nitrogen content of each corresponding organ type. Whole-plant
130 nitrogen biomass (g) was calculated as the sum of total leaf (g), stem (g), and
131 root (g) nitrogen biomass. Root nodule carbon biomass was not included in the
132 calculation of root carbon biomass; however, relative plant investment toward root
133 or root nodule standing stock was estimated as the ratio of root biomass to root
134 nodule biomass (g g^{-1}), following similar metrics to those adopted by Dovrat et al.
135 (2018) and Dovrat et al. (2020).

136 Carbon costs to acquire nitrogen (gC gN^{-1}) were estimated as the ratio of
137 total root carbon biomass (gC) to whole-plant nitrogen biomass (gN). This cal-
138 culation quantifies the relationship between carbon spent on nitrogen acquisition
139 and whole-plant nitrogen acquisition by using root carbon biomass as a proxy for

140 estimating the magnitude of carbon allocated toward nitrogen acquisition. This
141 calculation therefore assumes that the magnitude of root carbon standing stock is
142 proportional to carbon transferred to root nodules or mycorrhizae, or lost through
143 root exudation or turnover. This assumption has been supported in species that
144 associate with ectomycorrhizal fungi (Hobbie 2006; Hobbie and Hobbie 2008), but
145 is less clear in species that acquire nitrogen through non-symbiotic active uptake
146 or symbiotic nitrogen fixation. It is also unclear whether relationships between
147 root carbon standing stock and carbon transfer to root nodules are similar in mag-
148 nitude to carbon lost through exudation or when allocated toward other active
149 uptake pathways. Thus, because of the way we performed our measurements, our
150 proximal values of carbon costs to acquire nitrogen are underestimates.

151 2.2.3 *Statistical analyses*

152 We explored the effects of light and nitrogen availability on carbon costs to
153 acquire nitrogen using separate linear mixed-effects models for each species. Mod-
154 els included shade cover, nitrogen fertilization, and interactions between shade
155 cover and nitrogen fertilization as continuous fixed effects, and also included block
156 as a random intercept term. Three separate models for each species were built
157 with this independent variable structure for three different dependent variables: (i)
158 carbon costs to acquire nitrogen (gC gN^{-1}); (ii) whole-plant nitrogen biomass (de-
159 nominator of carbon cost to acquire nitrogen; gN); and (iii) root carbon biomass
160 (numerator of carbon cost to acquire nitrogen; gC). We constructed two additional
161 models for *G. max* with the same model structure described above to investigate
162 the effects of light availability and nitrogen fertilization on root nodule biomass

163 (g) and the ratio of root nodule biomass to root biomass (unitless).

164 We used Shapiro–Wilk tests of normality to determine whether species-
165 specific linear mixed-effects model residuals followed a normal distribution. None
166 of our models satisfied residual normality assumptions when models were fit using
167 untransformed data (Shapiro–Wilk: $P < 0.05$ in all cases). We attempted to satisfy
168 residual normality assumptions by first fitting models using dependent variables
169 that were natural-log transformed. If residual normality assumptions were still
170 not met (Shapiro–Wilk: $P < 0.05$), then models were fit using dependent variables
171 that were square root transformed. All residual normality assumptions were satis-
172 fied when models were fit with either a natural-log or square root transformation
173 (Shapiro–Wilk: $P > 0.05$ in all cases). Specifically, we natural-log transformed *G.*
174 *hirsutum* carbon costs to acquire nitrogen and *G. hirsutum* whole-plant nitrogen
175 biomass. We also square root transformed *G. max* carbon costs to acquire nitro-
176 gen, *G. max* whole-plant nitrogen biomass, root carbon biomass in both species,
177 *G. max* root nodule biomass, and the *G. max* ratio of root nodule biomass to root
178 biomass. We used the ‘lmer’ function in the ‘lme4’ R package (Bates et al. 2015)
179 to fit each model and the ‘Anova’ function in the ‘car’ R package (Fox and Weis-
180 berg 2019) to calculate Wald’s χ^2 to determine the significance ($\alpha = 0.05$) of each
181 fixed effect coefficient. Finally, we used the ‘emmeans’ R package (Lenth 2019)
182 to conduct post-hoc comparisons of our treatment combinations using Tukey’s
183 tests. Degrees of freedom for all Tukey’s tests were approximated using the Ken-
184 ward–Roger approach (Kenward and Roger 1997). All analyses and plots were
185 conducted in R version 4.0.1 (R Core Team 2021).

186 2.3 Results

187 2.3.1 *Carbon costs to acquire nitrogen*

188 Carbon costs to acquire nitrogen in *G. hirsutum* increased with increasing
189 light availability ($p < 0.001$; Table 2.1; Fig. 2.1) and decreased with increasing
190 nitrogen fertilization ($p < 0.001$; Table 2.1; Fig. 2.1). There was no interaction
191 between light availability and nitrogen fertilization ($p = 0.486$, Table 2.1; Fig.
192 2.1).

193 Carbon costs to acquire nitrogen in *G. max* also increased with increasing
194 light availability ($p < 0.001$, Table 2.1; Fig. 2.1) and decreased with increasing
195 nitrogen fertilization ($p < 0.001$; Table 2.1; Fig. 2.1). There was no interaction
196 between light availability and nitrogen fertilization ($p = 0.261$, Table 2.1; Fig.
197 2.1).

Table 2.1. Analysis of variance results exploring species-specific effects of light availability, nitrogen fertilization, and their interactions on carbon costs to acquire nitrogen, whole-plant nitrogen biomass, and root carbon biomass

	df	Carbon costs to acquire nitrogen			Whole-plant nitrogen biomass			Root carbon biomass		
		Coefficient	χ^2	p	Coefficient	χ^2	p	Coefficient	χ^2	p
<i>G. hirsutum</i>										
Intercept		1.594	-	-	-3.232	-	-	0.432	-	-
Light (L)	1	-1.09E-02	56.494	<0.001	-6.41E-03	91.275	<0.001	-2.62E-03	169.608	<0.001
Nitrogen (N)	1	-1.34E-03	54.925	<0.001	1.83E-03	118.784	<0.001	1.15E-04	2.901	0.089
L*N	1	3.88E-06	0.485	0.486	-1.34E-05	10.721	0.001	-1.67E-06	3.140	0.076
<i>G. max</i>										
Intercept		1.877	-	-	0.239	-	-	0.438	-	-
Light (L)	1	-7.67E-03	174.156	<0.001	-6.72E-04	39.799	<0.001	-2.55E-03	194.548	<0.001
Nitrogen (N)	1	-2.35E-04	21.948	<0.001	1.55E-04	70.771	<0.001	2.52E-04	19.458	<0.001
L*N	1	-2.89E-06	1.262	0.261	-6.32E-07	1.435	0.231	-3.16E-06	10.803	0.001

*Significance determined using Wald's χ^2 tests ($P=0.05$). P -values<0.05 are in bold and p -values between 0.05 and 0.1 are italicized. Negative coefficients for light treatments indicate a positive effect of increasing light availability on all response variables, as light availability is treated as percent shade cover in all linear mixed-effects models.

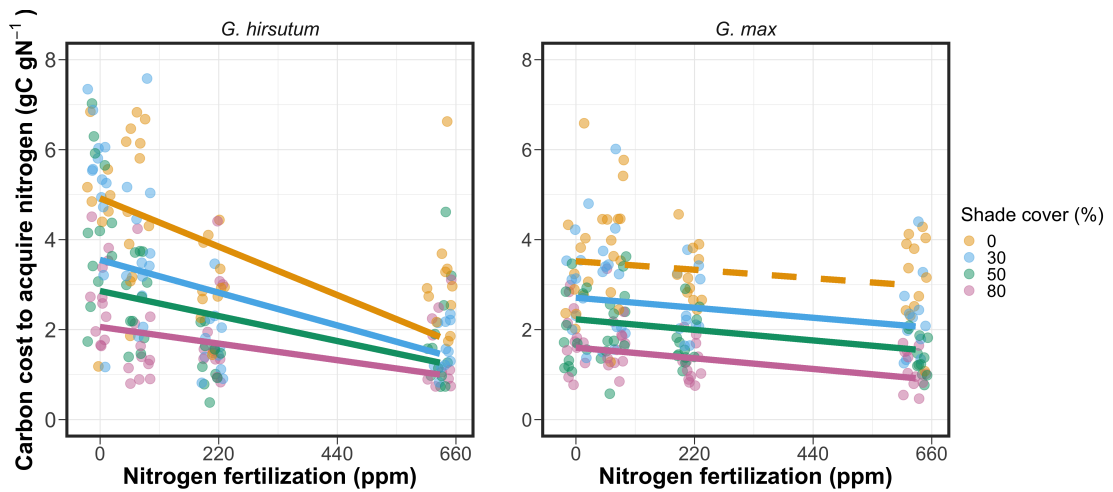


Figure 2.1. Relationships between soil nutrient fertilization and light availability on carbon costs to acquire nitrogen in *G. hirsutum* and *G. max*. Nitrogen fertilization treatments are represented on the x-axis. Shade cover treatments are represented through colored points and trendlines. Trendlines were created by back-transforming marginal mean slopes and intercepts from species-specific linear mixed-effects models. These values were calculated using the ‘emtrends’ and ‘emmmeans’ functions in the ‘emmeans’ R package (Lenth, 2019). Points are jittered for visibility. Yellow points and trendlines represent the 0% shade cover treatment, blue points and trendlines represent the 30% shade cover treatment, green points and trendlines represent the 50% shade cover treatment, and purple points and trendlines represent the 80% shade cover treatment. Solid trendlines indicate slopes that are significantly different from zero (Tukey: $p < 0.05$), while dashed trendlines indicate slopes that are not statistically different from zero.

198 2.3.2 *Whole plant nitrogen biomass*

199 Whole-plant nitrogen biomass in *G. hirsutum* was driven by an interaction
200 between light availability and nitrogen fertilization ($p = 0.001$; Table 2.1; Fig.
201 2.2). This interaction indicated a greater stimulation of whole-plant nitrogen
202 biomass by nitrogen fertilization as light levels increased (Table 2.1; Fig. 2.2).

203 Whole-plant nitrogen biomass in *G. max* increased with increasing light
204 availability ($p < 0.001$) and nitrogen fertilization ($p < 0.001$), with no interaction
205 between light availability and nitrogen fertilization ($p = 0.231$; Table 2.1; Fig.
206 2.2).

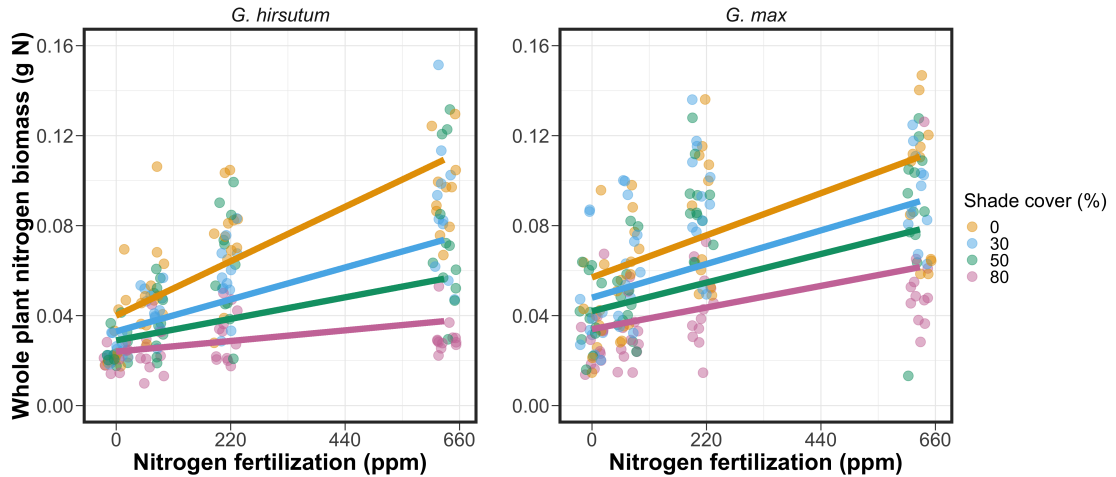


Figure 2.2. Relationships between soil nutrient fertilization and light availability on whole-plant nitrogen biomass in *G. hirsutum* and *G. max*. Whole-plant nitrogen biomass is the denominator of the carbon cost to acquire nitrogen calculation. Nitrogen fertilization treatments are represented on the x-axis. Shade cover treatments are represented through colored points and trendlines. Trendlines were created by back-transforming marginal mean slopes and intercepts from species-specific linear mixed-effects models. These values were calculated using the ‘emtrends’ and ‘emmmeans’ functions in the ‘emmeans’ R package (Lenth 2019). Points are jittered for visibility. Yellow points and trendlines represent the 0% shade cover treatment, blue points and trendlines represent the 30% shade cover treatment, green points and trendlines represent the 50% shade cover treatment, and purple points and trendlines represent the 80% shade cover treatment. Solid trendlines indicate slopes that are significantly different from zero (Tukey: $P < 0.05$), while dashed trendlines indicate slopes that are not statistically different from zero.

207 2.3.3 *Root carbon biomass*

208 Root carbon biomass in *G. hirsutum* significantly increased with increasing
209 light availability ($p < 0.001$; Table 2.1; Fig. 2.3) and marginally increased with
210 nitrogen fertilization ($p = 0.089$; Table 2.1; Fig. 2.3). There was also a marginal
211 interaction between light availability and nitrogen fertilization ($p = 0.076$; Table
212 2.1), driven by an increase in the positive response of root carbon biomass to
213 increasing nitrogen fertilization as light availability increased. This resulted in
214 significantly positive trends between root carbon biomass and nitrogen fertilization
215 in the two highest light treatments (Tukey: $p < 0.05$ in both cases; Table 2.3;
216 Fig. 2.3) and no effect of nitrogen fertilization in the two lowest light treatments
217 (Tukey: $p > 0.05$ in both cases; Table 2.3; Fig. 2.3).

218 There was an interaction between light availability and nitrogen fertiliza-
219 tion on root carbon biomass in *G. max* ($p = 0.001$; Table 2.1; Fig. 2.3). Post-hoc
220 analyses indicated that the positive effects of nitrogen fertilization on *G. max* root
221 carbon biomass increased with increasing light availability (Table 2.3; Fig. 2.3).
222 There were also positive individual effects of increasing nitrogen fertilization ($p <$
223 0.001) and light availability ($p < 0.001$) on *G. max* root carbon biomass (Table
224 2.1; Fig. 2.3).

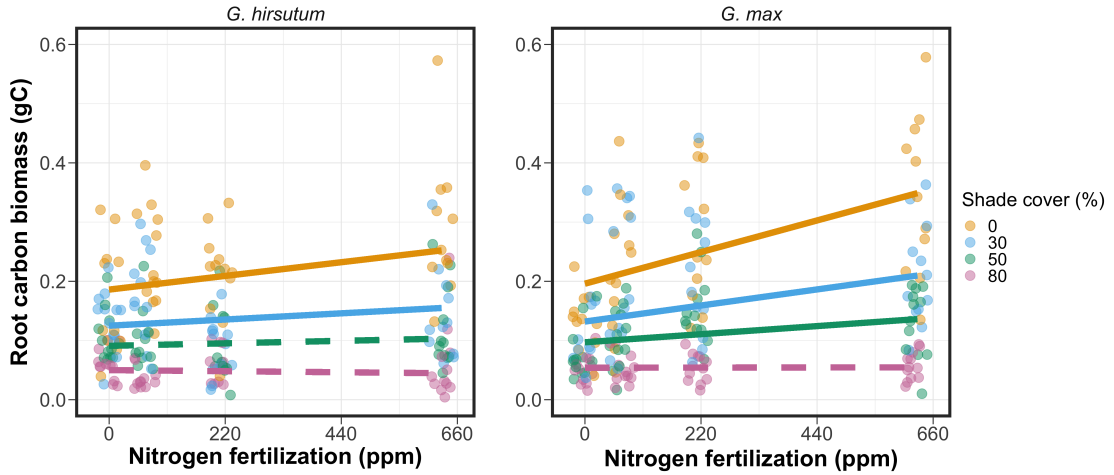


Figure 2.3. Relationships between soil nutrient fertilization and light availability on root carbon biomass in *G. hirsutum* and *G. max*. Root carbon biomass is the numerator of the carbon cost to acquire nitrogen calculation. Nitrogen fertilization treatments are represented on the x-axis. Shade cover treatments are represented through colored points and trendlines. Trendlines were created by back-transforming marginal mean slopes and intercepts from species-specific linear mixed-effects models. These values were calculated using the ‘emtrends’ and ‘emmmeans’ functions in the ‘emmeans’ R package (Lenth 2019). Points are jittered for visibility. Yellow points and trendlines represent the 0% shade cover treatment, blue points and trendlines represent the 30% shade cover treatment, green points and trendlines represent the 50% shade cover treatment, and purple points and trendlines represent the 80% shade cover treatment. Solid trendlines indicate slopes that are significantly different from zero (Tukey: $p < 0.05$), while dashed trendlines indicate slopes that are not statistically different from zero.

225 2.3.4 *Root nodule biomass*

226 Root nodule biomass in *G. max* increased with increasing light availability
227 ($p < 0.001$; Table 2.2; Fig. 2.4A) and decreased with increasing nitrogen fertiliza-
228 tion ($p < 0.001$; Table 2.2; Fig. 2.4A). There was no interaction between nitrogen
229 fertilization and light availability ($p = 0.133$; Table 2.2; Fig. 2.4A). The ratio of
230 root nodule biomass to root biomass did not change in response to light avail-
231 ability ($p = 0.481$; Table 2.2; Fig. 2.4B) but decreased with increasing nitrogen
232 fertilization ($p < 0.001$; Table 2.2; Fig. 2.4B). There was no interaction between
233 nitrogen fertilization and light availability on the ratio of root nodule biomass to
234 root biomass ($p = 0.621$; Table 2.2; Fig. 2.4B).

Table 2.2. Analysis of variance results exploring effects of light availability, nitrogen fertilization, and their interactions on *G. max* root nodule biomass and the ratio of root nodule biomass to root biomass*

	Nodule biomass			Nodule biomass: root biomass			
	df	Coefficient	χ^2	p	coefficient	χ^2	p
(Intercept)		0.302	-	-	0.448	-	-
Light (L)	1	-1.81E-03	72.964	<0.001	-8.76E-05	0.496	0.481
Nitrogen (N)	1	-2.83E-04	115.377	<0.001	-5.09E-04	156.476	<0.001
L*N	1	1.14E-06	2.226	0.133	-7.30E-07	0.244	0.621

*Significance determined using Wald's χ^2 tests ($\alpha = 0.05$). *p*-values less than 0.05 are in bold. Negative coefficients for light treatments indicate a positive effect of increasing light availability on all response variables, as light availability is treated as percent shade cover in all linear mixed-effects models. Root nodule biomass and nodule biomass: root biomass models were only constructed for *G. max* because *G. hirsutum* was not inoculated with *B. japonicum* and is not capable of forming root nodules.

Table 2.3. Slopes of the regression line describing the relationship between each dependent variable and nitrogen fertilization at each light level*

Shade cover	Carbon cost to acquire nitrogen	Whole-plant nitrogen biomass	Root carbon biomass	Root nodule biomass	Nodule biomass root biomass
<i>G. hirsutum</i>					
0%	-1.34E-03^a	1.83E-03^a	1.15E-04^b	-	-
30%	-1.22E-03^a	1.43E-03^a	1.17E-04^b	-	-
50%	-1.14E-03^a	1.17E-03^a	3.12E-05 ^b	-	-
80%	-1.02E-03^a	7.66E-04^a	-1.89E-06 ^b	-	-
<i>G. max</i>					
0%	-2.35E-04 ^b	1.55E-05^b	2.51E-04^b	-2.83E-04^b	-5.09E-04^b
30%	-3.22E-04^b	1.35E-05^b	1.57E-04^b	-2.49E-04^b	-5.31E-04^b
50%	-3.80E-04^b	1.23E-05^b	9.37E-05^b	-2.26E-04^b	-5.45E-04^b
80%	-4.66E-04^b	1.04E-05^b	-9.95E-07 ^b	-1.92E-04^b	-5.67E-04^b

*Slopes represent estimated marginal mean slopes from linear mixed-effects models described in the Methods. Slopes were calculated using the ‘emmeans’ R package (Lenth 2019). Superscripts indicate slopes fit to natural-log (^a) or square root (^b) transformed data. Slopes statistically different from zero (Tukey: $p < 0.05$) are indicated in bold. Marginally significant slopes (Tukey: $0.05 < p < 0.1$) are italicized.

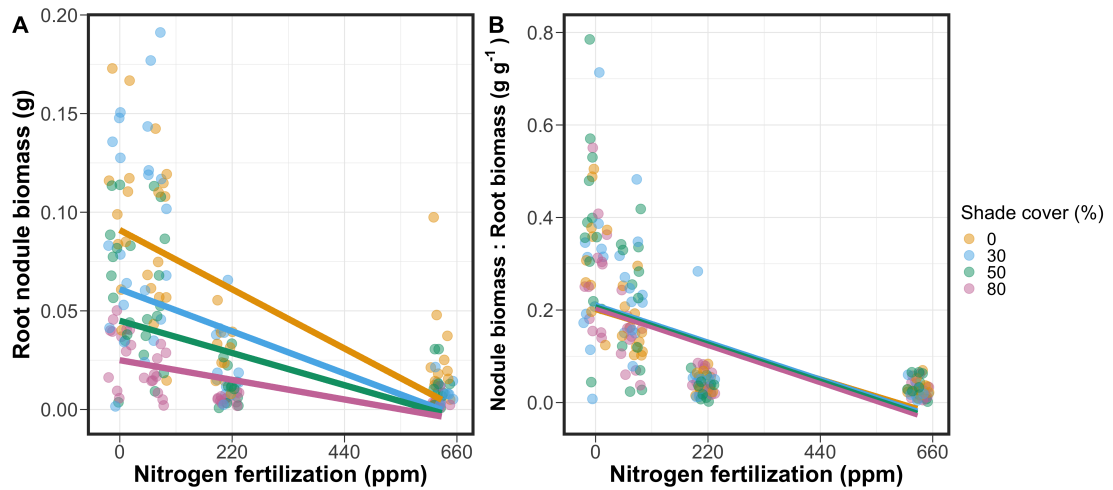


Figure 2.4. Effects of shade cover and nitrogen fertilization on root nodule biomass (A) and the ratio of root nodule biomass to root biomass (B) in *G. max*. Nitrogen fertilization treatments are represented on the x-axis. Shade cover treatments are represented through colored points and trendlines. Trendlines were created by back-transforming marginal mean slopes and intercepts from species-specific linear mixed-effects models. These values were calculated using the ‘emtrends’ and ‘emmeans’ functions in the ‘emmeans’ R package (Lenth 2019). Points are jittered for visibility. Yellow points and trendlines represent the 0% shade cover treatment, blue points and trendlines represent the 30% shade cover treatment, green points and trendlines represent the 50% shade cover treatment, and purple points and trendlines represent the 80% shade cover treatment. Solid trendlines indicate slopes that are significantly different from zero (Tukey: $p < 0.05$), while dashed trendlines indicate slopes that are not statistically different from zero.

235 2.4 Discussion

236 In this chapter, we determined the effects of light availability and soil ni-
237 trogen fertilization on root mass carbon costs to acquire nitrogen in *G. hirsutum*
238 and *G. max*. In support of our hypotheses, we found that carbon costs to acquire
239 nitrogen generally increased with increasing light availability and decreased with
240 increasing soil nitrogen fertilization in both species. These findings suggest that
241 carbon costs to acquire nitrogen are determined by factors that influence plant
242 nitrogen demand and soil nitrogen availability. In contrast to our second hypothe-
243 sis, root nodulation data suggested that *G. max* and *G. hirsutum* achieved similar
244 directional carbon cost responses to nitrogen fertilization despite a likely shift in
245 *G. max* allocation from nodulation to root biomass along the nitrogen fertilization
246 gradient (Fig. 2.4B).

247 Both *G. max* and *G. hirsutum* experienced an increase in carbon costs to
248 acquire nitrogen due to increasing light availability. These patterns were driven by
249 a larger increase in root carbon biomass than whole-plant nitrogen biomass. In-
250 creases in root carbon biomass due to factors that increase plant nitrogen demand
251 are a commonly observed pattern, as carbon allocated belowground provides sub-
252 strate needed to produce and maintain structures that satisfy aboveground plant
253 nitrogen demand (Nadelhoffer and Raich 1992; Giardina et al. 2005; Raich et al.
254 2014). Our findings suggest that plants allocate relatively more carbon for acquir-
255 ing nitrogen when demand increases over short temporal scales, which may cause
256 a temporary state of diminishing return due to asynchrony between belowground
257 carbon and whole-plant nitrogen responses to plant nitrogen demand (Kulmatiski
258 et al. 2017; Noyce et al. 2019). These responses might be attributed to a temporal

259 lag associated with producing structures that enhance nitrogen acquisition. For
260 example, fine roots (Matamala and Schlesinger 2000; Norby et al. 2004; Arndal
261 et al. 2018) and root nodules (Parvin et al. 2020) take time to build and first
262 require the construction of coarse roots. Thus, full nitrogen returns from these
263 investments may not occur immediately (Kayler et al. 2010; Kayler et al. 2017),
264 and may vary by species acquisition strategy. We speculate that increases in ni-
265 trogen acquisition from a given carbon investment may occur beyond the 5 week
266 scope of this experiment. A similar study conducted over a longer temporal scale
267 would address this.

268 Increasing soil nitrogen fertilization generally decreased carbon costs to
269 acquire nitrogen in both species. These patterns were driven by a larger increase
270 in whole-plant nitrogen biomass than root carbon biomass. In *G. hirsutum*, re-
271 ductions in carbon costs to acquire nitrogen may have been due to an increase in
272 per-root nitrogen uptake, allowing individuals to maximize the amount of nitro-
273 gen acquired from a belowground carbon investment. Interestingly, increased soil
274 nitrogen fertilization increased whole-plant nitrogen biomass in *G. max* despite
275 reductions in root nodule biomass that likely reduced the nitrogen-fixing capac-
276 ity of *G. max* (Andersen et al. 2005; Muñoz et al. 2016). While reductions in
277 root nodulation due to increased soil nitrogen availability are commonly observed
278 (Gibson and Harper 1985; Fujikake et al. 2003), our responses were observed in
279 tandem with increased root carbon biomass, implying that *G. max* shifted relative
280 carbon allocation from nitrogen fixation to soil nitrogen acquisition (Markham and
281 Zekveld 2007; Dovrat et al. 2020). This was likely because there was a reduction in
282 the carbon cost advantage of acquiring fixed nitrogen relative to soil nitrogen, and

283 suggests that species capable of associating with symbiotic nitrogen-fixing bacte-
284 ria shift their relative nitrogen acquisition pathway to optimize nitrogen uptake
285 (Rastetter et al. 2001). Future studies should further investigate these patterns
286 with a larger quantity of phylogenetically related species, or different varieties
287 of a single species that differ in their ability to form associations with symbiotic
288 nitrogen-fixing bacteria to more directly test the impact of nitrogen fixation on
289 the patterns observed in this study.

290 Carbon costs to acquire nitrogen are subsumed in the general discussion of
291 economic analogies to plant resource uptake (Bloom et al. 1985; Rastetter et al.
292 2001; Vitousek et al. 2002; Phillips et al. 2013; Terrer et al. 2018; Henneron et al.
293 2020). Despite this, terrestrial biosphere models rarely include these carbon costs
294 within their framework for predicting plant nitrogen uptake. There is currently
295 one plant resource uptake model, FUN, that quantitatively predicts carbon costs
296 to acquire nitrogen within a framework for predicting plant nitrogen uptake for
297 different nitrogen acquisition strategies (Fisher et al. 2010; Brzostek et al. 2014)

298 (Fisher et al. 2010; Brzostek et al. 2014). Iterations of FUN are currently
299 coupled to two terrestrial biosphere models: the Community Land Model 5.0 and
300 the Joint UK Land Environment Simulator (Shi et al. 2016; Lawrence et al.
301 2019; Clark et al. 2011). Recent work suggests that coupling FUN to CLM 5.0
302 caused a large overprediction of plant nitrogen uptake associated with nitrogen
303 fixation (Davies-Barnard et al. 2020). Thus, empirical data from manipulative
304 experiments that explicitly quantify carbon costs to acquire nitrogen in species
305 capable of associating with nitrogen-fixing bacteria across different environmental
306 contexts is an important step toward identifying potential biases in models such

307 as FUN.

308 Our findings broadly support the FUN formulation of carbon costs to ac-
309 quire nitrogen in response to soil nitrogen availability. FUN calculates carbon
310 costs to acquire nitrogen based on the sum of carbon costs to acquire nitrogen
311 via nitrogen fixation, mycorrhizal active uptake, non-mycorrhizal active uptake,
312 and retranslocation (Fisher et al. 2010; Brzostek et al. 2014). Carbon costs to
313 acquire nitrogen via mycorrhizal or non-mycorrhizal active uptake pathways are
314 derived as a function of nitrogen availability, root biomass, and two parameterized
315 values based on nitrogen acquisition strategy (Brzostek et al. 2014). Due to this,
316 FUN simulates a net decrease in carbon costs to acquire nitrogen with increasing
317 nitrogen availability for mycorrhizal and non-mycorrhizal active uptake pathways,
318 assuming constant root biomass. This was a pattern we observed in *G. hirsutum*
319 regardless of light availability. In contrast, FUN would not simulate a net change
320 in carbon costs to acquire nitrogen via nitrogen fixation due to nitrogen avail-
321 ability. This is because carbon costs to acquire nitrogen via nitrogen fixation are
322 derived from a well-established function of soil temperature, which is independent
323 of soil nitrogen availability (Houlton et al. 2008; Fisher et al. 2010). We observed
324 a net reduction in carbon costs to acquire nitrogen in *G. max*, except when in-
325 dividuals were grown under 0% shade cover (Fig. 2.1). While a net reduction of
326 carbon costs in response to nitrogen fertilization runs counter to nitrogen fixa-
327 tion carbon costs simulated by FUN, these patterns were likely because *G. max*
328 individuals switched their primary mode of nitrogen acquisition from symbiotic
329 nitrogen fixation to a non-symbiotic active uptake pathway (Fig. 2.4B).

330 It should be noted that the metric used in this study to determine carbon

331 costs to acquire nitrogen has several limitations. Most notably, this metric uses
332 root carbon biomass as a proxy for estimating the amount of carbon spent on
333 nitrogen acquisition. While it is true that most carbon allocated belowground
334 has at least an indirect structural role in acquiring soil resources, it remains un-
335 clear whether this assumption holds true for species that acquire nitrogen via
336 symbiotic nitrogen fixation. We also cannot quantify carbon lost through root
337 exudates or root turnover, which may increase due to factors that increase plant
338 nitrogen demand (Tingey et al. 2000; Phillips et al. 2011), and can increase the
339 magnitude of available nitrogen from soil organic matter through priming effects
340 on soil microbial communities (Uselman et al. 2000; Bengtson et al. 2012). It is
341 also not clear whether these assumptions hold under all environmental conditions,
342 such as those that shift belowground carbon allocation toward a different mode of
343 nitrogen acquisition (Taylor and Menge 2018; Friel and Friesen 2019) or between
344 species with different acquisition strategies. In this study, increasing soil nitrogen
345 fertilization increased carbon investment to roots relative to carbon transferred
346 to root nodules (Fig. 2.4B). By assuming that carbon allocated to root carbon
347 was proportional to carbon allocated to root nodules across all treatment com-
348 binations, these observed responses to soil nitrogen fertilization were likely to be
349 overestimated in *G. max*. We encourage future research to quantify these carbon
350 fates independently.

351 Researchers conducting pot experiments must carefully choose pot volume
352 to minimize the likelihood of pot volume-induced growth limitation (Poorter et al.
353 2012). Poorter et al. (2012) indicate that researchers are likely to avoid growth
354 limitations associated with pot volume if measurements are collected when the

355 plant biomass:pot volume ratio is less than 1 g L⁻¹. In this experiment, all treat-
356 ment combinations in both species had biomass:pot volume ratios less than 1 g
357 L⁻¹ except for *G. max* and *G. hirsutum* that were grown under 0% shade cover
358 and had received 630 ppm N. Specifically, *G. max* and *G. hirsutum* had average
359 respective biomass:pot volume ratios of 1.24±0.07 g L⁻¹ and 1.34±0.13 g L⁻¹, when
360 grown under 0% shade cover and received 630 ppm N (Supplementary Tables S2,
361 S3; Supplementary Fig. S1). If growth in this treatment combination was limited
362 by pot volume, then individuals may have had larger carbon costs to acquire ni-
363 trogen than would be expected if they were grown in larger pots. This pot volume
364 induced growth limitation could cause a reduction in per-root nitrogen uptake as-
365 sociated with more densely packed roots, which could reduce the positive effect
366 of nitrogen fertilization on whole-plant nitrogen biomass relative to root carbon
367 biomass (Poorter et al. 2012).

368 Growth limitation associated with pot volume provides a possible explana-
369 tion for the marginally insignificant effect of increasing nitrogen fertilization on *G.*
370 *max* carbon costs to acquire nitrogen when grown under 0% shade cover (Table
371 2.3; Fig. 2.1). This is because the regression line describing the relationship be-
372 tween carbon costs to acquire nitrogen and nitrogen fertilization in *G. max* grown
373 under 0% shade cover would have flattened if growth limitation had caused larger
374 than expected carbon costs to acquire nitrogen in the 0% shade cover, 630 ppm
375 N treatment combination. This may have been exacerbated by the fact that *G.*
376 *max* likely shifted relative carbon allocation from nitrogen fixation to soil nitrogen
377 acquisition, which could have increased the negative effect of more densely packed
378 roots on nitrogen uptake. These patterns could have also occurred in *G. hirsutum*

379 grown under 0% shade cover; however, there was no change in the effect of nitro-
380 gen fertilization on *G. hirsutum* carbon costs to acquire nitrogen grown under 0%
381 shade cover relative to other shade cover treatments. Regardless, the possibility
382 of growth limitation due to pot volume suggests that effects of increasing nitro-
383 gen fertilization on carbon costs to acquire nitrogen in both species grown under
384 0% shade cover could have been underestimated. Follow-up studies using a simi-
385 lar experimental design with a larger pot volume would be necessary in order to
386 determine whether these patterns were impacted by pot volume-induced growth
387 limitation.

388 In conclusion, this study provides empirical evidence that carbon costs to
389 acquire nitrogen are influenced by light availability and soil nitrogen fertilization
390 in a species capable of acquiring nitrogen via symbiotic nitrogen fixation and a
391 species not capable of forming such associations. We show that carbon costs to
392 acquire nitrogen generally increase with increasing light availability and decrease
393 with increasing nitrogen fertilization. This study provides important empirical
394 data needed to evaluate the formulation of carbon costs to acquire nitrogen in
395 terrestrial biosphere models, particularly carbon costs to acquire nitrogen that
396 are associated with symbiotic nitrogen fixation. Our findings broadly support
397 the general formulation of these carbon costs in the FUN biogeochemical model
398 in response to shifts in nitrogen availability. However, there is a need for future
399 studies to explicitly quantify carbon costs to acquire nitrogen under different en-
400 vironmental contexts, over longer temporal scales, and using larger selections of
401 phylogenetically related species. In addition, we suggest that future studies mini-
402 mize the limitations associated with the metric used here by explicitly measuring

403 belowground carbon fates independently.

404

Chapter 3

405 Soil nitrogen availability modifies leaf nitrogen economies in mature
406 temperate deciduous forests: a direct test of photosynthetic least-cost
407 theory

408 3.1 Introduction

409 Photosynthesis represents the largest carbon flux between the atmosphere
410 and land surface (IPCC 2021), and plays a central role in biogeochemical cycling
411 at multiple spatial and temporal scales (Vitousek and Howarth 1991; LeBauer and
412 Treseder 2008; Kaiser et al. 2015; Wieder et al. 2015). Therefore, carbon and
413 energy fluxes simulated by terrestrial biosphere models are sensitive to the formu-
414 lation of photosynthetic processes (Ziehn et al. 2011; Bonan et al. 2011; Booth
415 et al. 2012; Smith et al. 2016; Smith et al. 2017) and must be represented using
416 robust, empirically tested processes (Prentice et al. 2015; Wieder et al. 2019).
417 Current formulations of photosynthesis vary across terrestrial biosphere models
418 (Smith and Dukes 2013; Rogers et al. 2017), which causes variation in modeled
419 ecosystem processes (Knorr 2000; Knorr and Heimann 2001; Bonan et al. 2011;
420 Friedlingstein et al. 2014) and casts uncertainty on the ability of these models to
421 accurately predict terrestrial ecosystem responses and feedbacks to global change
422 (Zaehle et al. 2005; Schaefer et al. 2012; Davies-Barnard et al. 2020).

423 Terrestrial biosphere models commonly represent C₃ photosynthesis through
424 variants of the Farquhar et al. (1980) biochemical model (Smith and Dukes 2013;
425 Rogers 2014; Rogers et al. 2017). This well-tested photosynthesis model es-
426 timates leaf-level carbon assimilation, or photosynthetic capacity, as a function
427 of the maximum rate of Ribulose-1,5-bisphosphate carboxylase-oxygenase (Ru-

428 bisco) carboxylation (V_{cmax}) and the maximum rate of Ribulose-1,5-bisphosphate
429 (RuBP) regeneration (J_{max}) (Farquhar et al. 1980). Many terrestrial biosphere
430 models predict these model inputs based on plant functional group specific linear
431 relationships between leaf nutrient content and V_{cmax} (Smith and Dukes 2013;
432 Rogers 2014; Rogers et al. 2017) under the tenet that a large fraction of leaf
433 nutrients, and nitrogen (N) in particular, are partitioned toward building and
434 maintaining enzymes that support photosynthetic capacity, such as Rubisco (Brix
435 1971; Gulmon and Chu 1981; Evans 1989; Kattge et al. 2009; Walker et al. 2014).
436 Terrestrial biosphere models also predict leaf nutrient content from soil nutrient
437 availability based on the assumption that increasing soil nutrients generally in-
438 creases leaf nutrients (Firn et al. 2019; Li et al. 2020; Liang et al. 2020) which, in
439 the case of N, generally corresponds with an increase in photosynthetic processes
440 (Li et al. 2020; Liang et al. 2020).

441 Recent work calls the generality of relationships between soil nutrient avail-
442 ability, leaf nutrient content, and photosynthetic capacity into question, suggest-
443 ing instead that leaf nutrients and photosynthetic capacity are better predicted as
444 an integrated product of aboveground climate, leaf traits, and soil nutrient avail-
445 ability, rather than soil nutrient availability alone (Dong et al. 2017; Dong et al.
446 2020; Dong et al. 2022; Firn et al. 2019; Smith et al. 2019; Peng et al. 2021).
447 It has been reasoned that this result is because plants allocate added nutrients to
448 growth and storage rather than alterations in leaf chemistry (Smith et al. 2019),
449 perhaps as a result of nutrient limitation of primary productivity (LeBauer and
450 Treseder 2008; Fay et al. 2015). Additionally, recent work suggests that relation-
451 ships between leaf nutrient content and photosynthesis vary across environments,

452 and that the proportion of leaf nutrient content allocated to photosynthetic tis-
453 sue varies over space and time with plant acclimation and adaptation responses
454 to light availability, vapor pressure deficit, soil pH, soil nutrient availability, and
455 environmental factors that influence leaf mass per area (Pons and Pearcy 1994;
456 Niinemets and Tenhunen 1997; Evans and Poorter 2001; Hikosaka and Shigeno
457 2009; Ghimire et al. 2017; Onoda et al. 2017; Luo et al. 2021). The use of linear
458 relationships between leaf nutrient content and Vcmax to predict photosynthetic
459 capacity, as commonly used in terrestrial biosphere models (Rogers 2014), is not
460 capable of detecting such responses.

461 Photosynthetic least-cost theory provides an alternative framework for un-
462 derstanding relationships between soil nutrient availability, leaf nutrient content,
463 and photosynthetic capacity (Harrison et al. 2021). Leveraging a two-input mi-
464 croeconomics approach (Wright et al. 2003), the theory posits that plants accli-
465 mate to a given environment by optimizing leaf photosynthesis rates at the lowest
466 summed cost of using nutrients and water (Prentice et al. 2014; Wang et al. 2017;
467 Smith et al. 2019; Paillassa et al. 2020). Across resource availability gradients,
468 the theory predicts that optimal photosynthetic rates can be achieved by trading
469 less efficient use of a resource that is less costly to acquire (or more abundant)
470 for more efficient use of a resource more costly to acquire (or less abundant). For
471 example, an increase in soil nutrient availability should reduce the cost of acquir-
472 ing and using nutrients (Bae et al. 2015; Eastman et al. 2021; Perkowski et al.
473 2021), which could increase leaf nutrient investments in photosynthetic proteins to
474 allow similar photosynthetic rates to be achieved with higher nutrient use (lower
475 nutrient use efficiency) but lower water use (greater water use efficiency). The

476 theory suggests similar tradeoffs in response to increasing soil pH (Paillassa et al.
477 2020), specifically, that increasing soil pH should reduce the cost of acquiring soil
478 nutrients due to an increase in plant-available nutrient concentration (Paillassa
479 et al. 2020; Dong et al. 2022). The theory is also capable of reconciling dynamic
480 leaf nutrient-photosynthesis relationships at global scales (Luo et al. 2021).

481 Patterns expected from photosynthetic least-cost theory have recently re-
482 ceived empirical support both in global environmental gradient (Smith et al.
483 2019; Paillassa et al. 2020; Luo et al. 2021; Querejeta et al. 2022; Wester-
484 band et al. 2023) and local manipulative invasion (Bialic-Murphy et al. 2021)
485 studies. However, nutrient addition experiments that directly examine nutrient-
486 water use tradeoffs expected from the theory are rare (Guerrieri et al. 2011), and
487 only global gradient studies testing the theory have considered soil pH in their
488 analyses. As a result, there is a need to use nutrient addition and soil pH manu-
489 lation experiments to test mechanisms driving responses predicted by the theory.
490 Such experiments would also be useful to detect whether patterns expected from
491 theory translate to finer spatial scales.

492 In this study, we measured leaf responses to soil N availability in five decid-
493 uous tree species growing in the upper canopy of mature closed canopy temperate
494 forests in the northeastern United States. Soil N availability and pH were manip-
495 ulated through a N-by-pH field manipulation experiment with treatments applied
496 since 2011, eight years prior to measurement. Two different soil N treatments were
497 applied to increase N availability with opposing effects on soil pH. An additional
498 N-free acidifying treatment was expected to decrease soil pH. We hypothesized
499 that increased soil N availability would enable plants to increase nutrient uptake

500 and create more photosynthetic enzymes per leaf, allowing similar photosynthetic
501 rates achieved with lower leaf C_i:C_a and increased leaf N content allocated to
502 photosynthetic leaf tissue. We expected that this response would be driven by a
503 reduction in the cost of acquiring N, which would cause trees to sacrifice efficient
504 N use to enable more efficient use of other limiting resources (i.e., water). We
505 hypothesized similar leaf responses to increasing soil pH.

506 3.2 Methods

507 3.2.1 *Study site description*

508 We conducted this study in summer 2019 at three stands located within
509 a 20-km radius of Ithaca, NY, USA (42.444 °N, 76.502 °W). All stands contain
510 mature, closed-canopy forests dominated by deciduous tree species. Stands con-
511 tained abundant sugar maple (*Acer saccharum* Marshall), American beech (*Fagus*
512 *grandifolia* Ehrh.), and white ash (*Fraxinus americana* L.), accounting for 43%,
513 15%, and 17% of the total aboveground biomass across the three stands, respec-
514 tively, with less frequent red maple (*Acer rubrum* L.; 9% of total aboveground
515 biomass) and red oak occurrences (*Quercus rubra* L.; 10% of total aboveground
516 biomass). Soils at each site were broadly classified as a channery silt loam Incep-
517 tisols using the USDA NRCS Web Soil Survey data product (Soil Survey Staff
518 2022). Between 2006 and 2020, study sites averaged 972 mm of precipitation per
519 year and had an average temperature of 7.9 °C per a weather station located near
520 the Cornell University campus (42.449 °N, 76.449 °W) part of the NOAA NCEI
521 Global Historical Climatology Network (Menne et al. 2012).

522 3.2.2 *Experimental design*

523 Four 40 m x 40 m plots were set up at each site in 2009, each with an
524 additional 10 m buffer along plot perimeters (60 m x 60 m total). The plots
525 were set up as a nitrogen-by-pH field manipulation experiment, with one each of
526 four treatments at each site. Two nitrogen treatments were applied, both at 50
527 kg N ha⁻¹ yr⁻¹, as either sodium nitrate (NaNO₃) to raise soil pH, or ammonium
528 sulfate ((NH₄)₂SO₄) to acidify; an elemental sulfur treatment was selected to acid-
529 ify without N, applied at the same rate of S addition (57 kg S ha⁻¹ yr⁻¹); and
530 control plots received no additions. All amendments were added in pelletized form
531 using hand-held fertilizer spreaders to both the main plots and buffers. Amend-
532 ments were divided into three equal doses distributed across the growing season
533 from 2011-2017 and added as a single dose from 2018 onward. During 2019, plots
534 were fertilized during the week of May 20.

535 3.2.3 *Leaf gas exchange and trait measurements*

536 We sampled one leaf each from 6 to 10 individuals per plot between June
537 25 and July 12, 2019 for gas exchange measurements (Table S1). Leaves were
538 collected from deciduous broadleaf trees represented across all sites and plots and
539 were replicated in efforts to mimic the species abundance of each plot at each
540 site. We also attempted to collect leaves from the upper canopy to reduce differ-
541 ential shading effects on leaf physiology. Leaves were accessed by pulling down
542 small branches using an arborist's slingshot and weighted beanbag attached to a
543 throwline. Branches were immediately recut under deionized water and remained
544 submerged to reduce stomatal closure and avoid xylem embolism (as in Smith &

545 Dukes, 2018) until gas exchange data were collected.

546 Randomly selected leaves with little to no visible external damage were

547 attached to a Li-COR LI-6800 (Li-COR Bioscience, Lincoln, Nebraska, USA)

548 portable photosynthesis machine to measure net photosynthesis (A_{net} ; $\mu\text{mol m}^{-2} \text{s}^{-1}$),

549 stomatal conductance (g_{sw} ; $\text{mol m}^{-2} \text{s}^{-1}$), and intercellular CO_2 concentration

550 (C_i ; $\mu\text{mol mol}^{-1}$) at different reference CO_2 concentrations (C_a ; $\mu\text{mol mol}^{-1}$)

551 concentrations (i.e., an A_{net}/C_i curve) under saturating light conditions (2,000

552 $\mu\text{mol m}^{-2} \text{s}^{-1}$). Reference CO_2 concentrations followed the sequence: 400, 300,

553 200, 100, 50, 400, 400, 600, 800, 1000, 1200, 1500, and 2000 $\mu\text{mol mol}^{-1} \text{CO}_2$. Leaf

554 temperatures were not controlled in the cuvette and ranged from 21.8 °C to 31.7

555 °C (mean \pm SD: 27.2 ± 2.2 °C). A linear and second order log-polynomial nonlinear

556 regression suggested no effect of temperature on stomatal conductance measured

557 at 400 $\mu\text{mol mol}^{-1} \text{CO}_2$ or net photosynthesis measured at $\mu\text{mol mol}^{-1} \text{CO}_2$ (Ta-

558 ble S2-3; Fig. S1). All A_{net}/C_i curves were generated within one hour of branch

559 severance.

560 Leaf morphological and chemical traits were collected on the same leaf used

561 to generate each A_{net}/C_i curve. Images of each leaf were taken using a flat-bed

562 scanner to determine fresh leaf area using the ‘LeafArea’ R package (Katabuchi

563 2015), which automates leaf area calculations using ImageJ software (Schneider

564 et al. 2012). Each leaf was dried at 65°C for at least 48 hours, weighed, and

565 ground using a Retsch MM200 ball mill grinder (Verder Scientific, Inc., Newtown,

566 PA, USA) until homogenized. Leaf mass per area (M_{area} , g m^{-2}) was calculated

567 as the ratio of dry leaf biomass to fresh leaf area. Using a subsample of ground and

568 homogenized leaf biomass, leaf N content (N_{mass} ; gN g^{-1}) and leaf $\delta^{13}\text{C}$ (‰, rela-

569 tive to VPDB) were measured at the Cornell Stable Isotope Lab with an elemental
 570 analyzer (NC 2500, CE Instruments, Wigan, UK) interfaced to an isotope ratio
 571 mass spectrometer (Delta V Isotope Ratio Mass Spectrometer, ThermoFisher Sci-
 572 entific, Waltham, MA, USA). Leaf N content per unit leaf area (N_{area} ; gN m⁻²)
 573 was calculated by multiplying N_{mass} by M_{area} .

574 We used leaf $\delta^{13}\text{C}$ values to estimate χ (unitless), which is an isotope-
 575 derived estimate of the leaf $C_i:C_a$ ratio. While intercellular and atmospheric CO₂
 576 concentrations were directly measured during each A_{net}/C_i curve, deriving χ from
 577 $\delta^{13}\text{C}$ provides a more integrative estimate of the $C_i:C_a$ over an individual leaf's
 578 lifespan. We derived χ following the approach of Farquhar et al. (1989) described
 579 in Cernusak et al. (2013):

$$\chi = \frac{\Delta^{13}C - a}{b - a} \quad (3.1)$$

580 where $\Delta^{13}\text{C}$ represents the relative difference between leaf $\delta^{13}\text{C}$ (‰) and air $\delta^{13}\text{C}$
 581 (‰), and is calculated from the following equation:

$$\Delta^{13}C = \frac{\delta^{13}C_{\text{air}} - \delta^{13}C_{\text{leaf}}}{1 + \delta^{13}C_{\text{leaf}}} \quad (3.2)$$

582 where $\delta^{13}C_{\text{air}}$ is assumed to be -8‰ (Keeling et al. 1979; Farquhar et al. 1989), a
 583 represents the fractionation between ¹²C and ¹³C due to diffusion in air, assumed
 584 to be 4.4‰, and b represents the fractionation caused by Rubisco carboxylation,
 585 assumed to be 27‰ (Farquhar et al. 1989).

586 3.2.4 A_{net}/C_i curve-fitting and parameter estimation

587 We fit A_{net}/C_i curves of each individual using the ‘fitaci’ function in the
588 ‘plantecophys’ R package (Duursma 2015). This function estimates the maximum
589 rate of Rubisco carboxylation V_{cmax} ; $\mu\text{mol m}^{-2} \text{s}^{-1}$) and maximum rate of electron
590 transport for RuBP regeneration (J_{max} ; $\mu\text{mol m}^{-2} \text{s}^{-1}$) based on the Farquhar,
591 von Caemmerer, and Berry biochemical model of C₃ photosynthesis (Farquhar
592 et al. 1980). For each curve fit, we included triose phosphate utilization (TPU)
593 limitation to avoid underestimating J_{max} (Gregory et al. 2021). Curves were
594 visually examined to confirm the likely presence of TPU limitation.

595 We determined Michaelis-Menten coefficients for Rubisco affinity to CO₂
596 (K_c ; $\mu\text{mol mol}^{-1}$) and O₂ (K_o ; $\mu\text{mol mol}^{-1}$), and the CO₂ compensation point
597 (Γ^* ; $\mu\text{mol mol}^{-1}$) using leaf temperature and equations described in Medlyn et al.
598 (2002) and derived in Bernacchi et al. (2001). Specifically, K_c and K_o were
599 calculated as:

$$K_c = 404.9 * \exp^{\frac{79430(T_k - 298)}{298RT_k}} \quad (3.3)$$

600 and

$$K_o = 278.4 * \exp^{\frac{36380(T_k - 298)}{298RT_k}} \quad (3.4)$$

601 while Γ^* was calculated as:

$$\Gamma^* = 42.75 * \exp^{\frac{37830(T_k - 298)}{298RT_k}} \quad (3.5)$$

602 In all three equations, T_k is the leaf temperature (in Kelvin) during each A_{net}/C_i
603 curve and R is the universal gas constant ($8.314 \text{ J mol}^{-1} \text{ K}^{-1}$).

604 We standardized V_{cmax} and J_{max} estimates to 25°C using a modified Ar-
605 rhenius equation (Kattge and Knorr 2007):

$$k_{25} = \frac{k_{\text{obs}}}{e^{\frac{H_a(T_{\text{obs}} - T_{\text{ref}})}{T_{\text{ref}}RT_{\text{obs}}}} * \frac{1+e^{\frac{T_{\text{ref}}\Delta S - H_d}{T_{\text{obs}}}}}{1+e^{\frac{T_{\text{obs}}\Delta S - H_d}{T_{\text{obs}}}}}} \quad (3.6)$$

606 k_{25} represents the standardized V_{cmax} or J_{max} rate at 25°C , k_{obs} represents
607 the V_{cmax} or J_{max} estimate at the average leaf temperature measured inside the
608 cuvette during the A_{net}/C_i curve. H_a is the activation energy of V_{cmax} ($71,513$
609 J mol^{-1}) Kattge and Knorr (2007) or J_{max} ($49,884 \text{ J mol}^{-1}$) (Kattge and Knorr
610 2007). H_d represents the deactivation energy of both V_{cmax} and J_{max} ($200,000 \text{ J}$
611 mol^{-1}) (Medlyn et al. 2002), and R represents the universal gas constant (8.314
612 $\text{J mol}^{-1} \text{ K}^{-1}$). T_{ref} represents the standardized temperature of 298.15 K (25°C)
613 and T_{obs} represents the mean leaf temperature (in K) during each A_{net}/C_i curve.
614 ΔS is an entropy term that (Kattge and Knorr 2007) derived as a linear relation-
615 ship with average growing season temperature (T_g ; $^\circ\text{C}$), where:

$$\Delta S_{v_{\text{cmax}}} = -1.07 T_g + 668.39 \quad (3.7)$$

616 and

$$\Delta S_{j_{\text{max}}} = -0.75 T_g + 659.70 \quad (3.8)$$

617 We estimated T_g in Equations 3.7 and 3.8 based on mean daily (24-hour) air
618 temperature of the 30 days leading up to the day of each sample collection using
619 the same weather station reported in the site description. We then used V_{cmax25}
620 and J_{max25} estimates to calculate the ratio of J_{max25} to V_{cmax25} ($J_{max25}:V_{cmax25}$;
621 unitless).

622 3.2.5 *Proportion of leaf nitrogen allocated to photosynthesis and structure*

623 We used equations from Niinemets and Tenhunen (1997) to estimate the
624 proportion of leaf N content allocated to Rubisco and bioenergetics. The propor-
625 tion of leaf N allocated to Rubisco (ρ_{rub} ; gN gN⁻¹) was calculated as a function
626 of V_{cmax25} and N_{area} :

$$\rho_{rubisco} = \frac{V_{cmax25}N_r}{V_{cr}N_{area}} \quad (3.9)$$

627 where N_r is the amount of nitrogen in Rubisco, set to 0.16 gN (gN in Rubisco)⁻¹
628 and V_{cr} is the maximum rate of RuBP carboxylation per unit Rubisco protein,
629 set to 20.5 μmol CO₂ (g Rubisco)⁻¹. The proportion of leaf nitrogen allocated to
630 bioenergetics (ρ_{bioe} ; gN gN⁻¹) was similarly calculated as a function of J_{max25} and
631 N_{area} :

$$\rho_{bioe} = \frac{J_{max25}N_b}{J_{mc}N_{area}} \quad (3.10)$$

632 where N_b is the amount of nitrogen in cytochrome f, set to 0.12407 gN (μmol
633 cytochrome f)⁻¹ assuming a constant 1: 1: 1.2 cytochrome f: ferredoxin NADP
634 reductase: coupling factor molar ratio (Evans and Seemann 1989; Niinemets and

635 Tenhunen 1997), and J_{mc} is the capacity of electron transport per cytochrome f,
636 set to $156 \mu\text{mol electron} (\mu\text{mol cytochrome f})^{-1}\text{s}^{-1}$.

637 We estimated the proportion of leaf N content allocated to photosynthetic
638 tissue (ρ_{photo} ; gN gN^{-1}) as the sum of ρ_{rub} and ρ_{bioe} . This calculation is an un-
639 derestimate of the proportion of leaf N allocated to photosynthetic tissue because
640 it does not include N allocated to light harvesting proteins. This leaf N pool was
641 not included because we did not perform chlorophyll extractions on focal leaves.
642 However, the proportion of leaf N content allocated to light harvesting proteins
643 tends to be small relative to ρ_{rub} and ρ_{bioe} , and may scale with changes in ρ_{rub}
644 and ρ_{bioe} (Niinemets and Tenhunen 1997).

645 Finally, we estimated the proportion of leaf N content allocated to struc-
646 tural tissue (ρ_{str} ; gN gN^{-1}) using an empirical equation from Onoda et al. (2017):

$$N_{cw} = 0.000355 * M_{area}^{1.39} \quad (3.11)$$

647 where N_{cw} is the leaf N content allocated to cell walls (gN m^{-2}). ρ_{str} was estimated
648 by dividing N_{cw} by N_{area} .

649 3.2.6 *Tradeoffs between nitrogen and water use*

650 Photosynthetic nitrogen use efficiency (PNUE; $\mu\text{mol CO}_2 \text{ mol}^{-1} \text{ N s}^{-1}$)
651 was calculated by dividing A_{net} by N_{area} , first converting N_{area} to mol N m^{-2}
652 using the molar mass of N (14 g mol^{-1}). We used χ as an indicator of water
653 use efficiency, which exploratory analyses suggest had similar responses to soil N
654 availability and pH as intrinsic water use efficiency measured from gas exchange

655 (A_{net}/g_s). Tradeoffs between nitrogen and water use were determined by cal-
656 culating the ratio of N_{area} to χ ($N_{\text{area}}:\chi$; g N m⁻²) and V_{cmax25} to χ ($V_{\text{cmax25}}:\chi$;
657 $\mu\text{mol m}^{-2} \text{s}^{-1}$). This approach is similar to tradeoff calculations in which nitrogen-
658 water use tradeoffs are measured as the ratio of N_{area} or V_{cmax25} to g_s (Paillassa
659 et al. 2020; Bialic-Murphy et al. 2021). In this study, we quantify these re-
660 lationships using χ in lieu of g_s because g_s rapidly changes with environmental
661 conditions and therefore may have been altered by recent tree branch severance
662 and/or placement in the cuvette.

663 3.2.7 *Soil nitrogen availability and pH*

664 To characterize soil N availability at the time of our leaf gas exchange
665 measurements, we used mixed bed resin bags to quantify mobile ammonium-N
666 and nitrate-N concentrations in each plot. Lycra mesh bags were filled with 5 g
667 of Dowex® Marathon MR-3 hydrogen and hydroxide form resin (MilliporeSigma,
668 Burlington, MA USA) and sealed with a zip tie. Each bag was activated by
669 soaking in 0.5 M HCl for 20 minutes, then in 2 M NaCl until pH of the saline
670 solution stabilized, as described in Allison et al. (2008). Five resin bags were
671 inserted about 10 cm below the soil surface at each plot on June 25, 2019: one
672 near each of the four plot corners and one near the plot center. All resin bags
673 were collected 24 days later on July 19, 2019 and were frozen until extracted.

674 Prior to anion and cation extraction, each resin bag was rinsed with ul-
675 trapure water (MilliQ IQ 7000; Millipore Sigma, Burlington, MA) to remove any
676 surface soil residues. Anions and cations were extracted from surface-cleaned resin
677 bags by individually soaking and shaking each bag in 100 mL of a 0.1 M HCl/2.0

678 M NaCl matrix for one hour. Using a microplate reader (Biotek Synergy H1;
679 Biotek Instruments, Winooski, VT USA), nitrate-N concentrations were quanti-
680 fied spectrophotometrically at 540 nm with the end product of a single reagent
681 vanadium (III) chloride reaction (Doane and Horwáth 2003), and ammonium-N
682 concentrations quantified at 650 nm with the end product of a modified phenol-
683 hypochlorite reaction (Weatherburn 1967; Rhine et al. 1998). Both the single
684 reagent vanadium (III) chloride and modified phenol-hypochlorite methodologies
685 have been well established for determining nitrate-N and ammonium-N concen-
686 trations in resin bag extracts (Arnone 1997; Allison et al. 2008). We used a
687 series of negative and positive controls throughout each well plate to verify the
688 accuracy and precision of our measurements, assaying each resin bag extract and
689 control in triplicate. Soil N availability was estimated as the sum of the nitrate-N
690 and ammonium-N concentration in each resin bag, normalized per g of resin and
691 duration in the field ($\mu\text{g N g}^{-1} \text{ resin d}^{-1}$), then subsequently averaged across all
692 resin bags in a plot for a plot-level mean.

693 Soil pH was measured on 0-10 cm mineral soil samples collected prior to
694 fertilization in 2019. Near each of the four plot corners, three 5.5 cm diameter soil
695 cores were collected after first removing the forest floor where present. Each set
696 of three cores was placed in a plastic bag, and later composited by hand mixing
697 and sieved to 4mm. Soil pH was determined for a 1:2 soil:water slurry (10 g field-
698 moist soil to 20 mL DI water) of each sample using an Accumet AB15 pH meter
699 with flushable junction probe (Fisher Scientific; Hampton, NH, USA), and was
700 estimated at the plot level as the mean soil pH within each plot.

701 3.2.8 *Statistical analyses*

702 We built two separate series of linear mixed-effects models to explore effects
703 of soil N availability, soil pH, species, and leaf N content on leaf physiological
704 traits. In the first series of linear mixed-effects models, we explored the effect
705 of soil N availability, soil pH, and species on leaf N content, leaf photosynthesis,
706 stomatal conductance, and nitrogen-water use tradeoffs. Models included plot-
707 level soil N availability and plot-level soil pH as continuous fixed effects, species
708 as a categorical fixed effect, and site as a categorical random intercept term.
709 Interaction terms between fixed effects were not included due to the small number
710 of experimental plots. We built a series of separate models with this independent
711 variable structure to quantify individual effects of soil N availability, soil pH,
712 and species on N_{area} , M_{area} , N_{mass} , A_{net} , V_{cmax25} , J_{max25} , $J_{\text{max25}}:V_{\text{cmax25}}$, ρ_{rubisco} ,
713 $\rho_{\text{bioenergetics}}$, ρ_{photo} , $\rho_{\text{structure}}$, χ , PNUE, $N_{\text{area}}:\chi$, and $V_{\text{cmax25}}:\chi$.

714 A second series of linear mixed-effects models were built to investigate
715 relationships between leaf N content and photosynthetic parameters. Statistical
716 models included N_{area} as a single continuous fixed effect with species and site des-
717 ignated as individual random intercept terms. We used this independent variable
718 structure to quantify individual effects of leaf N content on A_{net} , V_{cmax25} , J_{max25} ,
719 $J_{\text{max25}}:V_{\text{cmax25}}$, and χ .

720 For all linear mixed-effects models, we used Shapiro-Wilk tests of normal-
721 ity to determine whether linear mixed-effects models satisfied residual normality
722 assumptions. If residual normality assumptions were not met, then models were
723 fit using dependent variables that were natural log transformed. If residual nor-
724 mality assumptions were still not met (Shapiro-Wilk: $p < 0.05$), then models were

725 fit using dependent variables that were square root transformed. All residual nor-
726 mality assumptions for both sets of models that did not originally satisfy residual
727 normality assumptions were met with either a natural log or square root data
728 transformation (Shapiro-Wilk: $p > 0.05$ in all cases).

729 In the first series of models, models for N_{area} , M_{area} , N_{mass} , V_{cmax25} , J_{max25} ,
730 χ , $N_{\text{area}}:\chi$, and $V_{\text{cmax25}}:\chi$, ρ_{rubisco} , $\rho_{\text{bioenergetics}}$, ρ_{photo} , $\rho_{\text{structure}}$ satisfied residual
731 normality assumptions without data transformations (Shapiro-Wilk: $p > 0.05$ in
732 all cases). The model for $J_{\text{max25}}:V_{\text{cmax25}}$ satisfied residual normality assumptions
733 with a natural log data transformation, while models for A_{net} and PNUE each
734 satisfied residual normality assumptions with square root data transformations.
735 In the second series of models, models for V_{cmax25} , J_{max25} , χ , and $V_{\text{cmax25}}:\chi$ satisfied
736 residual normality assumptions without data transformations (Shapiro-Wilk: p
737 > 0.05 in all cases). The model for $J_{\text{max25}}:V_{\text{cmax25}}$ required a natural log data
738 transformation and the model for A_{net} required a square root data transformation
739 (Shapiro-Wilk: $p > 0.05$ in both cases).

740 In all models, we used the ‘lmer’ function in the ‘lme4’ R package (Bates
741 et al. 2015) to fit each model and the ‘Anova’ function in the ‘car’ R package (Fox
742 and Weisberg 2019) to calculate Type II Wald’s χ^2 and determine the significance
743 level ($\alpha = 0.05$) of each fixed effect coefficient. Finally, we used the ‘emmeans’
744 R package (Lenth, 2019) to conduct post-hoc comparisons using Tukey’s tests,
745 where degrees of freedom were approximated using the Kenward-Roger approach
746 (Kenward and Roger 1997). All analyses and plots were conducted in R version
747 4.1.1 (R Core Team 2021)). All figure regression lines and associated 95% confi-
748 dence interval error bars were plotted using predictions generated across the soil

749 nitrogen availability gradient using the ‘emmeans’ R package (Lenth 2019).

750 3.3 Results

751 3.3.1 *Leaf N content*

752 Increasing soil N availability generally increased N_{area} (Table 3.1; Fig.
753 3.1a). This pattern was driven by an increase in N_{mass} (Table 3.1; Fig. 3.1c)
754 and a marginal increase in M_{area} (Table 3.1; Fig. 3.1e) with increasing soil N
755 availability. There was no effect of soil pH on N_{area} , N_{mass} , or M_{area} (Table 3.1);
756 however, we did observe strong differences in N_{area} (Fig. 3.1b), N_{mass} (Fig. 3.1d),
757 and M_{area} (Fig. 3.1e) between species (Table 3.1).

Table 3.1. Effects of soil N availability, soil pH, and species on leaf N content per unit leaf area (N_{area}), leaf N content per unit leaf mass (N_{mass}), and leaf mass per unit leaf area (M_{area})

	N_{area}			N_{mass}			M_{area}			
	df	Coefficient	χ^2	p	Coefficient	χ^2	p	Coefficient	χ^2	p
Intercept	-	9.03E-01	-	-	1.68E+00	-	-	4.60E+01	-	-
Soil N	1	1.68E-02	11.990	0.001	1.25E-02	6.902	0.009	4.87E-01	4.143	0.042
Soil pH	1	9.28E-02	0.836	0.361	8.08E-02	0.663	0.415	4.05E+00	0.653	0.419
Species	4	-	72.128	<0.001	-	35.074	<0.001	-	29.869	<0.001

*Significance determined using Type II Wald χ^2 tests ($\alpha = 0.05$). P-values < 0.05 are in bold.

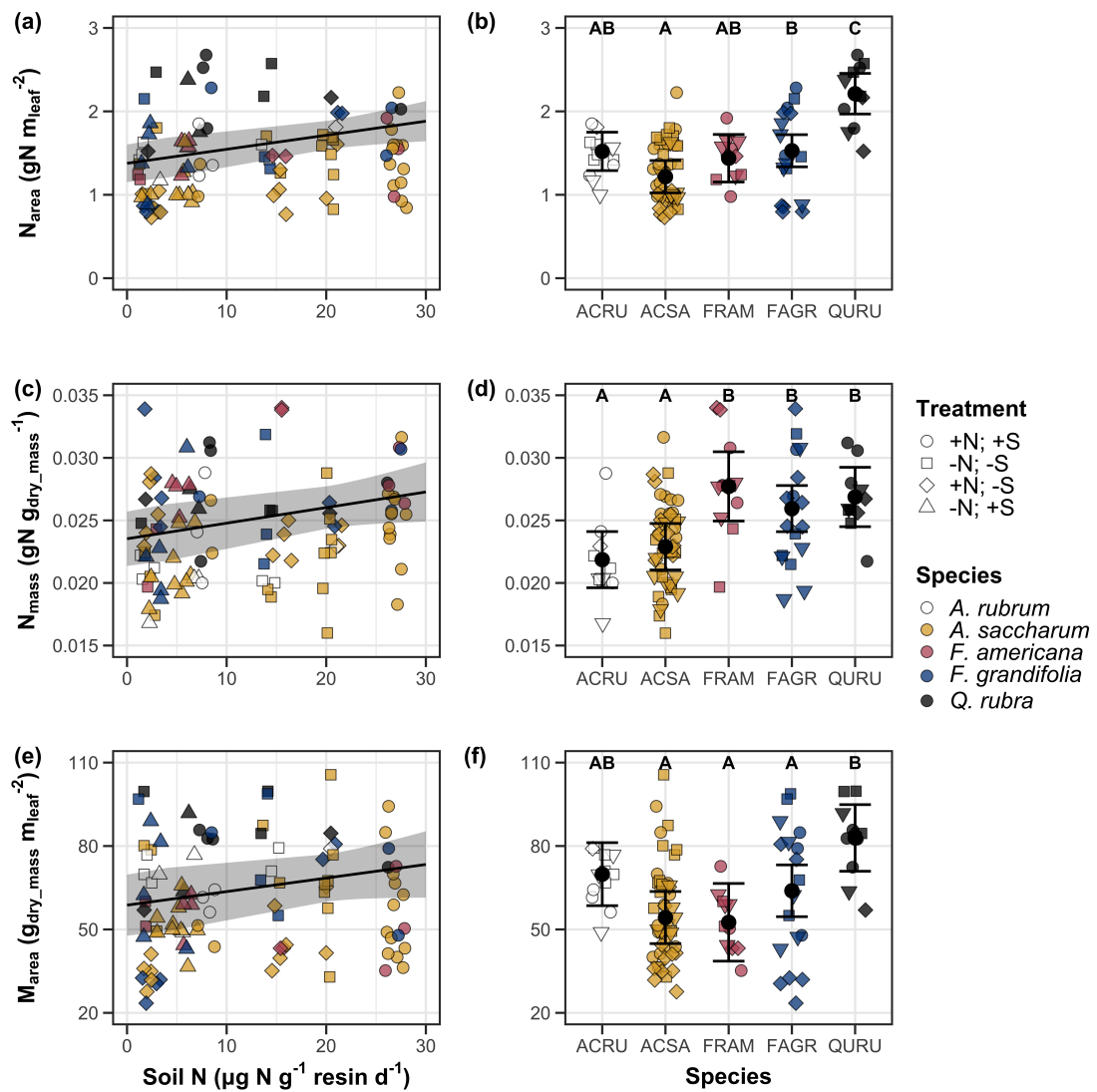


Figure 3.1. Effects of soil N availability and species on leaf N content per unit leaf area (a-b), leaf nitrogen content per unit leaf biomass (c-d), and leaf mass per unit leaf area (e-f). Soil N availability is represented on the x-axis in the left column of panels, while species is represented on the x-axis in the right column of panels. Tree species are represented as colored points and treatment plots are represented as shaped points, jittered for visibility. Species are abbreviated in the right column of panels through their assigned NRCS PLANTS Database symbol (USDA NRCS 2022), grouped along the x-axis per common mycorrhizal association, where the first three species commonly associate with arbuscular mycorrhizae (ACRU, ASCA, FAGR) and the second two species with ectomycorrhizae (FAGR, QURU). Trendlines are only included when the regression slope is statistically different from zero ($p < 0.05$).

758 3.3.2 *Net photosynthesis and leaf biochemistry*

759 Increasing soil N availability generally had no effect on A_{net} , V_{cmax25} , J_{max25} ,
760 or $J_{\text{max25}}:V_{\text{cmax25}}$ (Table 3.2, Figs. 3.2a, 3.2d, 3.2g). We also observed strong
761 species effects on all measured leaf photosynthetic traits (Table 3.2; Figs. 3.2b,
762 3.2e, 3.2h). Increasing soil pH had a marginal negative effect on A_{net} , but had no
763 effect on V_{cmax25} , J_{max25} , or $J_{\text{max25}}:V_{\text{cmax25}}$ (Table 3.2). There was a weak positive
764 effect of increasing N_{area} on A_{net} (Fig. 3.2c), but quite strong positive effects of
765 increasing N_{area} on V_{cmax25} and J_{max25} (Table 3.2; Fig. 3.2f and 3.2i).

Table 3.2. Effects of soil N availability, soil pH, species, and N_{area} on leaf biochemistry

	A_{net}			V_{cmax25}			J_{max25}			
	df	Coefficient	χ^2	p	Coefficient	χ^2	p	Coefficient	χ^2	p
(Intercept)	-	3.29E+00 ^b	-	-	6.38E+01	-	-	1.12E+02	-	-
Soil N	1	-1.23E-03 ^b	1.798	0.180	-3.84E-01	1.745	0.187	-6.70E-01	2.172	0.141
Soil pH	1	-3.09E-01 ^b	3.312	0.069	-4.91E+00	0.655	0.418	-8.18E+00	0.742	0.389
Species	4	-	11.838	0.019	-	31.748	<0.001	-	27.291	<0.001
(N_{area} int.)	-	6.59E-01 ^b	-	-	1.45E-01	-	-	2.86E+01	-	-
N_{area}	4	3.13E-01 ^b	4.790	0.029	2.43E+01	22.616	<0.001	4.04E+01	28.259	<0.001

	$J_{\text{max25}}:V_{\text{cmax25}}$			
	df	Coefficient	χ^2	p
(Intercept)	-	6.59E-01 ^a	-	-
Soil N	1	7.04E-04 ^a	0.088	0.767
Soil pH	1	-7.84E-03 ^a	0.025	0.874
Species	4	-	12.745	0.013
(N_{area} int.)	-	6.69E-01 ^a	-	-
N_{area}	4	-4.69E-02 ^a	1.142	0.285

*Significance determined using Type II Wald χ^2 tests ($\alpha = 0.05$). P -values < 0.05 are in bold, while p -values between 0.05 and 0.1 are italicized. Superscript letters indicate model coefficients fit to natural-log (^a) or square-root (^b) transformed data. Relationships between N_{area} and each response variable were fit using the second series of bivariate mixed-effects models, so model coefficients and results are independent from model coefficients and results reported for relationships between soil N, soil pH, and species for each response variable. Key: A_{net} – light saturated net photosynthesis rate; V_{cmax25} – maximum rate of Rubisco carboxylation at 25°C; J_{max25} – maximum rate of electron transport for RuBP regeneration at 25°C, $J_{\text{max25}}:V_{\text{cmax25}}$ – the ratio of J_{max25} to V_{cmax25} .

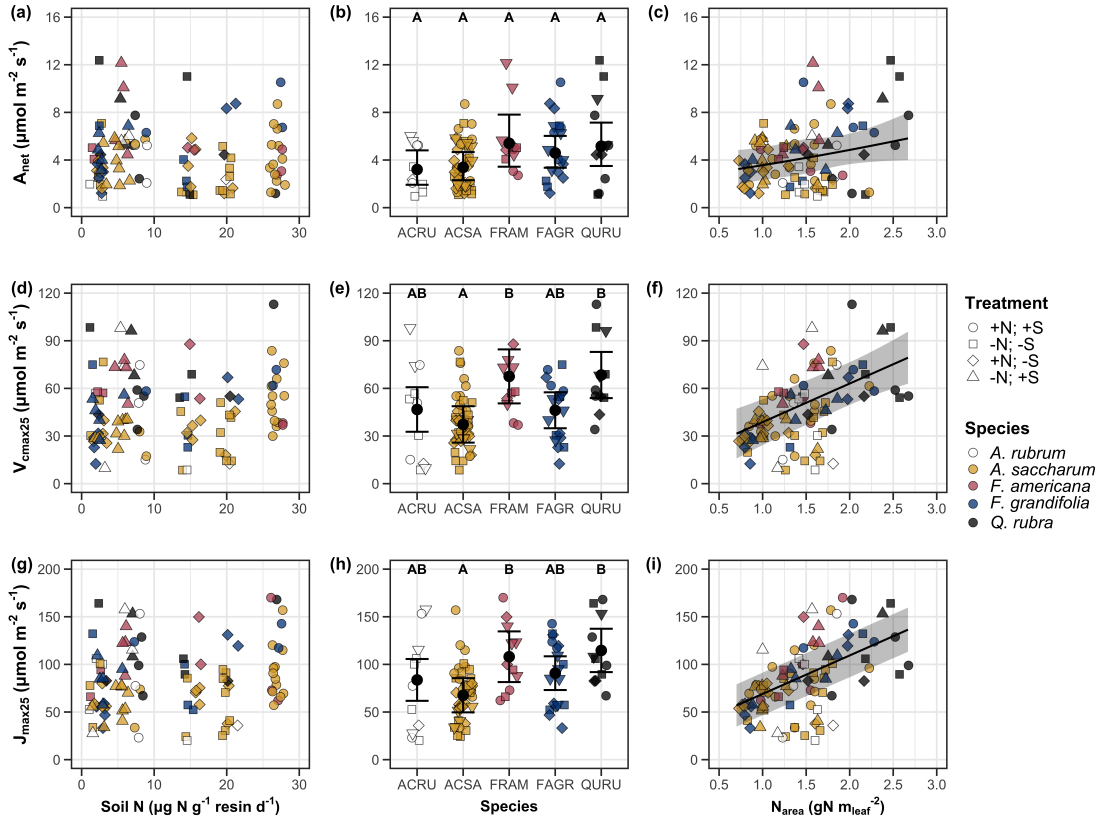


Figure 3.2. Effects of soil N availability (left column of panels), species (middle column of panels), and leaf N content per unit leaf area (right column of panels) on net photosynthesis (a-c), maximum Rubisco carboxylation rate (d-f), and maximum RuBP regeneration rate (g-i). Soil N availability is represented on the x-axis in the left column of panels, species is represented on the x-axis in the middle column of panels, and leaf N content per unit leaf area is represented continuously on the x-axis in the right column of panels. Species abbreviations and position along the x-axis in the middle column of panels, colored points, shapes, and trendlines are as explained in Figure 3.1.

766 3.3.3 *Leaf N allocation*

767 Neither soil N availability nor soil pH affected the proportion of leaf N
768 allocated to Rubisco or bioenergetics (Table 3.3; Fig. 3.3a, Fig. 3.3c), nor was
769 there any subsequent effect on the proportion of leaf N allocated to photosynthesis
770 (Table 3.3; Fig. 3.3f). We also found no effect of soil N availability or soil pH on
771 the proportion of leaf N allocated to structure (Table 3.3; Fig 3.3g). Species varied
772 in the proportion of leaf N allocated to Rubisco, photosynthesis, and structure (Fig
773 3.3b, Fig. 3.3d, Fig 3.3h), with no detectable species effect on the proportion of
774 leaf N allocated to bioenergetics (Table 3.3).

Table 3.3. Effects of soil N availability, soil pH, and species on the proportion of leaf nitrogen content allocated to photosynthesis, Rubisco, bioenergetics, and structure

	ρ_{photo}			ρ_{rub}			ρ_{bioe}			
	df	Coefficient	χ^2	p	Coefficient	χ^2	p	Coefficient	χ^2	p
Intercept	-	4.93E-01	-	-	4.17E-01	-	-	7.64E-02	-	-
Soil N	1	-1.23E-03	0.521	0.470	-1.04E-03	0.501	0.479	-1.77E-04	0.557	0.455
Soil pH	1	-4.37E-02	1.581	0.209	-3.70E-02	1.511	0.219	-6.84E-03	1.941	0.164
Species	4	-	13.106	0.011	-	14.152	0.007	-	7.300	0.121

	ρ_{str}			
	df	Coefficient	χ^2	p
Intercept	-	9.77E-02	-	-
Soil N	1	-2.29E-04	1.165	0.280
Soil pH	1	-1.87E-03	0.179	0.672
Species	4	-	16.428	0.002

*Significance determined using Type II Wald χ^2 tests ($\alpha = 0.05$). P-values < 0.05 are in bold. Key: ρ_{photo} - proportion of leaf nitrogen content allocated to photosynthesis; ρ_{rub} - proportion of leaf nitrogen content allocated to Rubisco; ρ_{bioe} - proportion of leaf nitrogen content allocated to bioenergetics; ρ_{str} - proportion of leaf nitrogen content allocated to structure.

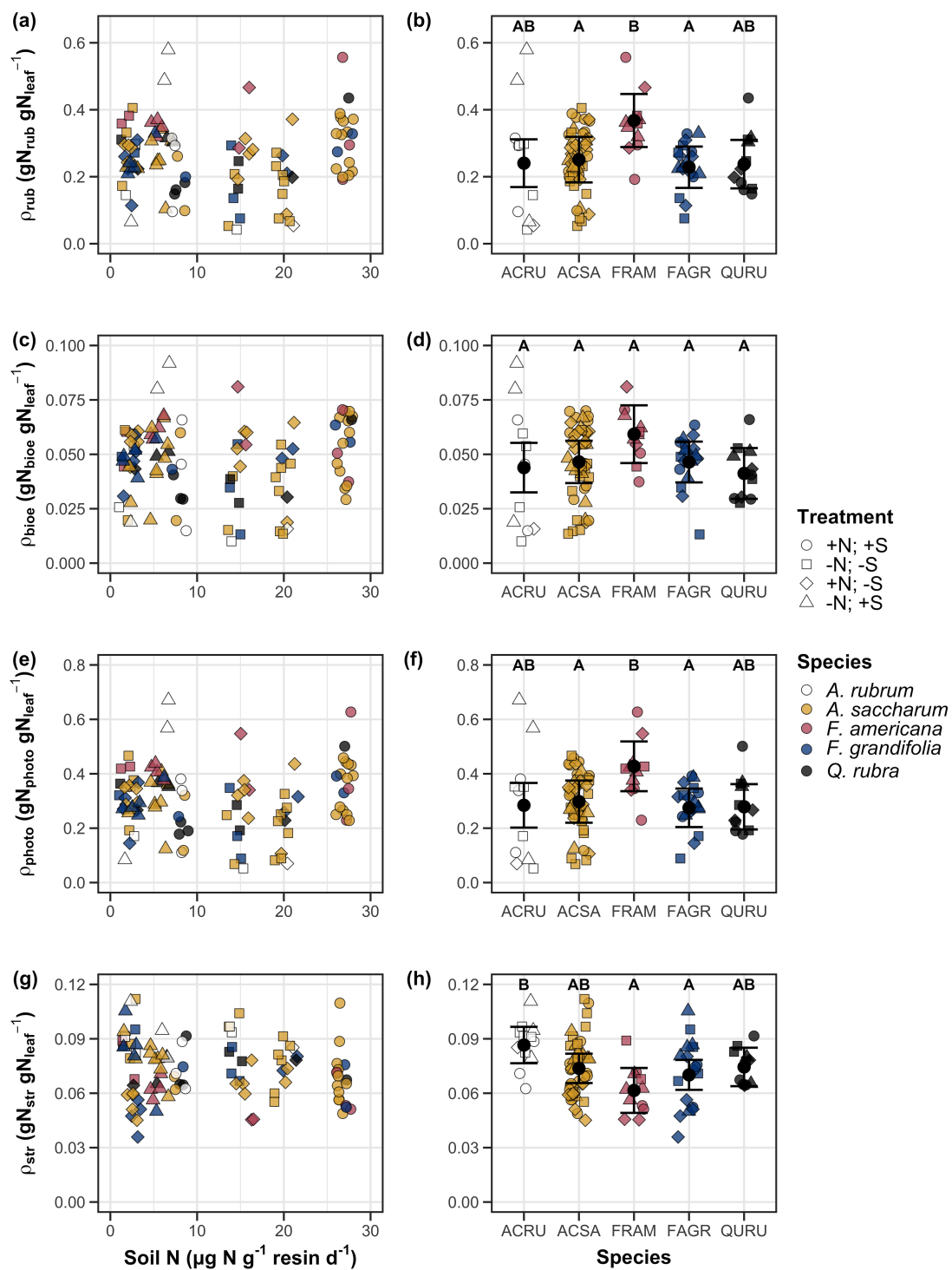


Figure 3.3. Effects of soil nitrogen availability and species on the proportion of leaf nitrogen content allocated to Rubisco (a-b), bioenergetics (c-d), photosynthesis (e-f), and structure (g-h)

775 3.3.4 *Tradeoffs between nitrogen and water use*

776 Although soil N availability did not affect χ (Table 3.4; Fig. 3.4a), increasing
777 soil N availability decreased PNUE (Table 3.4; Fig. 3.4d) and increased the
778 ratio of $N_{\text{area}}:\chi$ (Table 3.4; Fig. 3.4f). Specifically, this response yielded a 26%
779 reduction in PNUE and 37% stimulation in $N_{\text{area}}:\chi$ across the soil nitrogen avail-
780 ability gradient. There was no apparent effect of soil N availability on $V_{\text{cmax25}}:\chi$
781 (Table 3.4; Fig. 3.4h). Increasing soil pH had a weak marginal negative effect
782 on PNUE, but did not influence χ , $N_{\text{area}}:\chi$, or $V_{\text{cmax25}}:\chi$ (Table 3.4). We also
783 observed differences in χ (Fig. 3.4b), PNUE (Fig. 3.4e), $N_{\text{area}}:\chi$ (Fig. 3.4g), and
784 $V_{\text{cmax25}}:\chi$ (Fig. 3.4i) between species (Table 3.4). Finally, increasing N_{area} had a
785 strong negative effect on χ (Table 3.4; Fig. 3.4c) and a strong positive effect on
786 $V_{\text{cmax25}}:\chi$ (Table 3.4; Fig. 3.4j).

Table 3.4. Effects of soil N availability, soil pH, species, and N_{area} on tradeoffs between nitrogen and water use

	χ			PNUE			$N_{\text{area}}:\chi$			
	df	Coefficient	χ^2	p	Coefficient	χ^2	p	Coefficient	χ^2	p
(Intercept)	-	8.12E-01	-	-	9.57E+00	-	-	9.19E-01	-	-
Soil N	1	-1.14E-03	1.698	0.193	-6.63E-02	6.396	0.011	2.60E-02	9.533	0.002
Soil pH	1	-1.91E-02	1.087	0.297	-9.25E-01	2.843	<i>0.092</i>	2.03E-01	1.321	0.250
Species	4	-	18.843	0.001	-	13.454	0.009	-	52.983	<0.001
(N_{area} int.)	-	8.93E-01	-	-	-	-	-	-	-	-
N_{area}	1	-1.11E-01	80.606	<0.001	-	-	-	-	-	-

	$V_{\text{cmax25}}:\chi$			
	df	Coefficient	χ^2	p
(Intercept)	-	7.20E+01	-	-
Soil N	1	3.99E-01	0.963	0.326
Soil pH	1	-3.12E+00	0.138	0.711
Species	4	-	31.450	<0.001
(N_{area} int.)	-	1.18E+01	-	-
N_{area}	4	3.87E+01	32.797	<0.001

55

*Significance determined using Type II Wald χ^2 tests ($\alpha = 0.05$). P -values < 0.05 are in bold, while p -values between 0.05 and 0.1 are italicized. Superscript letters indicate model coefficients fit to natural-log ^(a) or square-root ^(b) transformed data. Relationships between N_{area} and each response variable were fit using the second series of bivariate mixed-effects models, so model coefficients and results are independent from model coefficients and results reported for relationships between soil N, soil pH, and species for each response variable. Key: χ - isotope-derived estimate of the $C_i:C_a$; PNUE - photosynthetic N use efficiency, ratio of net photosynthesis to leaf N content per unit leaf area; $N_{\text{area}}:\chi$ - ratio of N_{area} to χ ; $V_{\text{cmax25}}:\chi$ - ratio of V_{cmax25} to χ .

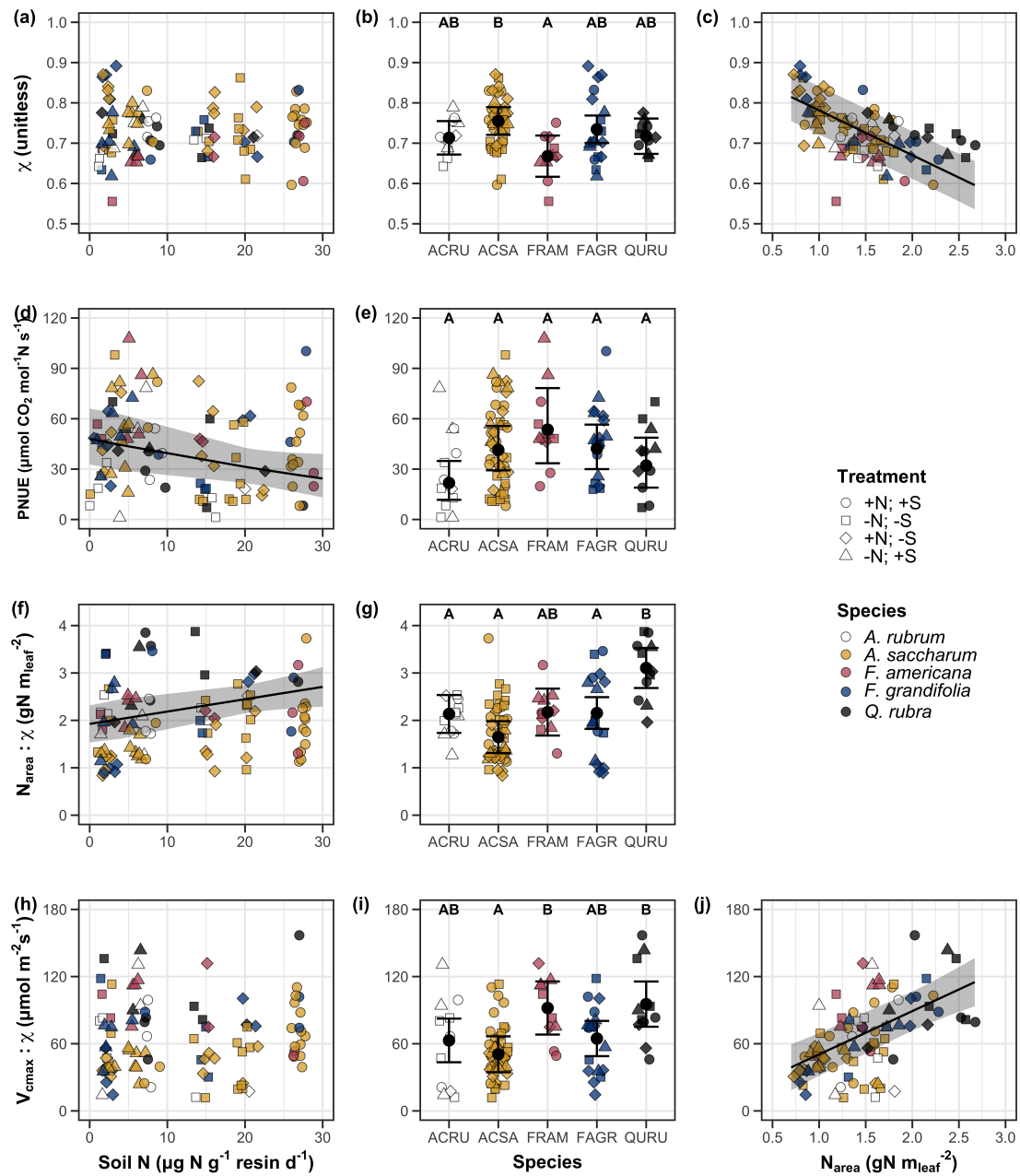


Figure 3.4. Effects of soil nitrogen availability and species on the proportion of leaf nitrogen content allocated to Rubisco (a-b), bioenergetics (c-d), photosynthesis (Rubisco + bioenergetics; e-f), and structure (g-h). Soil nitrogen availability is represented on the x-axis in the left column of panels and species are represented on the x-axis in the right column of panels. Species abbreviations and position along the x-axis in the middle column of panels, colored points, shapes, trendlines, error bars, and compact lettering are as explained in Figure 3.1.

787 3.4 Discussion

788 Photosynthetic least-cost theory provides an explanation for understand-
789 ing relationships between soil nutrient availability, leaf nutrient allocation, and
790 photosynthetic capacity. The theory suggests that plants acclimate to a given
791 environment by optimizing leaf photosynthesis rates at the lowest summed cost
792 of using nutrients and water Prentice et al. (2014), Wang et al. (2017), Smith
793 et al. (2019), Paillassa et al. (2020). The theory predicts that an increase in
794 soil nutrient availability should allow similar photosynthesis rates to be achieved
795 with increased leaf nutrient content and photosynthetic capacity (i.e., V_{cmax25} and
796 J_{max25}) at lower leaf $C_i:C_a$ (χ), resulting in an increase in water use efficiency,
797 decrease in nutrient use efficiency, and increase in both leaf nutrient content and
798 photosynthetic capacity per unit χ . The theory predicts similar leaf responses to
799 increasing soil pH under acidic conditions, presumably due to generally faster nu-
800 trient cycle dynamics and consequent reductions in the cost of acquiring nutrients
801 relative to water with increasing soil pH (Wang et al. 2017; Paillassa et al. 2020;
802 Dong et al. 2020).

803 Supporting the theory, we showed that increasing soil N availability was
804 associated with increased leaf N content (Fig 3.1a, 3.1c), a pattern that reduced
805 photosynthetic N use efficiency (Fig 3.4d) and increased leaf N content per unit
806 χ (Fig 3.4f). Increasing soil N coincided with slight, but non-significant decreases
807 in χ and increases in V_{cmax25} and J_{max25} ($p < 0.2$, Table 3.2). The positive trend
808 between soil N availability and photosynthetic capacity was supported by the con-
809 current strong increase in leaf N content with increasing soil N availability, which
810 resulted in no change in the proportion of leaf N content allocated to photosynthe-

811 sis across the soil N availability gradient. Additionally, leaf N content exhibited a
812 strong negative correlation with χ , indicative of strong nitrogen-water use trade-
813 offs at the leaf level. Responses tended to vary more due to soil N availability
814 than soil pH. Overall, these findings are consistent with the nutrient-water use
815 tradeoffs predicted from theory.

816 3.4.1 *Soil nitrogen availability modifies tradeoffs between nitrogen and water use*

817 In support of expected least-cost outcomes and past environmental gradient
818 studies (Dong et al. 2017; Paillassa et al. 2020), we found that increasing soil N
819 availability was associated with increased leaf N content. Soil N availability had
820 smaller impacts on measures of net photosynthesis and χ , which led to reductions
821 in PNUE and increases in leaf N content per unit χ , as expected from theory.
822 Photosynthetic least-cost theory suggests that reductions in PNUE should be
823 driven by an increase in the proportion of leaf N allocated to photosynthetic tissue,
824 a pattern that should allow plants to achieve optimal photosynthetic rates with
825 greater photosynthetic capacity to make better use of available light. Contrasting
826 theory predictions, we found no effect of soil N availability on photosynthetic
827 capacity. However, photosynthetic capacity did tend to increase with increasing
828 soil N availability ($p < 0.20$; Table 3.2) resulting in no effect of soil N availability on
829 the relative fraction of leaf N allocated to photosynthesis, Rubisco, or bioenergetics
830 (Fig. 3.3). These lines of evidence support the idea that trees use additional N
831 to support increased leaf N allocation toward photosynthetic tissue and enhance
832 photosynthetic capacity (Wright et al. 2003).

833 Soil N availability had a stronger effect on leaf N than photosynthetic ca-

834 pacity. This pattern suggests that additional plant N uptake due to increased
835 soil N availability was also being used to support non-photosynthetic N pools,
836 possibly to structural tissue or stress-induced amino acid and polyamine synthe-
837 sis (Minocha et al. 2000; Onoda et al. 2004; Bubier et al. 2011). While we
838 found no change in the proportion of leaf N allocated to leaf structural tissue, the
839 overall stimulation in leaf N content with increasing soil N availability suggests an
840 increase in the net amount of N invested in leaf structural tissue along the N avail-
841 ability gradient. Importantly, leaf N allocated to structure was calculated using
842 an empirical relationship between M_{area} and the amount of leaf N allocated to cell
843 walls (Onoda et al. 2017). As the generality of relationships between M_{area} and
844 the amount of leaf N allocated to cell walls has been called into question (Harrison
845 et al. 2009), future work should consider explicitly measuring N allocation to cell
846 wall tissue and stress-induced amino acid synthesis to confirm these patterns.

847 In opposition to patterns expected from least cost theory, increasing soil
848 N availability had no apparent effect on χ (Fig. 3.4a). Interestingly, despite
849 the null effect of soil N availability on χ , we observed a strong negative effect of
850 increasing N_{area} on χ (Fig. 3.4c), consistent with the nitrogen-water use tradeoffs
851 expected from theory. The null response of χ to increasing soil N availability may
852 have been due to a lack of water limitation in the system, given that the area
853 received approximately 20% more precipitation (1167 mm) during the 12-month
854 period leading up to our measurement period than normally expected (972 mm).
855 However, droughts can and do occur in temperate forests of the northeastern
856 United States (Sweet et al. 2017), so the observed increase in leaf N content
857 with increasing soil N availability could be a strategy that allows trees to hedge

858 bets against drier than normal growing seasons (Onoda et al. 2004; Onoda et al.
859 2017; Hallik et al. 2009). As was suggested in Paillassa et al. (2020), and more
860 recently by Querejeta et al. (2022), negative effects of soil N availability on χ may
861 increase with increasing aridity. This strategy would be especially advantageous if
862 it allows individuals growing in arid regions to maintain carbon assimilation rates
863 with reduced water loss. Future work should attempt to quantify interactive roles
864 of climate and soil nitrogen availability on nitrogen-water use tradeoffs, which
865 could be done by leveraging coordinated and multi-factor nutrient (Borer et al.
866 2014) and water (Knapp et al. 2017) manipulation experiments across broad
867 climatic gradients.

868 3.4.2 *Soil pH did not modify tradeoffs between nitrogen and water usage*

869 While the primary purpose of this study was to examine the role of soil N
870 availability on nitrogen-water use tradeoffs, our experimental design manipulated
871 both soil N and pH, providing an opportunity to isolate the roles of these variables.
872 Previous correlational studies along environmental gradients identified soil pH as
873 a particularly important factor that can modify tradeoffs between nutrient and
874 water use (Smith et al. 2019; Paillassa et al. 2020; Westerband et al. 2023)
875 and the proportion of leaf nitrogen allocated to photosynthesis (Luo et al. 2021).
876 Such studies implied that these patterns may be driven by reductions in the cost of
877 acquiring nutrients relative to water with increasing pH, which may be exacerbated
878 in acidic soils.

879 Consistent with theory (Wright et al. 2003; Prentice et al. 2014), our
880 results indicate that increasing soil pH was negatively associated with PNUE.

881 However, there was no effect of soil pH on leaf N content, χ , or leaf N content per
882 unit χ , most likely because the experimental N additions increased soil N sup-
883 ply while both increasing (sodium nitrate) and decreasing (ammonium sulfate)
884 soil pH. These results suggest that soil pH did not play a major role in modify-
885 ing expected photosynthetic least-cost theory patterns, contrasting findings from
886 Paillassa et al. (2020) and other gradient studies that note positive effects of in-
887 creasing soil pH on leaf N content, Rubisco carboxylation, and χ (Viet et al. 2013;
888 Cornwell et al. 2018; Luo et al. 2021). Instead, null responses to soil pH show
889 that leaf photosynthetic parameters depend more on soil N availability than pH
890 per se, and that inferences from gradient studies might be confounding covariation
891 between N availability and soil acidity.

892 3.4.3 *Species identity explains a large amount of variation in leaf and whole*
893 *plant traits*

894 Species generally explained a larger amount of variation in measured leaf
895 traits than soil N availability or soil pH. Interspecies variation is an important
896 factor to consider when deducing mechanisms that drive photosynthetic least-
897 cost theory, particularly for species that form distinct mycorrhizal associations or
898 have different photosynthetic pathways, growth forms, or leaf habit (Espelta et al.
899 2005; Adams et al. 2016; Bialic-Murphy et al. 2021; Scott and Smith 2022). The
900 need to consider species may also be important when comparing nutrient-water
901 use tradeoffs in early and late successional species, or in species with different
902 resource economic strategies (Abrams and Mostoller 1995; Ellsworth and Reich
903 1996; Wright et al. 2004; Reich 2014; Onoda et al. 2017; Ziegler et al. 2020).

904 A strength of the study design and sampling effort is that it controls for
905 many species differences that should modify nitrogen-water use tradeoffs expected
906 from theory. All tree species measured in this study shared the leaf habit of decid-
907 uous broadleaves, were growing in forests of similar successional stage, but differed
908 in mycorrhizal association and consequent resource economic strategies. As stands
909 tended to be dominated by trees that associate with arbuscular mycorrhizae (*Frax-*
910 *inus* and both *Acer* species made up 70% of total aboveground biomass across
911 stands), ecosystem biogeochemical cycle dynamics may be more closely aligned
912 to the inorganic nutrient economy proposed in Phillips et al. (2013), which may
913 promote stronger nitrogen-water use tradeoffs in tree species that associate with
914 arbuscular mycorrhizae. This result was not observed here, as photosynthetic
915 properties varied as much within as across the two mycorrhizal associations rep-
916 resented. Given the high variability in measured photosynthetic traits within
917 and across species, effects of mycorrhizal association likely require more intensive
918 sampling efforts to detect than were possible here.

919 3.4.4 *Implications for photosynthetic least-cost theory model development*

920 In the field, soil nutrient availability is heterogeneous across time and space
921 (Table S4). Unaccounted within-plot heterogeneity may have contributed to the
922 low amount of variation explained by soil N availability in our statistical mod-
923 els, as resin bags are a coarse surrogate for soil N availability. Despite this, we
924 still observed evidence for nutrient-water use tradeoffs, suggesting that observed
925 responses reported here may be an underestimate toward the net effect of soil
926 N availability on these tradeoffs. While we urge caution in the interpretation of

927 these results, they do provide a promising baseline for future studies investigating
928 patterns expected from photosynthetic least-cost theory at finer spatiotemporal
929 resolutions.

930 The general stronger relationship between leaf N content and photosynthetic parameters versus between leaf N content and soil N availability suggests
931 that leaf N content is more directly tied to photosynthesis than soil N availability. While this could be due to the high spatiotemporal heterogeneity of soil N
932 availability, principles from photosynthetic least-cost theory suggest that leaf N
933 content is the downstream product of leaf nutrient demand to build and maintain
934 photosynthetic machinery, which is set by aboveground environmental conditions
935 such as light availability, CO₂, temperature, or vapor pressure deficit (Smith
936 et al. 2019; Paillassa et al. 2020; Peng et al. 2021; Westerband et al. 2023). The
937 stronger relationship between leaf N and photosynthetic parameters paired with
938 the strong negative relationship between leaf N and χ could indicate a relatively
939 stronger effect of climate on leaf N-photosynthesis relationships than soil resource
940 availability. However, the short distance between plots and across sites limited
941 our ability to test this mechanism.

944 Variation in soil pH affected least cost responses less than variations in
945 soil N availability, in part because experimental treatments directly increased soil
946 N and affected soil pH in opposite directions. While soil pH has been shown
947 to drive nitrogen-water tradeoffs in global gradient analyses (Viet et al. 2013;
948 Paillassa et al. 2020), these responses may be due to covariations between soil pH
949 and nutrient cycling rather than a role of pH per se. The direct manipulations
950 of soil pH and soil N availability in this study allowed us to partly disentangle

951 these factors and show that variation in N availability matters more for least-cost
952 tradeoffs than pH alone.

953 3.4.5 *Conclusions*

954 Increasing soil N availability generally increased leaf N content (both area-
955 and mass-based), but did not significantly influence χ . This shift in leaf N led
956 to a reduction in PNUE, and an increase in leaf N per unit χ with increasing
957 soil N availability. Despite null effects of soil N availability on χ , we observed a
958 strong negative relationship between leaf N content and χ . These results provide
959 empirical support for the nutrient-water use tradeoffs expected from photosyn-
960 thetic least-cost theory in response to soil nutrient availability, but suggest that
961 all tenets of the theory may not hold in every environment. These results exper-
962 imentially test previous work suggesting that leaf water-nitrogen economies vary
963 across gradients of soil nutrient availability and pH, and show that variations in
964 nutrient availability matter more for determining variation in leaf photosynthetic
965 traits than soil pH.

966

Chapter 4

967 The relative cost of resource use for photosynthesis drives variance in
968 leaf nitrogen content across climate and soil resource availability
969 gradients

970 4.1 Introduction

971 Terrestrial biosphere models, which comprise the land surface component of
972 Earth system models, are sensitive to the formulation of photosynthetic processes
973 (Knorr 2000; Ziehn et al. 2011; Booth et al. 2012). This is because photosynthe-
974 sis is the largest carbon flux between the atmosphere and terrestrial biosphere,
975 and is constrained by ecosystem carbon and nutrient cycles (Hungate et al. 2003;
976 LeBauer and Treseder 2008; IPCC 2021; Fay et al. 2015). Many terrestrial bio-
977 sphere models formulate photosynthesis by parameterizing photosynthetic capac-
978 ity within plant functional groups through empirical linear relationships between
979 area-based leaf nitrogen content (N_{area}) and the maximum carboxylation rate
980 of Ribulose-1,5-bisphosphate carboxylase/oxygenase (Kattge et al. 2009; Rogers
981 2014; Rogers et al. 2017). Models are also beginning to include connected carbon-
982 nitrogen cycles (Wieder et al. 2015; Shi et al. 2016; Davies-Barnard et al. 2020;
983 Braghiere et al. 2022), which allows leaf photosynthesis to be predicted directly
984 through changes in N_{area} and indirectly through changes in soil nitrogen avail-
985 ability (e.g., LPJ-GUESS, Smith et al., 2014; CLM5.0, Lawrence et al., 2019).
986 Despite recent model developments, open questions remain regarding the gen-
987 erality of ecological relationships between soil nitrogen availability, leaf nitrogen
988 content, and leaf photosynthesis across edaphic and climatic gradients.

989 Empirical support for positive relationships between soil nitrogen avail-

ability and N_{area} is abundant (Firn et al. 2019; Liang et al. 2020), and is a result often attributed to the high nitrogen cost of building and maintaining Rubisco (Evans 1989; Evans and Seemann 1989; Onoda et al. 2004; Onoda et al. 2017; Dong et al. 2020). Such patterns imply that positive relationships between soil nitrogen availability and N_{area} should cause an increase in leaf photosynthesis and photosynthetic capacity by increasing the maximum rate of Rubisco carboxylation through increased investments to Rubisco construction and maintenance. This integrated N_{area} -photosynthesis response to soil nitrogen availability has been observed both in manipulative experiments and across environmental gradients (Field and Mooney 1986; Evans 1989; Walker et al. 2014; Li et al. 2020), and is thought to be driven by ecosystem nitrogen limitation, which limits its primary productivity globally (LeBauer and Treseder 2008; Fay et al. 2015). However, this response is not consistently observed, as recent studies note variable N_{area} -photosynthesis relationships across soil nitrogen availability gradients (Liang et al. 2020; Luo et al. 2021) and that aboveground growing conditions (e.g., light availability, temperature, vapor pressure deficit) or species identity traits (e.g., photosynthetic pathway, nitrogen acquisition strategy) may be more important for explaining variance in N_{area} and photosynthetic capacity across time and space (Adams et al. 2016; Dong et al. 2017; Dong et al. 2020; Dong et al. 2022; Smith et al. 2019; Peng et al. 2021; Westerband et al. 2023).

1010 4.2 Methods

1011 4.2.1 textit{Site descriptions and sampling methodology}

1012 We collected leaf and soil samples from 24 open grassland sites across cen-
1013 tral and eastern Texas in summer 2020 and summer 2021 (Fig. 4.1). Twelve
1014 sites were visited between June and July 2020 and 14 sites (11 unique from 2020)
1015 were visited between May and June 2021 (Table 1). We explicitly chose sites
1016 that maximized variability in precipitation and edaphic variability between sites
1017 while minimizing temperature variability across the environmental gradient (Ta-
1018 ble 1). No site with personally communicated or anecdotal evidence of grazing
1019 or disturbance (e.g., mowing, feral hog activity, etc.) were used. We collected
1020 leaf material from three individuals each of the five most abundant species at ran-
1021 dom locations at each site, only selecting species that were broadly classified as
1022 graminoid, forb/herb, shrub, or subshrub growth habits per the USDA PLANTS
1023 database (USDA NRCS 2022). All collected leaves were fully expanded with no
1024 visible herbivory or other external damage and also free from shading by nearby
1025 shrubs or trees. Five soil samples were collected from 0-15cm below the soil sur-
1026 face at each site near the leaf collection sample locations. Soil samples were later
1027 mixed together by hand to create one composite soil sample per site.

1028 4.2.2 Leaf trait measurements

1029 Images of each leaf were taken immediately following each site visit using
1030 a flat-bed scanner. Fresh leaf area was determined from each image using the
1031 'LeafArea' R package (Katabuchi 2015), which automates leaf area calculations
1032 using ImageJ software (Schneider et al. 2012). Each leaf was dried at 65°C for at

1033 least 48 hours to a constant mass, weighed, and manually ground in a mortar and
1034 pestle until homogenized. Leaf mass per area (M_{area} ; g m⁻²) was calculated as the
1035 ratio of dry leaf biomass to fresh leaf area. Subsamples of dried and homogenized
1036 leaf tissue were used to measure leaf nitrogen content (N_{mass} ; gN g⁻¹) through el-
1037 emental combustion analysis (Costech-4010, Costech Instruments, Valencia, CA).
1038 Leaf nitrogen content per unit leaf area (N_{area} ; gN m⁻²) was then calculated as
1039 the product of N_{mass} and M_{area} .

1040 Subsamples of dried and homogenized leaf tissue were sent to the University
1041 of California-Davis Stable Isotope Facility to determine leaf $\delta^{13}\text{C}$. Leaf $\delta^{13}\text{C}$ values
1042 were determined using an elemental analyzer (PDZ Europa ANCA-GSL; Sercon
1043 Ltd., Chestshire, UK) interfaced to an isotope ratio mass spectrometer (PDZ
1044 Europa 20-20 Isotope Ratio Mass Spectrometer, Sercon Ltd., Chestshire, UK).
1045 We used leaf $\delta^{13}\text{C}$ values (‰; relative to Vienna Pee Dee Belemnite international
1046 reference standard) to estimate the ratio of intercellular (C_i) to extracellular (C_a)
1047 CO₂ ratio (leaf $C_i:C_a$, χ ; unitless) following the approach of Farquhar et al. (1989)
1048 described in Cernusak et al. (2013). We derived χ as:

$$\chi = \frac{C_i}{C_a} = \frac{\Delta^{13}\text{C} - a}{b - a} \quad (4.1)$$

1049 where $\Delta^{13}\text{C}$ represents the relative difference between leaf $\delta^{13}\text{C}$ (‰) and air $\delta^{13}\text{C}$
1050 (‰), and is calculated as:

$$\Delta^{13}\text{C} = \frac{\delta^{13}\text{C}_{\text{air}} - \delta^{13}\text{C}_{\text{leaf}}}{1 + \delta^{13}\text{C}_{\text{leaf}}} \quad (4.2)$$

1051 $\delta^{13}\text{C}_{\text{air}}$, traditionally assumed to be -8‰ (Keeling et al. 1979; Farquhar et al.

1052 1989), was calculated as a function of calendar year t using an empirical equation
1053 derived in Feng (1999):

$$\delta^{13}C_{air} = -6.429 - 0.006e^{0.0217(t-1740)} \quad (4.3)$$

1054 This calculation resulted in $\delta^{13}C_{air}$ values for 2020 and 2021 as -9.04 and -9.09,
1055 respectively. a represents the fractionation between ^{12}C and ^{13}C due to diffusion
1056 in air, assumed to be 4.4‰, and b represents the fractionation caused by Rubisco
1057 carboxylation, assumed to be 27‰ (Farquhar et al. 1989). For C_4 species, b in
1058 Eqn. 4.1 was set to 6.3‰, and was derived from:

$$b = c + (d \cdot \phi) \quad (4.4)$$

1059 Where c was set to -5.7‰ and d was set to 30‰ (Farquhar et al. 1989). ϕ , which
1060 is the bundle sheath leakiness term, was set to 0.4. All χ values less than 0.2 and
1061 greater than 1.0 were assumed to be incorrect and removed.

1062 We derived the unit cost of resource use (β) using leaf χ and site climate
1063 data with equations first described in Prentice et al. (2014) and simplified in
1064 Lavergne et al. (2020):

$$\beta = 1.6\eta^* D \frac{\chi - (\frac{\Gamma^*}{C_a})^2}{(1 - \chi)^2(K_m + \Gamma^*)} \quad (4.5)$$

1065 where η^* is the viscosity of water relative to 25°C, calculated using elevation
1066 and mean air temperature of the seven days leading up to each site visit following
1067 equations in Huber et al. (2009). D represents vapor pressure deficit (Pa), set

1068 to the mean vapor pressure deficit of the seven days leading up to each site visit,
1069 C_a represents atmospheric CO₂ concentration, arbitrarily set to 420 $\mu\text{mol mol}^{-1}$
1070 CO₂. K_m (Pa) is the Michaelis-Menten coefficient for Rubisco affinity to CO₂ and
1071 O₂, calculated as:

$$K_m = K_c \cdot \left(1 + \frac{O_i}{K_o}\right) \quad (4.6)$$

1072 where K_c (Pa) and K_o (Pa) are the Michaelis-Menten coefficients for Rubisco
1073 affinity to CO₂ and O₂, respectively, and O_i is the intercellular O₂ concentration.
1074 Γ^* (Pa) is the CO₂ compensation point in the absence of dark respiration. K_c , K_o ,
1075 and Γ^* were determined using equations described in Medlyn et al. (2002) and
1076 derived in Bernacchi et al. (2001), invoking an elevation correction for atmospheric
1077 pressure as explained in Stocker et al. (2020).

1078

placeholder for Table 1

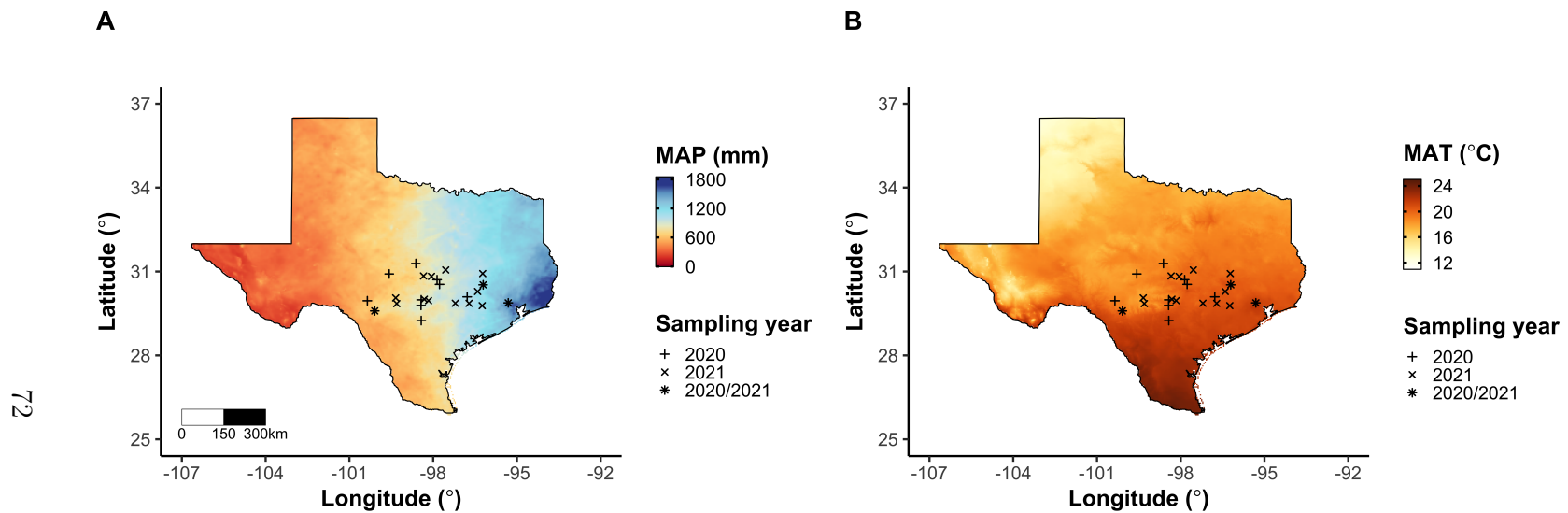


Figure 4.1. Maps that detail site locations along 2006-2020 mean annual precipitation (panel A) and mean annual temperature (panel B) gradients in Texas, USA. Precipitation and temperature data were plotted at a 4-km grid resolution and are masked to include only grid cells that occur in the Texas state boundary in the United States. In both panels, open circles refer to sites visited in 2020, open triangles to sites visited in 2021, and closed circles to sites visited in 2020 and 2021. The scale bar in panel A also applies to panel B.

1079 4.3 Results

1080 4.4 Discussion

1081

Chapter 5

1082 **1083**

Optimal resource investment to photosynthetic capacity maximizes
nutrient allocation to whole plant growth under elevated CO₂

1084 5.1 Introduction

1085 Terrestrial ecosystems are regulated by complex carbon and nitrogen cy-
1086 cles. As a result, terrestrial biosphere models, which are beginning to include
1087 coupled carbon and nitrogen cycles (Shi et al. 2016; Davies-Barnard et al. 2020;
1088 Braghieri et al. 2022), must accurately represent these cycles under different
1089 environmental scenarios to reliably simulate carbon and nitrogen atmosphere-
1090 biosphere fluxes (Hungate et al. 2003; Prentice et al. 2015). While the inclusion
1091 of coupled carbon and nitrogen cycles tends to reduce model uncertainty (Arora
1092 et al. 2020), large uncertainty in role of soil nitrogen availability and nitrogen ac-
1093 quisition strategy on leaf and whole plant acclimation responses to CO₂ remains
1094 (Smith and Dukes 2013; Terrer et al. 2018; Smith and Keenan 2020). This source
1095 of uncertainty likely contributes to the widespread divergence in future carbon
1096 and nitrogen flux simulations across terrestrial biosphere models (Friedlingstein
1097 et al. 2014; Zaehle et al. 2014; Meyerholt et al. 2020).

1098 Plants grown under elevated CO₂ generally have less leaf nitrogen content
1099 than those grown under ambient CO₂, a response that often corresponds with
1100 reductions in photosynthetic capacity and stomatal conductance at the leaf-level
1101 and biomass stimulation over time at the whole plant level (Curtis 1996; Drake
1102 et al. 1997; Ainsworth et al. 2002; Makino 2003; Morgan et al. 2004; Ainsworth
1103 and Long 2005; Ainsworth and Rogers 2007; Smith and Dukes 2013; Poorter et al.
1104 2022). As net primary productivity is generally limited by nitrogen availability

1105 (Vitousek and Howarth 1991; LeBauer and Treseder 2008; Fay et al. 2015), and
1106 soil nitrogen availability is often positively correlated with leaf nitrogen content
1107 and photosynthetic capacity (Field and Mooney 1986; Evans and Seemann 1989;
1108 Evans 1989; Walker et al. 2014; Firn et al. 2019; Liang et al. 2020), some
1109 have hypothesized that leaf and whole plant acclimation responses to CO₂ are
1110 constrained by soil nitrogen availability. The progressive nitrogen limitation hy-
1111 pothesis predicts that elevated CO₂ will increase plant nitrogen demand, which
1112 will increase plant nitrogen uptake and progressively deplete soil nitrogen if soil
1113 nitrogen supply does not exceed plant nitrogen demand (Luo et al. 2004). The
1114 hypothesis predicts that this response should result in strong acute stimulations in
1115 whole plant growth and primary productivity that diminish over time as nitrogen
1116 becomes more limiting. Assuming a positive relationship between soil nitrogen
1117 availability, leaf nitrogen content, and photosynthetic capacity, this hypothesis
1118 also implies that progressive reductions in soil nitrogen availability should be the
1119 mechanism that drives the downregulation in leaf nitrogen content and photosyn-
1120 thetic capacity under elevated CO₂. This hypothesis has received some support
1121 from free air CO₂ enrichment experiments (Reich et al. 2006; Norby et al. 2010),
1122 although is not consistently observed across experiments (Finzi et al. 2006; Moore
1123 et al. 2006; Liang et al. 2016).

1124 While possible that progressive nitrogen limitation may determine leaf and
1125 whole plant acclimation responses to CO₂, growing evidence indicates that leaf ni-
1126 trogen and photosynthetic capacity are more strongly determined through above-
1127 ground growing conditions than by soil resource availability (Dong et al. 2017;
1128 Dong et al. 2020; Dong et al. 2022; Smith et al. 2019; Smith and Keenan 2020;

1129 Paillassa et al. 2020; Peng et al. 2021; Querejeta et al. 2022; Westerband et al.
1130 2023), and satellite-derived chlorophyll fluorescence data indicate that increasing
1131 atmospheric CO₂ may decrease leaf and canopy demand for nitrogen (Dong et al.
1132 2022). Together, results from these studies suggest that the downregulation in
1133 leaf nitrogen content and photosynthetic capacity due to increasing CO₂ may not
1134 be as tightly linked to progressive nitrogen limitation as previously hypothesized.

1135 A unification of optimal coordination and photosynthetic least-cost the-
1136 ories predicts that leaves acclimate to elevated CO₂ by downregulating nitrogen
1137 allocation to Ribulose-1,5-bisphosphate (RuBP) carboxylase/oxygenase (Rubisco)
1138 to optimize resource use efficiencies at the leaf level, which allows for greater re-
1139 source allocation to whole plant growth (Drake et al. 1997; Wright et al. 2003;
1140 Prentice et al. 2014; Smith et al. 2019). The theory predicts that the downregu-
1141 lation in nitrogen allocation to Rubisco results in a stronger downregulation in the
1142 maximum rate of Rubisco carboxylation (V_{cmax}) than the maximum rate of RuBP
1143 regeneration (J_{max}), which maximizes photosynthetic efficiency by allowing net
1144 photosynthesis rates to be equally co-limited by Rubisco carboxylation and RuBP
1145 regeneration (Chen et al. 1993; Maire et al. 2012). This acclimation response
1146 allows plants to make more efficient use of available light while avoiding overin-
1147 vestment in Rubisco, which has high nitrogen and energetic costs of building and
1148 maintaining (Evans 1989; Evans and Clarke 2019). Instead, additional acquired
1149 resources not needed to optimize leaf photosynthesis are allocated to the mainte-
1150 nance of structures that support whole plant growth (e.g., total leaf area, whole
1151 plant biomass, etc.) or to allocation processes not related to leaf photosynthesis
1152 or growth, such as plant defense mechanisms or leaf structural tissue. Regardless,

1153 optimized resource allocation at the leaf level should allow for greater resource
1154 allocation to whole plant growth. The theory indicates that leaf acclimation re-
1155 sponses to CO₂ should be independent of changes in soil nitrogen availability.
1156 While this leaf acclimation response maximizes nitrogen allocation to structures
1157 that support whole plant growth, the theory suggests that the positive effect of
1158 elevated CO₂ on whole plant growth may be further stimulated by soil nitrogen
1159 availability through a reduction in the cost of acquiring nitrogen (Bae et al. 2015;
1160 Perkowski et al. 2021; Lu et al. 2022).

1161 Plants acquire nitrogen by allocating photosynthetically derived carbon be-
1162 lowground in exchange for nitrogen through different nitrogen acquisition strate-
1163 gies. These nitrogen acquisition strategies can include direct uptake pathways
1164 such as mass flow or diffusion (Barber 1962), symbioses with mycorrhizal fungi or
1165 symbiotic nitrogen-fixing bacteria (Vance and Heichel 1991; Marschner and Dell
1166 1994; Smith and Read 2008; Udvardi and Poole 2013), or through the release
1167 of root exudates that prime free-living soil microbial communities (Phillips et al.
1168 2011; Wen et al. 2022). Plants cannot acquire nitrogen without first allocating
1169 carbon belowground, which implies an inherent carbon cost to the plant for acquir-
1170 ing nitrogen regardless of nitrogen acquisition strategy. Carbon costs to acquire
1171 nitrogen often vary in species with different nitrogen acquisition strategies and
1172 are dependent on external environmental factors such as atmospheric CO₂, light
1173 availability, and soil nitrogen availability (Brzostek et al. 2014; Terrer et al. 2016;
1174 Terrer et al. 2018; Allen et al. 2020; Perkowski et al. 2021; Lu et al. 2022), which
1175 suggests that acquisition strategy may be an important factor in determining ef-
1176 fects of soil nitrogen availability on leaf and whole plant acclimation responses to

1177 elevated CO₂.

1178 A recent meta-analysis using data across 20 grassland and forest CO₂ en-
1179 richment experiments suggested that species which acquire nitrogen from sym-
1180 biotic nitrogen-fixing bacteria had reduced costs of nitrogen acquisition under
1181 elevated CO₂ (Terrer et al. 2018). Findings from this meta-analysis indicated
1182 that reductions in costs of nitrogen acquisition in species that form associations
1183 with symbiotic nitrogen-fixing bacteria under elevated CO₂ may drive stronger
1184 stimulations in whole plant growth and downregulations in V_{cmax} than species that
1185 associate with arbuscular mycorrhizal fungi (Smith and Keenan 2020), which gen-
1186 erally have higher costs of nitrogen acquisition under elevated CO₂ (Terrer et al.
1187 2018). However, plant investments in symbiotic nitrogen fixation generally de-
1188 cline with increasing nitrogen availability (Dovrat et al. 2018; Perkowski et al.
1189 2021), a response that has been previously inferred to be the result of a shift in
1190 the dominant mode of nitrogen acquisition to direct uptake pathways as costs of
1191 direct uptake decrease with increasing soil nitrogen availability (Rastetter et al.
1192 2001; Perkowski et al. 2021). Thus, effects of symbiotic nitrogen fixation on plant
1193 acclimation responses to CO₂ should decline with increasing soil nitrogen avail-
1194 ability, although manipulative experiments that directly test these patterns are
1195 rare.

1196 Here, we conducted a 7-week growth chamber experiment using *Glycine*
1197 *max* L. (Merr.) to examine the effects of soil nitrogen fertilization and inocula-
1198 tion with symbiotic nitrogen-fixing bacteria on leaf and whole plant acclimation
1199 responses to elevated CO₂. Following patterns expected from theory, we hypoth-
1200 esized that individual leaves should acclimate to elevated CO₂ by more strongly

1201 downregulating V_{cmax} relative to J_{max} , allowing leaf photosynthesis to approach
1202 optimal coordination. We expected this response to correspond with a stronger
1203 downregulation in leaf nitrogen content than V_{cmax} and J_{max} , which would in-
1204 crease the fraction of leaf nitrogen content allocated to photosynthesis and photo-
1205 synthetic nitrogen use efficiency. At the whole-plant level, we hypothesized that
1206 plants would acclimate to elevated CO₂ by stimulating whole plant growth and
1207 productivity, a response that would be driven by a strong positive response of
1208 total leaf area and aboveground biomass to elevated CO₂. We predicted that
1209 leaf acclimation responses to elevated CO₂ would be independent of soil nitro-
1210 gen fertilization and inoculation with symbiotic nitrogen-fixing bacteria; however,
1211 we expected that increasing soil nitrogen fertilization would increase the posi-
1212 tive effect of elevated CO₂ on measures of whole plant growth due to a stronger
1213 reduction in the cost of acquiring nitrogen under elevated CO₂ with increasing
1214 fertilization. We also expected stronger stimulations in whole plant growth due
1215 to inoculation, but that this effect would only be apparent under low fertilization
1216 due to a reduction in root nodulation with increasing fertilization.

1217 5.2 Methods

1218 5.2.1 *Seed treatments and experimental design*

1219 *Glycine max* L. (Merr) seeds were planted in 144 6-liter surface sterilized
1220 pots (NS-600, Nursery Supplies, Orange, CA, USA) containing a steam-sterilized
1221 70:30 v:v mix of Sphagnum peat moss (Premier Horticulture, Quakertown, PA,
1222 USA) to sand (Pavestone, subsidiary of Quikrete Companies, Atlanta, GA, USA).
1223 Before planting, all *G. max* seeds were surface sterilized in 2% sodium hypochlorite

1224 for 3 minutes, followed by three separate 3-minute washes with ultrapure water
1225 (MilliQ 7000; MilliporeSigma, Burlington, MA USA). A subset of surface steril-
1226 ized seeds were inoculated with *Bradyrhizobium japonicum* (Verdesian N-Dure™
1227 Soybean, Cary, NC, USA) in a slurry following manufacturer recommendations
1228 (3.12 g inoculant and 241 g deionized water per 1 kg seed).

1229 Seventy-two pots were randomly planted with surface-sterilized seeds inoc-
1230 ulated with *B. japonicum*, while the remaining 72 pots were planted with surface-
1231 sterilized uninoculated seeds. Thirty-six pots within each inoculation treatment
1232 were randomly placed in one of two atmospheric CO₂ treatments (ambient and
1233 1000 μmol mol⁻¹ CO₂). Pots within each unique inoculation-by-CO₂ treatment
1234 combination randomly received one of nine soil nitrogen fertilization treatments
1235 equivalent to 0, 35, 70, 105, 140, 210, 280, 350, or 630 ppm N. Nitrogen fertil-
1236 ization treatments were created using a modified Hoagland solution (Hoagland
1237 and Arnon 1950) designed to keep concentrations of other macronutrients and
1238 micronutrients equivalent across treatments (Table S1). Pots received the same
1239 fertilization treatment throughout the entire duration experiment, which were ap-
1240 plied twice per week in 150 mL doses as topical agents to the soil surface through-
1241 out the duration of the experiment. This experimental design yielded a fully
1242 factorial experiment with four replicates per unique fertilization-by-inoculation-
1243 by-CO₂ combination.

1244 5.2.2 *Growth chamber conditions*

1245 Upon experiment initiation, pots were randomly placed in one of six Per-
1246 cival LED-41L2 growth chambers (Percival Scientific Inc., Perry, IA, USA) over

1247 two experimental iterations due to chamber space limitation. two iterations were
1248 conducted such that one iteration included all elevated CO₂ pots and the second
1249 iteration included all ambient CO₂ pots. Average (\pm SD) CO₂ concentrations
1250 across chambers throughout the experiment were $439 \pm 5 \mu\text{mol mol}^{-1}$ for the
1251 ambient CO₂ treatment and $989 \pm 4 \mu\text{mol mol}^{-1}$ for the elevated CO₂ treatment.

1252 Daytime growing conditions were simulated using a 16-hour photoperiod,
1253 with incoming light radiation set to chamber maximum (mean \pm SD: 1240 ± 32
1254 $\mu\text{mol m}^{-2} \text{s}^{-1}$ across chambers), air temperature set to 25°C, and relative humid-
1255 ity set to 50%. The remaining 8 hours simulated nighttime growing conditions,
1256 with incoming light radiation set to 0 $\mu\text{mol m}^{-2} \text{s}^{-1}$, chamber temperature set
1257 to 17°C, and relative humidity set to 50%. Transitions between daytime and
1258 nighttime growing conditions were simulated by ramping incoming light radiation
1259 in 45-minute increments and temperature in 90-minute increments over a 3-hour
1260 period (Table S2).

1261 Including the two, 3-hour ramping periods, pots grew under average (\pm
1262 SD) daytime light intensity of $1049 \pm 27 \mu\text{mol m}^{-2} \text{s}^{-1}$. In the elevated CO₂
1263 iteration, pots grew under $24.0 \pm 0.2^\circ\text{C}$ during the day, $16.4 \pm 0.8^\circ\text{C}$ during the
1264 night, and $51.6 \pm 0.4\%$ relative humidity. In the ambient CO₂ iteration, pots grew
1265 under $23.9 \pm 0.2^\circ\text{C}$ during the day, $16.0 \pm 1.4^\circ\text{C}$ during the night, and $50.3 \pm 0.2\%$
1266 relative humidity. We accounted for climatic differences across the six chambers
1267 by shuffling the same group of pots daily throughout the growth chambers. This
1268 process was done by iteratively moving the group of pots on the top rack of a
1269 chamber to the bottom rack of the same chamber, while simultaneously moving
1270 the group of pots on the bottom rack of a chamber to the top rack of the adjacent

1271 chamber. We moved pots within and across chambers every day throughout the
1272 course of each experiment iteration.

1273 5.2.3 *Leaf gas exchange measurements*

1274 Gas exchange measurements were collected for all individuals on the sev-
1275 enth week of development. All gas exchange measurements were collected on
1276 the center leaf of the most recent fully expanded trifoliate leaf set. Specifi-
1277 cally, we measured net photosynthesis (A_{net} ; $\mu\text{mol m}^{-2} \text{s}^{-1}$), stomatal conduc-
1278 tance (g_{sw} ; $\text{mol m}^{-2} \text{s}^{-1}$), and intercellular CO_2 (C_i ; $\mu\text{mol mol}^{-1}$) concentrations
1279 across a range of atmospheric CO_2 concentrations (i.e., an A_{net}/C_i curve) using the
1280 Dynamic Assimilation Technique™. The Dynamic Assimilation Technique™ has
1281 been shown to correspond well with traditional steady-state CO_2 response curves
1282 in *G. max* (Saathoff and Welles 2021). A_{net}/C_i curves were generated along a
1283 reference CO_2 ramp down from $420 \mu\text{mol mol}^{-1} \text{CO}_2$ to $20 \mu\text{mol mol}^{-1} \text{CO}_2$, fol-
1284 lowed by a ramp up from $420 \mu\text{mol mol}^{-1} \text{CO}_2$ to $1620 \mu\text{mol mol}^{-1} \text{CO}_2$ after
1285 a 90-second wait period at $420 \mu\text{mol mol}^{-1} \text{CO}_2$. The ramp rate for each curve
1286 was set to $200 \mu\text{mol mol}^{-1} \text{min}^{-1}$, logging every five seconds, which generated 96
1287 data points per response curve. All A_{net}/C_i curves were generated after A_{net} and
1288 g_{sw} stabilized in a LI-6800 cuvette set to a 500 mol s^{-1} , 10,000 rpm mixing fan
1289 speed, 1.5 kPa vapor pressure deficit, 25°C leaf temperature, $2000 \mu\text{mol m}^{-2} \text{s}^{-1}$
1290 incoming light radiation, and initial reference CO_2 set to $420 \mu\text{mol mol}^{-1}$.

1291 With the same focal leaf used to generate A_{net}/C_i curves, we measured
1292 dark respiration (R_{d25} ; $\mu\text{mol m}^{-2} \text{s}^{-1}$) following at least a 30-minute period of
1293 darkness. Measurements were collected on a 5-second log interval for 60 seconds

1294 after stabilizing in a LI-6800 cuvette set to a 500 mol s^{-1} , 10,000 rpm mixing fan
1295 speed, 1.5 kPa vapor pressure deficit, 25°C leaf temperature, and $420 \mu\text{mol mol}^{-1}$
1296 reference CO_2 concentration (for both CO_2 concentrations), with incoming light
1297 radiation set to $0 \mu\text{mol m}^{-2} \text{ s}^{-1}$. A single dark respiration value was determined
1298 for each focal leaf by calculating the mean dark respiration value (i.e. the absolute
1299 value of A_{net} during the logging period) across the logging interval.

1300 5.2.4 *Leaf trait measurements*

1301 The focal leaf used to generate A_{net}/C_i curves and dark respiration was
1302 harvested immediately following gas exchange measurements. Images of each focal
1303 leaf were curated using a flat-bed scanner to determine wet leaf area using the
1304 'LeafArea' R package (Katabuchi 2015), which automates leaf area calculations
1305 using ImageJ software (Schneider et al. 2012). Each leaf was dried at 65°C for
1306 at least 48 hours, and subsequently weighed and ground until homogenized. Leaf
1307 mass per area (M_{area} ; g m^{-2}) was calculated as the ratio of dry leaf biomass
1308 to fresh leaf area. Using subsamples of ground and homogenized leaf tissue, we
1309 measured leaf nitrogen content (N_{mass} ; gN g^{-1}) through elemental combustion
1310 analysis (Costech-4010, Costech, Inc., Valencia, CA, USA). Leaf nitrogen content
1311 per unit leaf area (N_{area} ; gN m^{-2}) was calculated by multiplying N_{mass} and M_{area} .

1312 We extracted chlorophyll content from a second leaf in the same trifoliolate
1313 leaf set as the focal leaf used to generate A_{net}/C_i curves. Prior to chlorophyll
1314 extraction, we used a cork borer to punch between 3 and 5 0.6 cm^2 disks from
1315 the leaf. Separate images of each punched leaf and set of leaf disks were curated
1316 using a flat-bed scanner to determine wet leaf area, again quantified using the

1317 'LeafArea' R package (Katabuchi 2015). The punched leaf was dried and weighed
1318 after at least 65°C in the drying oven to determine Marea of the chlorophyll leaf.

1319 Leaf disks were shuttled into a test tube containing 10mL dimethyl sul-
1320 foxide, vortexed, and incubated at 65degreeC for 120 minutes (Barnes et al.
1321 1992). Incubated test tubes were vortexed again before loaded in 150 μ L trip-
1322 licate aliquots to a 96-well plate. Dimethyl sulfoxide was also loaded in a 150
1323 μ L triplicate aliquot as a blank. Absorbance measurements at 649.1 nm ($A_{649.1}$)
1324 and 665.1 nm ($A_{665.1}$) were read in each well using a plate reader (Biotek Synergy
1325 H1; Biotek Instruments, Winooski, VT USA) (Wellburn 1994), with triplicates
1326 subsequently averaged and corrected by the mean of the blank absorbance value.
1327 Blank-corrected absorbance values were used to estimate Chl_a (μ g mL $^{-1}$) and
1328 Chl_b (μ g mL $^{-1}$) following equations from Wellburn (1994):

$$Chl_a = 12.47A_{665.1} - 3.62A_{649.1} \quad (5.1)$$

1329 and

$$Chl_b = 25.06A_{665.1} - 6.50A_{649.1} \quad (5.2)$$

1330 Chl_a and Chl_b were converted to mmol mL $^{-1}$ using the molar mass of chlorophyll a
1331 (893.51 g mol $^{-1}$) and the molar mass of chlorophyll b (907.47 g mol $^{-1}$), then added
1332 together to calculate total chlorophyll content in the dimethyl sulfoxide extractant
1333 (mmol mL $^{-1}$). Total chlorophyll content was multiplied by the volume of the
1334 dimethyl sulfoxide extractant (10 mL) and converted to area-based chlorophyll
1335 content by dividing by the total area of the leaf disks (Chl_{area} ; mmol m $^{-2}$). Mass-
1336 based chlorophyll content (Chl_{mass} ; mmol g $^{-1}$) was calculated by dividing Chl_{area}

1337 by the leaf mass per area of the punched leaf.

1338 5.2.5 *A/C_i curve fitting and parameter estimation*

1339 We fit A_{net}/C_i curves of each individual using the ‘fitaci’ function in the
1340 ‘plantecophys’ R package (Duursma 2015). This function estimates the maximum
1341 rate of Rubisco carboxylation V_{cmax} ; $\mu\text{mol m}^{-2} \text{s}^{-1}$) and maximum rate of electron
1342 transport for RuBP regeneration (J_{max} ; $\mu\text{mol m}^{-2} \text{s}^{-1}$) based on the Farquhar bio-
1343 chemical model of C₃ photosynthesis (Farquhar et al. 1980). Triose phosphate
1344 utilization (TPU) limitation was included in all curve fits, and all curve fits in-
1345 cluded measured dark respiration values. As A_{net}/C_i curves were generated using
1346 a common leaf temperature, curves were fit using Michaelis-Menton coefficients
1347 for Rubisco affinity to CO₂ (K_c ; $\mu\text{mol mol}^{-1}$) and O₂ (K_o ; $\mu\text{mol mol}^{-1}$), and the
1348 CO₂ compensation point (Γ^* ; $\mu\text{mol mol}^{-1}$) reported in Bernacchi et al. (2001).
1349 Specifically, K_c was set to 404.9 $\mu\text{mol mol}^{-1}$, K_o was set to 278.4 $\mu\text{mol mol}^{-1}$, and
1350 Γ^* was set to 42.75 $\mu\text{mol mol}^{-1}$. The use of a common leaf temperature across
1351 curves and dark respiration measurements also eliminated the need to manually
1352 temperature standardize rate estimates. For clarity, we reference V_{cmax} , J_{max} , and
1353 R_d estimates throughout the rest of the paper as $V_{\text{cmax}25}$, $J_{\text{max}25}$, and R_{d25} .

1354 5.2.6 Stomatal limitation

1355 We quantified the extent by which stomatal conductance limited photo-
1356 synthesis (l; unitless) following equations originally described in Farquhar and
1357 Sharkey (1982). Stomatal limitation was calculated as:

$$l = 1 - \frac{A_{net}}{A_{mod}} \quad (5.3)$$

1358 where A_{mod} represents the photosynthetic rate where $C_i = C_a$. A_{mod} was calcu-

1359 lated as:

$$A_{mod} = V_{cmax25} - \frac{420 - \Gamma^*}{420 + K_m} - R_{d25} \quad (5.4)$$

1360 K_m is the Michaelis-Menten coefficient for Rubisco-limited photosynthesis, calcu-

1361 lated as:

$$K_m = K_c \cdot \left(1 + \frac{O_i}{K_o}\right) \quad (5.5)$$

1362 where O_i refers to leaf intercellular O_2 concentrations, set to $210 \mu\text{mol mol}^{-1}$.

1363 5.2.7 *Proportion of leaf nitrogen allocated to photosynthesis and structure*

1364 We used equations from Niinemets and Tenhunen (1997) to estimate the

1365 proportion of leaf N content allocated to Rubisco bioenergetics, and light harvest-

1366 ing proteins. The proportion of leaf N allocated to Rubisco (ρ_{rub} ; gN gN^{-1}) was

1367 calculated as a function of V_{cmax25} and N_{area} :

$$\rho_{rubisco} = \frac{V_{cmax25} N_r}{V_{cr} N_{area}} \quad (5.6)$$

1368 where N_r is the amount of nitrogen in Rubisco, set to $0.16 \text{ gN (gN in Rubisco)}^{-1}$

1369 and V_{cr} is the maximum rate of RuBP carboxylation per unit Rubisco protein,

1370 set to $20.5 \mu\text{mol CO}_2 (\text{g Rubisco})^{-1}$. The proportion of leaf nitrogen allocated to

1371 bioenergetics (ρ_{bioe} ; gN gN^{-1}) was similarly calculated as a function of J_{max25} and

1372 N_{area} :

$$\rho_{\text{bioe}} = \frac{J_{\text{max}25} N_b}{J_{\text{mc}} N_{\text{area}}} \quad (5.7)$$

1373 where N_b is the amount of nitrogen in cytochrome f, set to 0.12407 gN (μmol cytochrome f) $^{-1}$ assuming a constant 1: 1: 1.2 cytochrome f: ferredoxin NADP reductase: coupling factor molar ratio (Evans and Seemann 1989; Niinemets and Tenhunen 1997), and J_{mc} is the capacity of electron transport per cytochrome f, set to 156 μmol electron (μmol cytochrome f) $^{-1}\text{s}^{-1}$.

1378 The proportion of leaf nitrogen allocated to light harvesting proteins was calculated as a function of Chl_{mass} and N_{mass} :

$$\rho_{\text{light}} = \frac{Chl_{\text{mass}}}{N_{\text{mass}} c_b} \quad (5.8)$$

1380 where c_b is the stoichiometry of the light-harvesting chlorophyll complexes of photosystem II, set to 2.75 mmol chlorophyll (gN in chlorophyll) $^{-1}$. We used the N_{mass} value of the focal leaf used to generate A_{net}/C_i curves instead of the leaf used to extract chlorophyll content, as the two leaves are from the same trifoliolate leaf set and are highly correlated with each other (Figure SX).

1385 The proportion of leaf nitrogen content allocated to photosynthetic tissue (ρ_{photo} ; gN gN $^{-1}$) was estimated as the sum of ρ_{rubisco} , ρ_{bioe} , and ρ_{light} .

1387 Finally, the proportion of leaf N content allocated to structural tissue (ρ_{str} ; gN gN $^{-1}$) was estimated as:

$$\rho_{\text{structure}} = \frac{N_{\text{cw}}}{N_{\text{area}}} \quad (5.9)$$

1389 where N_{cw} is the leaf N content allocated to cell walls (gN m^{-2}), calculated as a
1390 function of M_{area} using an empirical equation from Onoda et al. (2017):

$$N_{cw} = 0.000355 * M_{area}^{1.39} \quad (5.10)$$

1391 5.2.8 *Whole plant traits*

1392 Seven weeks after experiment initiation and immediately following gas ex-
1393 change measurements, we harvested all experimental individuals and separated
1394 biomass of each experimental individual into major organ types (leaves, stems,
1395 roots, and nodules when present). Fresh leaf area of all harvested leaves was mea-
1396 sured using an LI-3100C (Li-COR Biosciences, Lincoln, Nebraska, USA). Total
1397 fresh leaf area (cm^2) was calculated as the sum of all leaf areas, including the focal
1398 leaf used to collect gas exchange data and the focal leaf used to extract chlorophyll
1399 content. All harvested material was dried in an oven set to 65°C for at least 48
1400 hours, weighed, and ground to homogeneity. Leaves and nodules were manually
1401 ground either with a mortar and pestle, while stems and roots were ground using
1402 a Wiley mill (E3300 Mini Mill; Eberbach Corp., MI, USA). Total dry biomass (g)
1403 was calculated as the sum of dry leaf (including focal leaf for both the A_{net}/C_i
1404 curve and leaf used to extract chlorophyll content), stem, root, and root nodule
1405 biomass. We also quantified carbon and nitrogen content of each respective organ
1406 type through elemental combustion (Costech-4010, Costech, Inc., Valencia, CA,
1407 USA) using subsamples of ground and homogenized organ tissue.

1408 Following the approach explained in Perkowski et al. (2021), we calcu-
1409 lated structural carbon costs to acquire nitrogen as the ratio of total belowground

1410 carbon biomass to whole plant nitrogen biomass (N_{cost} ; gC gN⁻¹). Belowground
1411 carbon biomass (C_{bg} ; gC) was calculated as the sum of root carbon biomass
1412 and root nodule carbon biomass. Root carbon biomass and root nodule carbon
1413 biomass was calculated as the product of the organ biomass and the respective
1414 organ carbon content. Whole plant nitrogen biomass (N_{wp} ; gN) was similarly
1415 calculated as the sum of total leaf, stem, root, and root nodule nitrogen biomass,
1416 including the focal leaf used for A_{net}/C_i curve and chlorophyll extractions. Leaf,
1417 stem, root, and root nodule nitrogen biomass was calculated as the product of
1418 the organ biomass and the respective organ nitrogen content. This calculation
1419 only quantifies plant structural carbon costs to acquire nitrogen and does not
1420 include any additional costs of nitrogen acquisition associated with respiration,
1421 root exudation, or root turnover. An explicit explanation of the limitations for
1422 interpreting this calculation can be found in Perkowski et al. (2021) and Terrer
1423 et al. (2018).

1424 Finally, plant investments in nitrogen fixation were calculated as the ratio
1425 of root nodule biomass to root biomass, where increasing values indicate an in-
1426 crease in plant investments to nitrogen fixation (Dovrat et al. 2018; Dovrat et al.
1427 2020; Perkowski et al. 2021).

1428 5.2.9 *Statistical analyses*

1429 Any uninoculated pots that had substantial root nodule formation (nodule
1430 biomass: root biomass values greater than 0.05 g g⁻¹) were removed from our
1431 analyses. This was because they were assumed to have been colonized by symbiotic
1432 nitrogen-fixing bacteria from outside sources. This decision resulted in the removal

1433 of sixteen pots from our analysis: two pots in the elevated CO₂ treatment that
1434 received 35 ppm N, three pots in the elevated CO₂ treatment that received 70
1435 ppm N, one pot in the elevated CO₂ treatment that received 210 ppm N, two pots
1436 in the elevated CO₂ treatment that received 280 ppm N, two pots in the ambient
1437 CO₂ treatment that received 0 ppm N, three pots in the ambient CO₂ treatment
1438 that received 70 ppm N, two pots in the ambient CO₂ treatment that received
1439 105 ppm N, and one pot in the ambient CO₂ treatment that received 280 ppm N.

1440 We built a series of linear mixed effects models to investigate the impacts of
1441 CO₂ concentration, soil nitrogen fertilization, and inoculation with *B. japonicum*
1442 on *G. max* gas exchange, tradeoffs between nitrogen and water use, whole plant
1443 growth, and investment in nitrogen fixation. All models included CO₂ treatment
1444 as a categorical fixed effect, inoculation treatment as a categorical fixed effect,
1445 soil nitrogen fertilization as a continuous fixed effect, with interaction terms be-
1446 tween all three fixed effects. All models also accounted for climatic difference
1447 between chambers across experiment iterations by including a random intercept
1448 term that nested starting chamber rack by CO₂ treatment. Models with this
1449 independent variable structure were created for each of the following dependent
1450 variables: N_{area} , M_{area} , N_{mass} , Chl_{area} , V_{cmax25} , J_{max25} , $J_{\text{max25}}:V_{\text{cmax25}}$, R_{d25} , g_{sw} ,
1451 stomatal limitation, ρ_{rubisco} , ρ_{bioe} , ρ_{light} , ρ_{photo} , $\rho_{\text{structure}}$, N_{cost} , C_{bg} , N_{wp} , total
1452 biomass, total leaf area, nodule biomass, and the ratio of nodule biomass to root
1453 biomass.

1454 We used Shapiro-Wilk tests of normality to determine whether linear mixed
1455 effects models satisfied residual normality assumptions. If residual normality as-
1456 sumptions were not met (Shapiro-Wilk: $p < 0.05$), then models were fit using

1457 dependent variables that were natural log transformed. All residual normality
1458 assumptions that did not originally satisfy residual normality assumptions were
1459 met with either a natural log or square root data transformation (Shapiro-Wilk:
1460 $p > 0.05$ in all cases). Specifically, models for N_{area} , N_{mass} , Chl_{area} , V_{cmax25} ,
1461 J_{max25} , $J_{\text{max25}}:V_{\text{cmax25}}$, g_{sw} , stomatal limitation, ρ_{rubisco} , ρ_{bioe} , ρ_{light} , ρ_{photo} , and to-
1462 tal leaf area satisfied residual normality assumptions without data transformation.
1463 Models for M_{area} , $\rho_{\text{structure}}$, N_{cost} , C_{bg} , N_{wp} , and total biomass satisfied residual
1464 normality assumptions with a natural log data transformation, while models for
1465 nodule biomass and nodule biomass: root biomass satisfied residual normality
1466 assumptions with a square root data transformation.

1467 In all statistical models, we used the 'lmer' function in the 'lme4' R package
1468 (Bates et al. 2015) to fit each model and the 'Anova' function in the 'car' R
1469 package (Fox and Weisberg 2019) to calculate Type II Wald's χ^2 and determine the
1470 significance ($\alpha = 0.05$) of each fixed effect coefficient. We then used the 'emmeans'
1471 R package (Lenth 2019) to conduct post-hoc comparisons using Tukey's tests,
1472 where degrees of freedom were approximated using the Kenward-Roger approach
1473 (Kenward and Roger 1997). All analyses and plots were conducted in R version
1474 4.2.0 (R Core Team 2021).

1475 5.3 Results

1476 5.4 Discussion

1477

Chapter 6

1478

Conclusions

1479

References

- 1480 Abrams, M. D. and S. A. Mostoller (1995). Gas exchange, leaf structure and
1481 nitrogen in contrasting successional tree species growing in open and under-
1482 story sites during a drought. *Tree Physiology* 15(6), 361–370.
- 1483 Adams, M. A., T. L. Turnbull, J. I. Sprent, and N. Buchmann (2016). Legumes
1484 are different: Leaf nitrogen, photosynthesis, and water use efficiency. *Pro-
1485 ceedings of the National Academy of Sciences of the United States of Amer-
1486 ica* 113(15), 4098–4103.
- 1487 Ainsworth, E. A., P. A. Davey, C. J. Bernacchi, O. C. Dermody, E. A. Heaton,
1488 D. J. Moore, P. B. Morgan, S. L. Naidu, H. S. Y. Ra, X. G. Zhu, P. S. Curtis,
1489 and S. P. Long (2002). A meta-analysis of elevated [CO₂] effects on soybean
1490 (*Glycine max*) physiology, growth and yield. *Global Change Biology* 8(8),
1491 695–709.
- 1492 Ainsworth, E. A. and S. P. Long (2005). What have we learned from 15 years of
1493 free-air CO₂ enrichment (FACE)? A meta-analytic review of the responses
1494 of photosynthesis, canopy properties and plant production to rising CO₂.
1495 *New Phytologist* 165(2), 351–372.
- 1496 Ainsworth, E. A. and A. Rogers (2007). The response of photosynthesis and
1497 stomatal conductance to rising [CO₂]: mechanisms and environmental in-
1498 teractions. *Plant, Cell and Environment* 30(3), 258–270.
- 1499 Allen, K., J. B. Fisher, R. P. Phillips, J. S. Powers, and E. R. Brzostek (2020).
1500 Modeling the carbon cost of plant nitrogen and phosphorus uptake across
1501 temperate and tropical forests. *Frontiers in Forests and Global Change* 3,

- 1502 1–12.
- 1503 Allison, S. D., C. I. Czimczik, and K. K. Treseder (2008). Microbial activity
1504 and soil respiration under nitrogen addition in Alaskan boreal forest. *Global
1505 Change Biology* 14(5), 1156–1168.
- 1506 Andersen, M. K., H. Hauggaard-Nielsen, P. Ambus, and E. S. Jensen (2005).
1507 Biomass production, symbiotic nitrogen fixation and inorganic N use in dual
1508 and tri-component annual intercrops. *Plant and Soil* 266(1-2), 273–287.
- 1509 Arndal, M. F., A. Tolver, K. S. Larsen, C. Beier, and I. K. Schmidt (2018). Fine
1510 root growth and vertical distribution in response to elevated CO₂, warming
1511 and drought in a mixed heathland–grassland. *Ecosystems* 21(1), 15–30.
- 1512 Arnone, J. A. (1997). Indices of plant N availability in an alpine grassland under
1513 elevated atmospheric CO₂. *Plant and Soil* 190(1), 61–66.
- 1514 Arora, V. K., A. Katavouta, R. G. Williams, C. D. Jones, V. Brovkin,
1515 P. Friedlingstein, J. Schwinger, L. Bopp, O. Boucher, P. Cadule, M. A.
1516 Chamberlain, J. R. Christian, C. Delire, R. A. Fisher, T. Hajima, T. Ilyina,
1517 E. Joetzjer, M. Kawamiya, C. D. Koven, J. P. Krasting, R. M. Law, D. M.
1518 Lawrence, A. Lenton, K. Lindsay, J. Pongratz, T. Raddatz, R. Séférian,
1519 K. Tachiiri, J. F. Tjiputra, A. Wiltshire, T. Wu, and T. Ziehn (2020).
1520 Carbon-concentration and carbon-climate feedbacks in CMIP6 models and
1521 their comparison to CMIP5 models. *Biogeosciences* 17(16), 4173–4222.
- 1522 Bae, K., T. J. Fahey, R. D. Yanai, and M. Fisk (2015). Soil nitrogen availabil-
1523 ity affects belowground carbon allocation and soil respiration in northern
1524 hardwood forests of New Hampshire. *Ecosystems* 18(7), 1179–1191.

- 1525 Barber, S. A. (1962). A diffusion and mass-flow concept of soil nutrient avail-
1526 ability. *Soil Science* 93(1), 39–49.
- 1527 Barnes, J. D., L. Balaguer, E. Manrique, S. Elvira, and A. W. Davison (1992).
1528 A reappraisal of the use of DMSO for the extraction and determination
1529 of chlorophylls a and b in lichens and higher plants. *Environmental and
1530 Experimental Botany* 32(2), 85–100.
- 1531 Bates, D., M. Mächler, B. Bolker, and S. Walker (2015). Fitting linear mixed-
1532 effects models using lme4. *Journal of Statistical Software* 67(1), 1–48.
- 1533 Bengtson, P., J. Barker, and S. J. Grayston (2012). Evidence of a strong cou-
1534 pling between root exudation, C and N availability, and stimulated SOM
1535 decomposition caused by rhizosphere priming effects. *Ecology and Evolu-
1536 tion* 2(8), 1843–1852.
- 1537 Bernacchi, C. J., E. L. Singsaas, C. Pimentel, A. R. Portis, and S. P. Long
1538 (2001). Improved temperature response functions for models of Rubisco-
1539 limited photosynthesis. *Plant, Cell and Environment* 24(2), 253–259.
- 1540 Bialic-Murphy, L., N. G. Smith, P. Voothuluru, R. M. McElderry, M. D.
1541 Roche, S. T. Cassidy, S. N. Kivlin, and S. Kalisz (2021). Invasion-induced
1542 root–fungal disruptions alter plant water and nitrogen economies. *Ecology
1543 Letters* 24(6), 1145–1156.
- 1544 Bloom, A. J., F. S. Chapin, and H. A. Mooney (1985). Resource limitation
1545 in plants - an economic analogy. *Annual Review of Ecology and Systemat-
1546 ics* 16(1), 363–392.
- 1547 Bonan, G. B., M. D. Hartman, W. J. Parton, and W. R. Wieder (2013). Evaluat-

- 1548 ing litter decomposition in earth system models with long-term litterbag ex-
1549 periments: an example using the Community Land Model version 4 (CLM4).
1550 *Global Change Biology* 19(3), 957–974.
- 1551 Bonan, G. B., P. J. Lawrence, K. W. Oleson, S. Levis, M. Jung, M. Reich-
1552 stein, D. M. Lawrence, and S. C. Swenson (2011). Improving canopy pro-
1553 cesses in the Community Land Model version 4 (CLM4) using global flux
1554 fields empirically inferred from FLUXNET data. *Journal of Geophysical Re-*
1555 *search* 116(G2), G02014.
- 1556 Booth, B. B. B., C. D. Jones, M. Collins, I. J. Totterdell, P. M. Cox, S. Sitch,
1557 C. Huntingford, R. A. Betts, G. R. Harris, and J. Lloyd (2012). High sen-
1558 sitivity of future global warming to land carbon cycle processes. *Environ-*
1559 *mental Research Letters* 7(2), 024002.
- 1560 Borer, E. T., W. S. Harpole, P. B. Adler, E. M. Lind, J. L. Orrock, E. W.
1561 Seabloom, and M. D. Smith (2014). Finding generality in ecology: A model
1562 for globally distributed experiments. *Methods in Ecology and Evolution* 5(1),
1563 65–73.
- 1564 Braghieri, R. K., J. B. Fisher, K. Allen, E. Brzostek, M. Shi, X. Yang, D. M.
1565 Ricciuto, R. A. Fisher, Q. Zhu, and R. P. Phillips (2022). Modeling global
1566 carbon costs of plant nitrogen and phosphorus acquisition. *Journal of Ad-*
1567 *vances in Modeling Earth Systems* 14(8), 1–23.
- 1568 Brix, H. (1971). Effects of nitrogen fertilization on photosynthesis and respi-
1569 ration in Douglas-fir. *Forest Science* 17(4), 407–414.
- 1570 Brzostek, E. R., J. B. Fisher, and R. P. Phillips (2014). Modeling the carbon
1571 cost of plant nitrogen acquisition: Mycorrhizal trade-offs and multipath

- 1572 resistance uptake improve predictions of retranslocation. *Journal of Geo-*
1573 *physical Research: Biogeosciences* 119, 1684–1697.
- 1574 Bubier, J. L., R. Smith, S. Juutinen, T. R. Moore, R. Minocha, S. Long, and
1575 S. Minocha (2011). Effects of nutrient addition on leaf chemistry, morphol-
1576 ogy, and photosynthetic capacity of three bog shrubs. *Oecologia* 167(2),
1577 355–368.
- 1578 Cernusak, L. A., N. Ubierna, K. Winter, J. A. M. Holtum, J. D. Marshall, and
1579 G. D. Farquhar (2013). Environmental and physiological determinants of
1580 carbon isotope discrimination in terrestrial plants. *New Phytologist* 200(4),
1581 950–965.
- 1582 Chen, J.-L., J. F. Reynolds, P. C. Harley, and J. D. Tenhunen (1993). Coor-
1583 dination theory of leaf nitrogen distribution in a canopy. *Oecologia* 93(1),
1584 63–69.
- 1585 Clark, D. B., L. M. Mercado, S. Sitch, C. D. Jones, N. Gedney, M. J. Best,
1586 M. Pryor, G. G. Rooney, R. L. H. Essery, E. Blyth, O. Boucher, R. J.
1587 Harding, C. Huntingford, and P. M. Cox (2011). The Joint UK Land Envi-
1588 ronment Simulator (JULES), model description. Part 2: Carbon fluxes and
1589 vegetation dynamics. *Geoscientific Model Development* 4(3), 701–722.
- 1590 Cornwell, W. K., J. H. C. Cornelissen, K. Amatangelo, E. Dorrepaal, V. T.
1591 Eviner, O. Godoy, S. E. Hobbie, B. Hoorens, H. Kurokawa, N. Pérez-
1592 Harguindeguy, H. M. Quested, L. S. Santiago, D. A. Wardle, I. J. Wright,
1593 R. Aerts, S. D. Allison, P. van Bodegom, V. Brovkin, A. Chatain, T. V.
1594 Callaghan, S. Díaz, E. Garnier, D. E. Gurvich, E. Kazakou, J. A. Klein,
1595 J. Read, P. B. Reich, N. A. Soudzilovskaia, M. V. Vaieretti, and M. Westoby

- 1596 (2008). Plant species traits are the predominant control on litter decomposition
1597 rates within biomes worldwide. *Ecology Letters* 11(10), 1065–1071.
- 1598 Cornwell, W. K., I. J. Wright, J. Turner, V. Maire, M. M. Barbour, L. A.
1599 Cernusak, T. E. Dawson, D. S. Ellsworth, G. D. Farquhar, H. Griffiths,
1600 C. Keitel, A. Knohl, P. B. Reich, D. G. Williams, R. Bhaskar, J. H. C. Cornelissen,
1601 A. Richards, S. Schmidt, F. Valladares, C. Körner, E.-D. Schulze,
1602 N. Buchmann, and L. S. Santiago (2018). Climate and soils together regulate
1603 photosynthetic carbon isotope discrimination within C₃ plants worldwide.
1604 *Global Ecology and Biogeography* 27(9), 1056–1067.
- 1605 Curtis, P. S. (1996). A meta-analysis of leaf gas exchange and nitrogen in trees
1606 grown under elevated carbon dioxide. *Plant, Cell and Environment* 19(2),
1607 127–137.
- 1608 Davies-Barnard, T., J. Meyerholt, S. Zaehle, P. Friedlingstein, V. Brovkin,
1609 Y. Fan, R. A. Fisher, C. D. Jones, H. Lee, D. Peano, B. Smith, D. Wårlind,
1610 and A. J. Wiltshire (2020). Nitrogen cycling in CMIP6 land surface models:
1611 progress and limitations. *Biogeosciences* 17(20), 5129–5148.
- 1612 Delaire, M., E. Frak, M. Sigogne, B. Adam, F. Beaujard, and X. Le Roux
1613 (2005). Sudden increase in atmospheric CO₂ concentration reveals strong
1614 coupling between shoot carbon uptake and root nutrient uptake in young
1615 walnut trees. *Tree Physiology* 25(2), 229–235.
- 1616 Doane, T. A. and W. R. Horwáth (2003). Spectrophotometric determination of
1617 nitrate with a single reagent. *Analytical Letters* 36(12), 2713–2722.
- 1618 Dong, N., I. C. Prentice, B. J. Evans, S. Caddy-Retalic, A. J. Lowe, and I. J.
1619 Wright (2017). Leaf nitrogen from first principles: field evidence for adaptive

- 1620** variation with climate. *Biogeosciences* 14(2), 481–495.
- 1621** Dong, N., I. C. Prentice, I. J. Wright, B. J. Evans, H. F. Togashi, S. Caddy-
- 1622** Retalic, F. A. McInerney, B. Sparrow, E. Leitch, and A. J. Lowe (2020).
- 1623** Components of leaf-trait variation along environmental gradients. *New Phytologist* 228(1), 82–94.
- 1624**
- 1625** Dong, N., I. C. Prentice, I. J. Wright, H. Wang, O. K. Atkin, K. J. Bloomfield,
- 1626** T. F. Domingues, S. M. Gleason, V. Maire, Y. Onoda, H. Poorter, and N. G.
- 1627** Smith (2022). Leaf nitrogen from the perspective of optimal plant function.
- 1628** *Journal of Ecology* 110(11), 2585–2602.
- 1629** Dong, N., I. J. Wright, J. M. Chen, X. Luo, H. Wang, T. F. Keenan, N. G.
- 1630** Smith, and I. C. Prentice (2022). Rising CO₂ and warming reduce global
- 1631** canopy demand for nitrogen. *New Phytologist* 235(5), 1692–1700.
- 1632** Dovrat, G., H. Bakhshian, T. Masci, and E. Sheffer (2020). The nitrogen eco-
- 1633** nomic spectrum of legume stoichiometry and fixation strategy. *New Phytol-*
- 1634** *ogist* 227(2), 365–375.
- 1635** Dovrat, G., T. Masci, H. Bakhshian, E. Mayzlish Gati, S. Golan, and E. Shef-
- 1636** fer (2018). Drought-adapted plants dramatically downregulate dinitrogen
- 1637** fixation: Evidences from Mediterranean legume shrubs. *Journal of Ecol-*
- 1638** *ogy* 106(4), 1534–1544.
- 1639** Drake, B. G., M. A. Gonzàlez-Meler, and S. P. Long (1997). More efficient
- 1640** plants: a consequence of rising atmospheric CO₂? *Annual Review of Plant*
- 1641** *Biology* 48, 609–639.
- 1642** Duursma, R. A. (2015). Plantecophys - An R Package for Analysing and Mod-

- 1643** elling Leaf Gas Exchange Data. *PLOS ONE* 10(11), e0143346.
- 1644** Eastman, B. A., M. B. Adams, E. R. Brzostek, M. B. Burnham, J. E. Carrara,
1645 C. Kelly, B. E. McNeil, C. A. Walter, and W. T. Peterjohn (2021). Altered
1646 plant carbon partitioning enhanced forest ecosystem carbon storage after 25
1647 years of nitrogen additions. *New Phytologist* 230(4), 1435–1448.
- 1648** Ellsworth, D. S. and P. B. Reich (1996). Photosynthesis and leaf nitrogen in five
1649 Amazonian tree species during early secondary succession. *Ecology* 77(2),
1650 581–594.
- 1651** Espelta, J. M., P. Cortés, M. Mangirón, and J. Retana (2005). Differences in
1652 biomass partitioning, leaf nitrogen content, and water use efficiency d13C
1653 result in similar performance of seedlings of two Mediterranean oaks with
1654 contrasting leaf habit. *Ecoscience* 12(4), 447–454.
- 1655** Evans, J. R. (1989). Photosynthesis and nitrogen relationships in leaves of C₃
1656 plants. *Oecologia* 78(1), 9–19.
- 1657** Evans, J. R. and V. C. Clarke (2019). The nitrogen cost of photosynthesis.
1658 *Journal of Experimental Botany* 70(1), 7–15.
- 1659** Evans, J. R. and H. Poorter (2001). Photosynthetic acclimation of plants to
1660 growth irradiance: the relative importance of specific leaf area and nitrogen
1661 partitioning in maximizing carbon gain. *Plant, Cell and Environment* 24(8),
1662 755–767.
- 1663** Evans, J. R. and J. R. Seemann (1989). The allocation of protein nitrogen in
1664 the photosynthetic apparatus: costs, consequences, and control. *Photosyn-*
1665 *thesis* 8, 183–205.

- 1666** Exbrayat, J.-F., A. A. Bloom, P. Falloon, A. Ito, T. L. Smallman, and
1667 M. Williams (2018). Reliability ensemble averaging of 21st century projec-
1668 tions of terrestrial net primary productivity reduces global and regional
1669 uncertainties. *Earth System Dynamics* 9(1), 153–165.
- 1670** Farquhar, G. D., J. R. Ehleringer, and K. T. Hubick (1989). Carbon Isotope
1671 Discrimination and Photosynthesis. *Annual Review of Plant Physiology and*
1672 *Plant Molecular Biology* 40(1), 503–537.
- 1673** Farquhar, G. D. and T. D. Sharkey (1982). Stomatal conductance and photo-
1674 synthesis. *Annual Review of Plant Physiology* 33(1), 317–345.
- 1675** Farquhar, G. D., S. von Caemmerer, and J. A. Berry (1980). A biochemical
1676 model of photosynthetic CO₂ assimilation in leaves of C3 species.
1677 *Planta* 149(1), 78–90.
- 1678** Fay, P. A., S. M. Prober, W. S. Harpole, J. M. H. Knops, J. D. Bakker, E. T.
1679 Borer, E. M. Lind, A. S. MacDougall, E. W. Seabloom, P. D. Wragg, P. B.
1680 Adler, D. M. Blumenthal, Y. M. Buckley, C. Chu, E. E. Cleland, S. L.
1681 Collins, K. F. Davies, G. Du, X. Feng, J. Firn, D. S. Gruner, N. Hagenah,
1682 Y. Hautier, R. W. Heckman, V. L. Jin, K. P. Kirkman, J. A. Klein, L. M.
1683 Ladwig, Q. Li, R. L. McCulley, B. A. Melbourne, C. E. Mitchell, J. L. Moore,
1684 J. W. Morgan, A. C. Risch, M. Schütz, C. J. Stevens, D. A. Wedin, and
1685 L. H. Yang (2015). Grassland productivity limited by multiple nutrients.
1686 *Nature Plants* 1(7), 15080.
- 1687** Feng, X. (1999). Trends in intrinsic water-use efficiency of natural trees for the
1688 past 100-200 years: A response to atmospheric CO₂ concentration. *Geochim-
ica et Cosmochimica Acta* 63(13-14), 1891–1903.

- 1690 Field, C. B. and H. A. Mooney (1986). The photosynthesis-nitrogen relationship
1691 in wild plants. In T. J. Givnish (Ed.), *On the Economy of Plant Form and*
1692 *Function*, pp. 25–55. Cambridge: Cambridge University Press.
- 1693 Finzi, A. C., D. J. P. Moore, E. H. DeLucia, J. Lichter, K. S. Hofmockel, R. B.
1694 Jackson, H. S. Kim, R. Matamala, H. R. McCarthy, R. Oren, J. S. Pippen,
1695 and W. H. Schlesinger (2006). Progressive nitrogen limitation of ecosystem
1696 processes under elevated CO₂ in a warm-temperate forest. *Ecology* 87(1),
1697 15–25.
- 1698 Firn, J., J. M. McGree, E. Harvey, H. Flores Moreno, M. Schutz, Y. M. Buckley,
1699 E. T. Borer, E. W. Seabloom, K. J. La Pierre, A. M. MacDougall, S. M.
1700 Prober, C. J. Stevens, L. L. Sullivan, E. Porter, E. Ladouceur, C. Allen,
1701 K. H. Moromizato, J. W. Morgan, W. S. Harpole, Y. Hautier, N. Eisen-
1702 hauer, J. P. Wright, P. B. Adler, C. A. Arnillas, J. D. Bakker, L. Biederman,
1703 A. A. D. Broadbent, C. S. Brown, M. N. Bugalho, M. C. Caldeira, E. E. Cle-
1704 land, A. Ebeling, P. A. Fay, N. Hagenah, A. R. Kleinhesselink, R. Mitchell,
1705 J. L. Moore, C. Nogueira, P. L. Peri, C. Roscher, M. D. Smith, P. D. Wragg,
1706 and A. C. Risch (2019). Leaf nutrients, not specific leaf area, are consistent
1707 indicators of elevated nutrient inputs. *Nature Ecology and Evolution* 3(3),
1708 400–406.
- 1709 Fisher, J. B., S. Sitch, Y. Malhi, R. A. Fisher, C. Huntingford, and S.-Y. Tan
1710 (2010). Carbon cost of plant nitrogen acquisition: A mechanistic, globally
1711 applicable model of plant nitrogen uptake, retranslocation, and fixation.
1712 *Global Biogeochemical Cycles* 24(1), 1–17.
- 1713 Fox, J. and S. Weisberg (2019). *An R companion to applied regression* (Third

- 1714 edit ed.). Thousand Oaks, California: Sage.
- 1715 Franklin, O., R. E. McMurtrie, C. M. Iversen, K. Y. Crous, A. C. Finzi, D. Tis-
- 1716 sue, D. S. Ellsworth, R. Oren, and R. J. Norby (2009). Forest fine-root
- 1717 production and nitrogen use under elevated CO₂: contrasting responses
- 1718 in evergreen and deciduous trees explained by a common principle. *Global*
- 1719 *Change Biology* 15(1), 132–144.
- 1720 Friedlingstein, P., M. Meinshausen, V. K. Arora, C. D. Jones, A. Anav, S. K.
- 1721 Liddicoat, and R. Knutti (2014). Uncertainties in CMIP5 climate projections
- 1722 due to carbon cycle feedbacks. *Journal of Climate* 27(2), 511–526.
- 1723 Friel, C. A. and M. L. Friesen (2019). Legumes modulate allocation to rhizobial
- 1724 nitrogen fixation in response to factorial light and nitrogen manipulation.
- 1725 *Frontiers in Plant Science* 10, 1316.
- 1726 Fujikake, H., A. Yamazaki, N. Ohtake, K. Sueoshi, S. Matsuhashi, T. Ito,
- 1727 C. Mizuniwa, T. Kume, S. Hoshimoto, N.-S. Ishioka, S. Watanabe, A. Osa,
- 1728 T. Sekine, H. Uchida, A. Tsuji, and T. Ohyama (2003). Quick and reversible
- 1729 inhibition of soybean root nodule growth by nitrate involves a decrease in
- 1730 sucrose supply to nodules. *Journal of Experimental Botany* 54(386), 1379–
- 1731 1388.
- 1732 Ghimire, B., W. J. Riley, C. D. Koven, J. Kattge, A. Rogers, P. B. Reich, and
- 1733 I. J. Wright (2017). A global trait-based approach to estimate leaf nitro-
- 1734 gen functional allocation from observations:. *Ecological Applications* 27(5),
- 1735 1421–1434.
- 1736 Giardina, C. P., M. D. Coleman, J. E. Hancock, J. S. King, E. A. Lilleskov,
- 1737 W. M. Loya, K. S. Pregitzer, M. G. Ryan, and C. C. Trettin (2005). The

- 1738 response of belowground carbon allocation in forests to global change. In
1739 D. Binkley and O. Manyailo (Eds.), *Tree Species Effects on Soils: Implications for Global Change* (Volume 55 ed.), Chapter Chapter 7, pp. 119–154.
1740 Berlin/Heidelberg: Springer-Verlag.
- 1741
- 1742 Gibson, A. H. and J. E. Harper (1985). Nitrate effect on nodulation of soybean
1743 by *Bradyrhizobium japonicum*. *Crop Science* 25(3), 497–501.
- 1744 Gill, A. L. and A. C. Finzi (2016). Belowground carbon flux links biogeochemical
1745 cycles and resource-use efficiency at the global scale. *Ecology Letters* 19(12),
1746 1419–1428.
- 1747 Goll, D. S., V. Brovkin, B. R. Parida, C. H. Reick, J. Kattge, P. B. Reich, P. M.
1748 van Bodegom, and Ü. Niinemets (2012). Nutrient limitation reduces land
1749 carbon uptake in simulations with a model of combined carbon, nitrogen
1750 and phosphorus cycling. *Biogeosciences Discussions* 9(3), 3173–3232.
- 1751 Gregory, L. M., A. M. McClain, D. M. Kramer, J. D. Pardo, K. E. Smith, O. L.
1752 Tessmer, B. J. Walker, L. G. Ziccardi, and T. D. Sharkey (2021, oct). The
1753 triose phosphate utilization limitation of photosynthetic rate: Out of global
1754 models but important for leaf models. *Plant, Cell and Environment* 44(10),
1755 3223–3226.
- 1756 Guerrieri, R., M. Mencuccini, L. J. Sheppard, M. Saurer, M. P. Perks, P. Levy,
1757 M. A. Sutton, M. Borghetti, and J. Grace (2011). The legacy of enhanced
1758 N and S deposition as revealed by the combined analysis of $\delta^{13}\text{C}$, $\delta^{18}\text{O}$ and
1759 $\delta^{15}\text{N}$ in tree rings. *Global Change Biology* 17(5), 1946–1962.
- 1760 Gulmon, S. L. and C. C. Chu (1981). The effects of light and nitrogen on photo-
1761 synthesis, leaf characteristics, and dry matter allocation in the chaparral

- 1762** shrub, <i>Diplacus aurantiacus</i>. *Oecologia* 49(2), 207–212.
- 1763** Gutschick, V. P. (1981). Evolved strategies in nitrogen acquisition by plants.
- 1764** *The American Naturalist* 118(5), 607–637.
- 1765** Hallik, L., Ü. Niinemets, and I. J. Wright (2009). Are species shade and drought
- 1766** tolerance reflected in leaf-level structural and functional differentiation in
- 1767** Northern Hemisphere temperate woody flora? *New Phytologist* 184(1), 257–
- 1768** 274.
- 1769** Harrison, M. T., E. J. Edwards, G. D. Farquhar, A. B. Nicotra, and J. R.
- 1770** Evans (2009). Nitrogen in cell walls of sclerophyllous leaves accounts for
- 1771** little of the variation in photosynthetic nitrogen-use efficiency. *Plant, Cell*
- 1772** and *Environment* 32(3), 259–270.
- 1773** Harrison, S. P., W. Cramer, O. Franklin, I. C. Prentice, H. Wang,
- 1774** Å. Bränström, H. de Boer, U. Dieckmann, J. Joshi, T. F. Keenan,
- 1775** A. Lavergne, S. Manzoni, G. Mengoli, C. Morfopoulos, J. Peñuelas,
- 1776** S. Pietsch, K. T. Rebel, Y. Ryu, N. G. Smith, B. D. Stocker, and I. J.
- 1777** Wright (2021). Eco-evolutionary optimality as a means to improve vegeta-
- 1778** tion and land-surface models. *New Phytologist* 231(6), 2125–2141.
- 1779** Henneron, L., P. Kardol, D. A. Wardle, C. Cros, and S. Fontaine (2020). Rhizo-
- 1780** sphere control of soil nitrogen cycling: a key component of plant economic
- 1781** strategies. *New Phytologist* 228(4), 1269–1282.
- 1782** Hikosaka, K. and A. Shigeno (2009). The role of Rubisco and cell walls in the
- 1783** interspecific variation in photosynthetic capacity. *Oecologia* 160(3), 443–
- 1784** 451.

- 1785 Hoagland, D. R. and D. I. Arnon (1950). The water culture method for growing
1786 plants without soil. *California Agricultural Experiment Station: 347* 347(2),
1787 1–32.
- 1788 Hobbie, E. A. (2006). Carbon allocation to ectomycorrhizal fungi correlates
1789 with belowground allocation in culture studies. *Ecology* 87(3), 563–569.
- 1790 Hobbie, E. A. and J. E. Hobbie (2008). Natural abundance of ^{15}N in nitrogen-
1791 limited forests and tundra can estimate nitrogen cycling through mycorrhizal
1792 fungi: a review. *Ecosystems* 11(5), 815–830.
- 1793 Hoek, T. A., K. Axelrod, T. Biancalani, E. A. Yurtsev, J. Liu, and J. Gore
1794 (2016). Resource availability modulates the cooperative and competitive na-
1795 ture of a microbial cross-feeding mutualism. *PLOS Biology* 14(8), e1002540.
- 1796 Höglberg, M. N., M. J. I. Briones, S. G. Keel, D. B. Metcalfe, C. Campbell, A. J.
1797 Midwood, B. Thornton, V. Hurry, S. Linder, T. Näsholm, and P. Höglberg
1798 (2010). Quantification of effects of season and nitrogen supply on tree below-
1799 ground carbon transfer to ectomycorrhizal fungi and other soil organisms in
1800 a boreal pine forest. *New Phytologist* 187(2), 485–493.
- 1801 Höglberg, P., M. N. Höglberg, S. G. Göttlicher, N. R. Betson, S. G. Keel, D. B.
1802 Metcalfe, C. Campbell, A. Schindlbacher, V. Hurry, T. Lundmark, S. Linder,
1803 and T. Näsholm (2008). High temporal resolution tracing of photosynthate
1804 carbon from the tree canopy to forest soil microorganisms. *New Phytolo-*
1805 *gist* 177(1), 220–228.
- 1806 Houlton, B. Z., Y.-P. Wang, P. M. Vitousek, and C. B. Field (2008). A uni-
1807 fying framework for dinitrogen fixation in the terrestrial biosphere. *Na-*
1808 *ture* 454(7202), 327–330.

- 1809 Huber, M. L., R. A. Perkins, A. Laesecke, D. G. Friend, J. V. Sengers, M. J.
1810 Assael, I. N. Metaxa, E. Vogel, R. Mareš, and K. Miyagawa (2009). New
1811 international formulation for the viscosity of H₂O. *Journal of Physical and*
1812 *Chemical Reference Data* 38(2), 101–125.
- 1813 Hungate, B. A., J. S. Dukes, M. R. Shaw, Y. Luo, and C. B. Field (2003).
1814 Nitrogen and climate change. *Science* 302(5650), 1512–1513.
- 1815 IPCC (2021). *Climate Change 2021: The Physical Science Basis. Contribution*
1816 *of Working Group I to the Sixth Assessment Report of the Intergovernmental*
1817 *Panel on Climate Change*. Cambridge University Press.
- 1818 Johnson, N. C., J. H. Graham, and F. A. Smith (1997). Functioning of mycor-
1819 rhizal associations along the mutualism-parasitism continuum. *New Phytol-*
1820 *ogist* 135(4), 575–585.
- 1821 Kaiser, C., M. R. Kilburn, P. L. Clode, L. Fuchslueger, M. Koranda, J. B. Cliff,
1822 Z. M. Solaiman, and D. V. Murphy (2015). Exploring the transfer of recent
1823 plant photosynthates to soil microbes: mycorrhizal pathway vs direct root
1824 exudation. *New Phytologist* 205(4), 1537–1551.
- 1825 Katabuchi, M. (2015). LeafArea: An R package for rapid digital analysis of leaf
1826 area. *Ecological Research* 30(6), 1073–1077.
- 1827 Kattge, J. and W. Knorr (2007). Temperature acclimation in a biochemical
1828 model of photosynthesis: a reanalysis of data from 36 species. *Plant, Cell*
1829 *and Environment* 30(9), 1176–1190.
- 1830 Kattge, J., W. Knorr, T. Raddatz, and C. Wirth (2009). Quantifying photosyn-
1831 thetic capacity and its relationship to leaf nitrogen content for global-scale

- 1832** terrestrial biosphere models. *Global Change Biology* 15(4), 976–991.
- 1833** Kayler, Z., A. Gessler, and N. Buchmann (2010). What is the speed of link
- 1834** between aboveground and belowground processes? *New Phytologist* 187(4),
- 1835** 885–888.
- 1836** Kayler, Z., C. Keitel, K. Jansen, and A. Gessler (2017). Experimental evi-
- 1837** dence of two mechanisms coupling leaf-level C assimilation to rhizosphere
- 1838** CO₂ release. *Environmental and Experimental Botany* 135,
- 1839** 21–26.
- 1840** Keeling, C. D., W. G. Mook, and P. P. Tans (1979, jan). Recent trends in the
- 1841** ¹³C/¹²C ratio of atmospheric carbon dioxide.
- 1842** *Nature* 277(5692), 121–123.
- 1843** Kenward, M. G. and J. H. Roger (1997). Small sample inference for fixed effects
- 1844** from restricted maximum likelihood. *Biometrics* 53(3), 983.
- 1845** Knapp, A. K., M. L. Avolio, C. Beier, C. J. W. Carroll, S. L. Collins, J. S.
- 1846** Dukes, L. H. Fraser, R. J. Griffin-Nolan, D. L. Hoover, A. Jentsch, M. E.
- 1847** Loik, R. P. Phillips, A. K. Post, O. E. Sala, I. J. Slette, L. Yahdjian, and
- 1848** M. D. Smith (2017). Pushing precipitation to the extremes in distributed
- 1849** experiments: recommendations for simulating wet and dry years. *Global*
- 1850** *Change Biology* 23(5), 1774–1782.
- 1851** Knorr, W. (2000). Annual and interannual CO₂ exchanges of the
- 1852** terrestrial biosphere: process-based simulations and uncertainties. *Global*
- 1853** *Ecology and Biogeography* 9(3), 225–252.
- 1854** Knorr, W. and M. Heimann (2001). Uncertainties in global terrestrial biosphere

- 1855 modeling: 1. A comprehensive sensitivity analysis with a new photosynthesis
1856 and energy balance scheme. *Global Biogeochemical Cycles* 15(1), 207–225.
- 1857 Kulmatiski, A., P. B. Adler, J. M. Stark, and A. T. Tredennick (2017). Water
1858 and nitrogen uptake are better associated with resource availability than
1859 root biomass. *Ecosphere* 8(3), e01738.
- 1860 Lavergne, A., D. Sandoval, V. J. Hare, H. Graven, and I. C. Prentice (2020).
1861 Impacts of soil water stress on the acclimated stomatal limitation of pho-
1862 tosythesis: Insights from stable carbon isotope data. *Global Change Biol-*
1863 *ogy* 26(12), 7158–7172.
- 1864 Lawrence, D. M., R. A. Fisher, C. D. Koven, K. W. Oleson, S. C. Swen-
1865 son, G. B. Bonan, N. Collier, B. Ghimire, L. Kampenhout, D. Kennedy,
1866 E. Kluzek, P. J. Lawrence, F. Li, H. Li, D. L. Lombardozzi, W. J. Riley,
1867 W. J. Sacks, M. Shi, M. Vertenstein, W. R. Wieder, C. Xu, A. A. Ali,
1868 A. M. Badger, G. Bisht, M. Broeke, M. A. Brunke, S. P. Burns, J. Buzan,
1869 M. Clark, A. Craig, K. M. Dahlin, B. Drewniak, J. B. Fisher, M. Flanner,
1870 A. M. Fox, P. Gentine, F. M. Hoffman, G. Keppel-Aleks, R. Knox, S. Ku-
1871 mar, J. Lenaerts, L. R. Leung, W. H. Lipscomb, Y. Lu, A. Pandey, J. D.
1872 Pelletier, J. Perket, J. T. Randerson, D. M. Ricciuto, B. M. Sanderson,
1873 A. Slater, Z. M. Subin, J. Tang, R. Q. Thomas, M. Val Martin, and X. Zeng
1874 (2019). The Community Land Model Version 5: description of new features,
1875 benchmarking, and impact of forcing uncertainty. *Journal of Advances in*
1876 *Modeling Earth Systems* 11(12), 4245–4287.
- 1877 LeBauer, D. S. and K. K. Treseder (2008). Nitrogen limitation of net primary
1878 productivity. *Ecology* 89(2), 371–379.

- 1879 Lenth, R. (2019). emmeans: estimated marginal means, aka least-squares
1880 means.
- 1881 Li, W., H. Zhang, G. Huang, R. Liu, H. Wu, C. Zhao, and N. G. McDowell
1882 (2020). Effects of nitrogen enrichment on tree carbon allocation: A global
1883 synthesis. *Global Ecology and Biogeography* 29(3), 573–589.
- 1884 Liang, J., X. Qi, L. Souza, and Y. Luo (2016). Processes regulating progressive
1885 nitrogen limitation under elevated carbon dioxide: a meta-analysis. *Biogeosciences*
1886 13(9), 2689–2699.
- 1887 Liang, X., T. Zhang, X. Lu, D. S. Ellsworth, H. BassiriRad, C. You, D. Wang,
1888 P. He, Q. Deng, H. Liu, J. Mo, and Q. Ye (2020). Global response patterns of
1889 plant photosynthesis to nitrogen addition: A meta-analysis. *Global Change
Biology* 26(6), 3585–3600.
- 1890 Lu, J., J. Yang, C. Keitel, L. Yin, P. Wang, W. Cheng, and F. A. Dijkstra
1891 (2022). Belowground Carbon Efficiency for Nitrogen and Phosphorus Ac-
1892 quisition Varies Between *Lolium perenne* and *Trifolium repens* and Depends
1893 on Phosphorus Fertilization. *Frontiers in Plant Science* 13, 1–9.
- 1894 Luo, X., T. F. Keenan, J. M. Chen, H. Croft, I. C. Prentice, N. G. Smith,
1895 A. P. Walker, H. Wang, R. Wang, C. Xu, and Y. Zhang (2021). Global
1896 variation in the fraction of leaf nitrogen allocated to photosynthesis. *Nature
Communications* 12(1), 4866.
- 1897 Luo, Y., W. S. Currie, J. S. Dukes, A. C. Finzi, U. A. Hartwig, B. A. Hungate,
1898 R. E. McMurtrie, R. Oren, W. J. Parton, D. E. Pataki, R. M. Shaw, D. R.
1899 Zak, and C. B. Field (2004). Progressive nitrogen limitation of ecosystem
1900 responses to rising atmospheric carbon dioxide. *BioScience* 54(8), 731–739.
- 1901
- 1902

- 1903 Maire, V., P. Martre, J. Kattge, F. Gastal, G. Esser, S. Fontaine, and J.-F.
1904 Soussana (2012). The coordination of leaf photosynthesis links C and N
1905 fluxes in C₃ plant species. *PLoS ONE* 7(6), e38345.
- 1906 Makino, A. (2003). Rubisco and nitrogen relationships in rice: leaf photosyn-
1907 thesis and plant growth. *Soil Science and Plant Nutrition* 49(3), 319–327.
- 1908 Markham, J. H. and C. Zekveld (2007). Nitrogen fixation makes biomass al-
1909 location to roots independent of soil nitrogen supply. *Canadian Journal of*
1910 *Botany* (9), 787–793.
- 1911 Marschner, H. and B. Dell (1994). Nutrient uptake in mycorrhizal symbiosis.
1912 *Plant and Soil* 159(1), 89–102.
- 1913 Matamala, R. and W. H. Schlesinger (2000). Effects of elevated atmospheric
1914 CO₂ on fine root production and activity in an intact tem-
1915 perate forest ecosystem. *Global Change Biology* 6(8), 967–979.
- 1916 Medlyn, B. E., E. Dreyer, D. S. Ellsworth, M. Forstreuter, P. C. Harley,
1917 M. U. F. Kirschbaum, X. Le Roux, P. Montpied, J. Strassmeyer, A. Wal-
1918 croft, K. Wang, and D. Loustau (2002). Temperature response of parameters
1919 of a biochemically based model of photosynthesis. II. A review of experimen-
1920 tal data. *Plant, Cell and Environment* 25(9), 1167–1179.
- 1921 Menge, D. N. L., S. A. Levin, and L. O. Hedin (2008). Evolutionary tradeoffs can
1922 select against nitrogen fixation and thereby maintain nitrogen limitation.
1923 *Proceedings of the National Academy of Sciences* 105(5), 1573–1578.
- 1924 Menne, M. J., I. Durre, R. S. Vose, B. E. Gleason, and T. G. Houston (2012).
1925 An overview of the global historical climatology network-daily database.

- 1926** *Journal of Atmospheric and Oceanic Technology* 29(7), 897–910.
- 1927** Meyerholt, J., K. Sickel, and S. Zaehle (2020). Ensemble projections elucidate effects of uncertainty in terrestrial nitrogen limitation on future carbon uptake. *Global Change Biology* 26(7), 3978–3996.
- 1928**
- 1929**
- 1930** Meyerholt, J., S. Zaehle, and M. J. Smith (2016). Variability of projected terrestrial biosphere responses to elevated levels of atmospheric
- 1931** CO₂ due to uncertainty in biological nitrogen fixation. *Bio-*
- 1932** *geosciences* 13(5), 1491–1518.
- 1933**
- 1934** Minocha, R., S. Long, A. H. Magill, J. D. Aber, and W. H. McDowell (2000).
- 1935** Foliar free polyamine and inorganic ion content in relation to soil and soil
- 1936** solution chemistry in two fertilized forest stands at the Harvard Forest,
- 1937** Massachusetts. *Plant and Soil* 222(1-2), 119–137.
- 1938** Moore, D. J., S. Aref, R. M. Ho, J. S. Pippen, J. G. Hamilton, and E. H. De
- 1939** Lucia (2006). Annual basal area increment and growth duration of *Pinus*
- 1940** *taeda* in response to eight years of free-air carbon dioxide enrichment. *Global*
- 1941** *Change Biology* 12(8), 1367–1377.
- 1942** Morgan, J. A., D. E. Pataki, C. Körner, H. Clark, S. J. Del Gross, J. M.
- 1943** Grünzweig, A. K. Knapp, A. R. Mosier, P. C. D. Newton, P. A. Niklaus,
- 1944** J. B. Nippert, R. S. Nowak, W. J. Parton, H. W. Polley, and M. R. Shaw
- 1945** (2004). Water relations in grassland and desert ecosystems exposed to ele-
- 1946** vated atmospheric CO₂. *Oecologia* 140(1), 11–25.
- 1947** Muñoz, N., X. Qi, M. W. Li, M. Xie, Y. Gao, M. Y. Cheung, F. L. Wong, and
- 1948** H.-M. Lam (2016). Improvement in nitrogen fixation capacity could be part
- 1949** of the domestication process in soybean. *Heredity* 117(2), 84–93.

- 1950** Nadelhoffer, K. J. and J. W. Raich (1992). Fine root production estimates and
- 1951** belowground carbon allocation in forest ecosystems. *Ecology* 73(4), 1139–
- 1952** 1147.
- 1953** Niinemets, Ü. and J. D. Tenhunen (1997). A model separating leaf struc-
- 1954** tural and physiological effects on carbon gain along light gradients for the
- 1955** shade-tolerant species *< i>Acer saccharum</i>*. *Plant, Cell and Environ-*
- 1956** *ment* 20(7), 845–866.
- 1957** Norby, R. J., J. Ledford, C. D. Reilly, N. E. Miller, and E. G. O'Neill
- 1958** (2004). Fine-root production dominates response of a deciduous forest to
- 1959** atmospheric CO₂ enrichment. *Proceedings of the National Academy of Sci-*
- 1960** *ences* 101(26), 9689–9693.
- 1961** Norby, R. J., J. M. Warren, C. M. Iversen, B. E. Medlyn, and R. E. Mc-
- 1962** Murtrie (2010). CO₂ enhancement of forest productivity constrained by
- 1963** limited nitrogen availability. *Proceedings of the National Academy of Sci-*
- 1964** *ences* 107(45), 19368–19373.
- 1965** Noyce, G. L., M. L. Kirwan, R. L. Rich, and J. P. Megonigal (2019). Asyn-
- 1966** chronous nitrogen supply and demand produce nonlinear plant allocation
- 1967** responses to warming and elevated CO₂. *Proceedings of the*
- 1968** *National Academy of Sciences* 116(43), 21623–21628.
- 1969** Onoda, Y., K. Hikosaka, and T. Hirose (2004). Allocation of nitrogen to
- 1970** cell walls decreases photosynthetic nitrogen-use efficiency. *Functional Ecol-*
- 1971** *ogy* 18(3), 419–425.
- 1972** Onoda, Y., I. J. Wright, J. R. Evans, K. Hikosaka, K. Kitajima, Ü. Niinemets,
- 1973** H. Poorter, T. Tosens, and M. Westoby (2017). Physiological and structural

- 1974** tradeoffs underlying the leaf economics spectrum. *New Phytologist* 214(4),
- 1975** 1447–1463.
- 1976** Paillassa, J., I. J. Wright, I. C. Prentice, S. Pepin, N. G. Smith, G. Ethier,
- 1977** A. C. Westerband, L. J. Lamarque, H. Wang, W. K. Cornwell, and V. Maire
- 1978** (2020). When and where soil is important to modify the carbon and water
- 1979** economy of leaves. *New Phytologist* 228(1), 121–135.
- 1980** Parvin, S., S. Uddin, S. Tausz Posch, R. Armstrong, and M. Tausz (2020). Car-
- 1981** bon sink strength of nodules but not other organs modulates photosynthesis
- 1982** of faba bean (*i>Vicia faba</i>*) grown under elevated [CO₂] and different
- 1983** water supply. *New Phytologist* 227(1), 132–145.
- 1984** Peng, Y., K. J. Bloomfield, L. A. Cernusak, T. F. Domingues, and I. C. Pren-
- 1985** tice (2021). Global climate and nutrient controls of photosynthetic capacity.
- 1986** *Communications Biology* 4(1), 462.
- 1987** Perkowski, E. A., E. F. Waring, and N. G. Smith (2021). Root mass carbon
- 1988** costs to acquire nitrogen are determined by nitrogen and light availabil-
- 1989** ity in two species with different nitrogen acquisition strategies. *Journal of*
- 1990** *Experimental Botany* 72(15), 5766–5776.
- 1991** Phillips, R. P., E. R. Brzostek, and M. G. Midgley (2013). The mycorrhizal-
- 1992** associated nutrient economy: a new framework for predicting carbon-
- 1993** nutrient couplings in temperate forests. *New Phytologist* 199(1), 41–51.
- 1994** Phillips, R. P., A. C. Finzi, and E. S. Bernhardt (2011). Enhanced root ex-
- 1995** udation induces microbial feedbacks to N cycling in a pine forest under
- 1996** long-term CO₂ fumigation. *Ecology Letters* 14(2), 187–194.

- 1997** Pons, T. L. and R. W. Pearcy (1994). Nitrogen reallocation and photosynthetic acclimation in response to partial shading in soybean plants. *Physiologia Plantarum* 92(4), 636–644.
- 1998**
- 1999**
- 2000** Poorter, H., J. Bühler, D. Van Dusschoten, J. Climent, and J. A. Postma (2012).
- 2001** Pot size matters: A meta-analysis of the effects of rooting volume on plant growth. *Functional Plant Biology* 39(11), 839–850.
- 2002**
- 2003** Poorter, H., O. Knopf, I. J. Wright, A. A. Temme, S. W. Hogewoning, A. Graf,
- 2004** L. A. Cernusak, and T. L. Pons (2022). A meta-analysis of responses of C₃ plants to atmospheric CO₂: dose-response curves for 85 traits ranging from the molecular to the whole-plant level. *New Phytologist* 233(4), 1560–1596.
- 2005**
- 2006**
- 2007** Prentice, I. C., N. Dong, S. M. Gleason, V. Maire, and I. J. Wright (2014).
- 2008** Balancing the costs of carbon gain and water transport: testing a new theoretical framework for plant functional ecology. *Ecology Letters* 17(1), 82–91.
- 2009**
- 2010** Prentice, I. C., X. Liang, B. E. Medlyn, and Y.-P. Wang (2015). Reliable, robust and realistic: The three R's of next-generation land-surface modelling.
- 2011**
- 2012** *Atmospheric Chemistry and Physics* 15, 5987–6005.
- 2013** Querejeta, J. I., I. Prieto, C. Armas, F. Casanoves, J. S. Diémé, M. Diouf,
- 2014** H. Yossi, B. Kaya, F. I. Pugnaire, and G. M. Rusch (2022). Higher leaf nitrogen content is linked to tighter stomatal regulation of transpiration and more efficient water use across dryland trees. *New Phytologist* 235(4),
- 2015**
- 2016**
- 2017** 1351–1364.
- 2018** R Core Team (2021). R: A language and environment for statistical computing.
- 2019** Raich, J. W., D. A. Clark, L. Schwendenmann, and T. E. Wood (2014). Above-

- 2020** ground tree growth varies with belowground carbon allocation in a tropical rainforest environment. *PLoS ONE* 9(6), e100275.
- 2021**
- 2022** Rastetter, E. B., P. M. Vitousek, C. B. Field, G. R. Shaver, D. Herbert, and
- 2023** G. I. Ågren (2001). Resource optimization and symbiotic nitrogen fixation.
- 2024** *Ecosystems* 4(4), 369–388.
- 2025** Reich, P. B. (2014). The world-wide 'fast-slow' plant economics spectrum: a
- 2026** traits manifesto. *Journal of Ecology* 102(2), 275–301.
- 2027** Reich, P. B., S. E. Hobbie, T. Lee, D. S. Ellsworth, J. B. West, D. Tilman,
- 2028** J. M. H. Knops, S. Naeem, and J. Trost (2006). Nitrogen limitation con-
- 2029** strains sustainability of ecosystem response to CO₂. *Nature* 440(7086), 922–925.
- 2030**
- 2031** Rhine, E. D., R. L. Mulvaney, E. J. Pratt, and G. K. Sims (1998). Improving
- 2032** the Berthelot reaction for determining ammonium in soil extracts and water.
- 2033** *Soil Science Society of America Journal* 62(2), 473.
- 2034** Rogers, A. (2014). The use and misuse of V_{cmax} in Earth System Models. *Photo-*
- 2035** *tosynthesis Research* 119(1-2), 15–29.
- 2036** Rogers, A., B. E. Medlyn, J. S. Dukes, G. B. Bonan, S. Caemmerer, M. C.
- 2037** Dietze, J. Kattge, A. D. B. Leakey, L. M. Mercado, Ü. Niinemets, I. C.
- 2038** Prentice, S. P. Serbin, S. Sitch, D. A. Way, and S. Zaehle (2017). A roadmap
- 2039** for improving the representation of photosynthesis in Earth system models.
- 2040** *New Phytologist* 213(1), 22–42.
- 2041** Saathoff, A. J. and J. Welles (2021). Gas exchange measurements in the un-
- 2042** steady state. *Plant Cell and Environment* 44(11), 3509–3523.

- 2043** Saleh, A. M., M. Abdel-Mawgoud, A. R. Hassan, T. H. Habeeb, R. S. Yehia,
2044 and H. AbdElgawad (2020). Global metabolic changes induced by arbuscular
2045 mycorrhizal fungi in oregano plants grown under ambient and elevated levels
2046 of atmospheric CO₂. *Plant Physiology and Biochemistry* 151, 255–263.
- 2047** Schaefer, K., C. R. Schwalm, C. Williams, M. A. Arain, A. Barr, J. M. Chen,
2048 K. J. Davis, D. Dimitrov, T. W. Hilton, D. Y. Hollinger, E. Humphreys,
2049 B. Poulter, B. M. Racza, A. D. Richardson, A. Sahoo, P. Thornton, R. Var-
2050 gas, H. Verbeeck, R. Anderson, I. Baker, T. A. Black, P. Bolstad, J. Chen,
2051 P. S. Curtis, A. R. Desai, M. C. Dietze, D. Dragoni, C. M. Gough, R. F.
2052 Grant, L. Gu, A. K. Jain, C. Kucharik, B. E. Law, S. Liu, E. Lokipitiya,
2053 H. A. Margolis, R. Matamala, J. H. McCaughey, R. Monson, J. W. Munger,
2054 W. Oechel, C. Peng, D. T. Price, D. Ricciuto, W. J. Riley, N. Roulet,
2055 H. Tian, C. Tonitto, M. Torn, E. Weng, and X. Zhou (2012). A model-
2056 data comparison of gross primary productivity: Results from the North
2057 American Carbon Program site synthesis. *Journal of Geophysical Research:*
2058 *Biogeosciences* 117(G3), G03010.
- 2059** Schneider, C. A., W. S. Rasband, and K. W. Eliceiri (2012). NIH Image to
2060 ImageJ: 25 years of image analysis. *Nature Methods* 9(7), 671–675.
- 2061** Scott, H. G. and N. G. Smith (2022). A Model of C4 Photosynthetic Acclimation
2062 Based on Least-Cost Optimality Theory Suitable for Earth System Model
2063 Incorporation. *Journal of Advances in Modeling Earth Systems* 14(3), 1–16.
- 2064** Shi, M., J. B. Fisher, E. R. Brzostek, and R. P. Phillips (2016). Carbon cost
2065 of plant nitrogen acquisition: Global carbon cycle impact from an improved
2066 plant nitrogen cycle in the Community Land Model. *Global Change Biol-*

- 2067** *ogy* 22(3), 1299–1314.
- 2068** Shi, M., J. B. Fisher, R. P. Phillips, and E. R. Brzostek (2019). Neglecting
2069 plant–microbe symbioses leads to underestimation of modeled climate im-
2070 pacts. *Biogeosciences* 16(2), 457–465.
- 2071** Smith, N. G. and J. S. Dukes (2013). Plant respiration and photosynthesis in
2072 global-scale models: incorporating acclimation to temperature and CO₂.
2073 *Global Change Biology* 19(1), 45–63.
- 2074** Smith, N. G. and T. F. Keenan (2020). Mechanisms underlying leaf photosyn-
2075 thetic acclimation to warming and elevated CO₂ as inferred from least-cost
2076 optimality theory. *Global Change Biology* 26(9), 5202–5216.
- 2077** Smith, N. G., T. F. Keenan, I. C. Prentice, H. Wang, I. J. Wright, Ü. Niinemets,
2078 K. Y. Crous, T. F. Domingues, R. Guerrieri, F. oko Ishida, J. Kattge, E. L.
2079 Kruger, V. Maire, A. Rogers, S. P. Serbin, L. Tarvainen, H. F. Togashi,
2080 P. A. Townsend, M. Wang, L. K. Weerasinghe, and S.-X. Zhou (2019).
2081 Global photosynthetic capacity is optimized to the environment. *Ecology*
2082 *Letters* 22(3), 506–517.
- 2083** Smith, N. G., D. L. Lombardozzi, A. Tawfik, G. B. Bonan, and J. S. Dukes
2084 (2017). Biophysical consequences of photosynthetic temperature acclimation
2085 for climate. *Journal of Advances in Modeling Earth Systems* 9(1), 536–547.
- 2086** Smith, N. G., S. L. Malyshev, E. Shevliakova, J. Kattge, and J. S. Dukes
2087 (2016). Foliar temperature acclimation reduces simulated carbon sensitivity
2088 to climate. *Nature Climate Change* 6(4), 407–411.
- 2089** Smith, S. E. and D. J. Read (2008). *Mycorrhizal Symbiosis*. Academic Press.

- 2090 Soil Survey Staff (2022). Web Soil Survey.
- 2091 Soudzilovskaia, N. A., J. C. Douma, A. A. Akhmetzhanova, P. M. van Bode-
- 2092 gom, W. K. Cornwell, E. J. Moens, K. K. Treseder, and J. H. C. Cornelissen
- 2093 (2015). Global patterns of plant root colonization intensity by mycorrhizal
- 2094 fungi explained by climate and soil chemistry. *Global Ecology and Biogeog-*
- 2095 *raphy* 24(3), 371–382.
- 2096 Stocker, B. D., H. Wang, N. G. Smith, S. P. Harrison, T. F. Keenan, D. San-
- 2097 doval, T. Davis, and I. C. Prentice (2020). P-model v1.0: An optimality-
- 2098 based light use efficiency model for simulating ecosystem gross primary pro-
- 2099 duction. *Geoscientific Model Development* 13(3), 1545–1581.
- 2100 Sulman, B. N., E. Shevliakova, E. R. Brzostek, S. N. Kivlin, S. L. Malyshev,
- 2101 D. N. L. Menge, and X. Zhang (2019). Diverse mycorrhizal associations
- 2102 enhance terrestrial C storage in a global model. *Global Biogeochemical Cy-*
- 2103 *cles* 33(4), 501–523.
- 2104 Sweet, S. K., D. W. Wolfe, A. DeGaetano, and R. Benner (2017). Anatomy
- 2105 of the 2016 drought in the Northeastern United States: Implications for
- 2106 agriculture and water resources in humid climates. *Agricultural and Forest*
- 2107 *Meteorology* 247, 571–581.
- 2108 Taylor, B. N. and D. N. L. Menge (2018). Light regulates tropical symbiotic
- 2109 nitrogen fixation more strongly than soil nitrogen. *Nature Plants* 4(9), 655–
- 2110 661.
- 2111 Terrer, C., S. Vicca, B. A. Hungate, R. P. Phillips, and I. C. Prentice (2016).
- 2112 Mycorrhizal association as a primary control of the CO₂ fertilization effect.
- 2113 *Science* 353(6294), 72–74.

- 2114** Terrer, C., S. Vicca, B. D. Stocker, B. A. Hungate, R. P. Phillips, P. B. Reich,
2115 A. C. Finzi, and I. C. Prentice (2018). Ecosystem responses to elevated CO₂
2116 governed by plant–soil interactions and the cost of nitrogen acquisition. *New*
2117 *Phytologist* 217(2), 507–522.
- 2118** Thomas, R. Q., E. N. J. Brookshire, and S. Gerber (2015). Nitrogen limita-
2119 tion on land: how can it occur in Earth system models? *Global Change*
2120 *Biology* 21(5), 1777–1793.
- 2121** Thomas, R. Q., S. Zaehle, P. H. Templer, and C. L. Goodale (2013). Global pat-
2122 terns of nitrogen limitation: confronting two global biogeochemical models
2123 with observations. *Global Change Biology* 19(10), 2986–2998.
- 2124** Thornton, P. E., J.-F. Lamarque, N. A. Rosenbloom, and N. M. Mahowald
2125 (2007). Influence of carbon-nitrogen cycle coupling on land model response
2126 to CO₂ fertilization and climate variability. *Global Bioge-
ochemical Cycles* 21(4), GB4018.
- 2128** Tingey, D. T., D. L. Phillips, and M. G. Johnson (2000). Elevated CO₂ and
2129 conifer roots: effects on growth, life span and turnover. *New Phytolo-
gist* 147(1), 87–103.
- 2131** Udvardi, M. and P. S. Poole (2013). Transport and metabolism in legume-
2132 rhizobia symbioses. *Annual Review of Plant Biology* 64, 781–805.
- 2133** USDA NRCS (2022). The PLANTS Database.
- 2134** Uselman, S. M., R. G. Qualls, and R. B. Thomas (2000). Effects of increased
2135 atmospheric CO₂, temperature, and soil N availability on root exudation of
2136 dissolved organic carbon by a N-fixing tree (*Robinia pseudoacacia* L.). *Plant*

- 2137 *and Soil* 222, 191–202.
- 2138 van Diepen, L. T. A., E. A. Lilleskov, K. S. Pregitzer, and R. M. Miller (2007).
- 2139 Decline of arbuscular mycorrhizal fungi in northern hardwood forests ex-
- 2140 posed to chronic nitrogen additions. *New Phytologist* 176(1), 175–183.
- 2141 Vance, C. P. and G. H. Heichel (1991). Carbon in N₂ fixation: Limitation or
- 2142 exquisite adaptation. *Annual Review of Plant Physiology and Plant Molec-*
- 2143 *ular Biology* 42(1), 373–392.
- 2144 Viet, H. D., J.-H. Kwak, K.-S. Lee, S.-S. Lim, M. Matsushima, S. X. Chang,
- 2145 K.-H. Lee, and W.-J. Choi (2013). Foliar chemistry and tree ring δ¹³C of
- 2146 *Pinus densiflora* in relation to tree growth along a soil pH gradient. *Plant*
- 2147 *and Soil* 363(1-2), 101–112.
- 2148 Vitousek, P. M., K. Cassman, C. C. Cleveland, T. Crews, C. B. Field, N. B.
- 2149 Grimm, R. W. Howarth, R. Marino, L. Martinelli, E. B. Rastetter, and
- 2150 J. I. Sprent (2002). Towards an ecological understanding of biological nitro-
- 2151 gen fixation. In *The Nitrogen Cycle at Regional to Global Scales*, pp. 1–45.
- 2152 Springer Netherlands.
- 2153 Vitousek, P. M. and R. W. Howarth (1991). Nitrogen limitation on land and in
- 2154 the sea: How can it occur? *Biogeochemistry* 13(2), 87–115.
- 2155 Vitousek, P. M., S. Porder, B. Z. Houlton, and O. A. Chadwick (2010).
- 2156 Terrestrial phosphorus limitation: mechanisms, implications, and nitro-
- 2157 gen–phosphorus interactions. *Ecological Applications* 20(1), 5–15.
- 2158 Walker, A. P., A. P. Beckerman, L. Gu, J. Kattge, L. A. Cernusak, T. F.
- 2159 Domingues, J. C. Scales, G. Wohlfahrt, S. D. Wullschleger, and F. I. Wood-

- 2160 ward (2014). The relationship of leaf photosynthetic traits - V_{cmax} and J_{max}
2161 - to leaf nitrogen, leaf phosphorus, and specific leaf area: a meta-analysis
2162 and modeling study. *Ecology and Evolution* 4(16), 3218–3235.
- 2163 Wang, H., I. C. Prentice, T. F. Keenan, T. W. Davis, I. J. Wright, W. K.
2164 Cornwell, B. J. Evans, and C. Peng (2017). Towards a universal model for
2165 carbon dioxide uptake by plants. *Nature Plants* 3(9), 734–741.
- 2166 Wang, W., Y. Wang, G. Hoch, Z. Wang, and J. Gu (2018). Linkage of root mor-
2167 phology to anatomy with increasing nitrogen availability in six temperate
2168 tree species. *Plant and Soil* 425(1-2), 189–200.
- 2169 Weatherburn, M. W. (1967). Phenol-hypochlorite reaction for determination of
2170 ammonia. *Analytical Chemistry* 39(8), 971–974.
- 2171 Wellburn, A. R. (1994). The spectral determination of chlorophylls a and b, as
2172 well as total carotenoids, using various solvents with spectrophotometers of
2173 different resolution. *Journal of Plant Physiology* 144(3), 307–313.
- 2174 Wen, Z., P. J. White, J. Shen, and H. Lambers (2022). Linking root exuda-
2175 tion to belowground economic traits for resource acquisition. *New Phytolo-*
2176 *gist* 233(4), 1620–1635.
- 2177 Westerband, A. C., I. J. Wright, V. Maire, J. Paillassa, I. C. Prentice, O. K.
2178 Atkin, K. J. Bloomfield, L. A. Cernusak, N. Dong, S. M. Gleason, C. Guil-
2179 herme Pereira, H. Lambers, M. R. Leishman, Y. Malhi, and R. H. Nolan
2180 (2023). Coordination of photosynthetic traits across soil and climate gradi-
2181 ents. *Global Change Biology* 29(3), 1–29.
- 2182 Wieder, W. R., C. C. Cleveland, W. K. Smith, and K. Todd-Brown (2015).

- 2183 Future productivity and carbon storage limited by terrestrial nutrient availability. *Nature Geoscience* 8(6), 441–444.
- 2184
- 2185 Wieder, W. R., D. M. Lawrence, R. A. Fisher, G. B. Bonan, S. J. Cheng, C. L.
- 2186 Goodale, A. S. Grandy, C. D. Koven, D. L. Lombardozzi, K. W. Oleson,
- 2187 and R. Q. Thomas (2019). Beyond static benchmarking: using experimental
- 2188 manipulations to evaluate land model assumptions. *Global Biogeochemical*
- 2189 *Cycles* 33(10), 1289–1309.
- 2190 Wright, I. J., P. B. Reich, and M. Westoby (2003). Least-cost input mixtures
- 2191 of water and nitrogen for photosynthesis. *The American Naturalist* 161(1),
- 2192 98–111.
- 2193 Wright, I. J., P. B. Reich, M. Westoby, D. D. Ackerly, Z. Baruch, F. Bongers,
- 2194 J. Cavender-Bares, T. Chapin, J. H. C. Cornelissen, M. Diemer, J. Flexas,
- 2195 E. Garnier, P. K. Groom, J. Gulias, K. Hikosaka, B. B. Lamont, T. Lee,
- 2196 W. Lee, C. Lusk, J. J. Midgley, M.-L. Navas, Ü. Niinemets, J. Oleksyn,
- 2197 N. Osada, H. Poorter, P. Poot, L. Prior, V. I. Pyankov, C. Roumet, S. C.
- 2198 Thomas, M. G. Tjoelker, E. J. Veneklaas, and R. Villar (2004). The world-
- 2199 wide leaf economics spectrum. *Nature* 428(6985), 821–827.
- 2200 Xu-Ri and I. C. Prentice (2017). Modelling the demand for new nitrogen fixation
- 2201 by terrestrial ecosystems. *Biogeosciences* 14(7), 2003–2017.
- 2202 Zaehle, S., B. E. Medlyn, M. G. De Kauwe, A. P. Walker, M. C. Dietze, T. Hick-
- 2203 ler, Y. Luo, Y. P. Wang, B. El-Masri, P. Thornton, A. Jain, S. Wang,
- 2204 D. Warlind, E. Weng, W. Parton, C. M. Iversen, A. Gallet-Budynek, H. Mc-
- 2205 carthy, A. C. Finzi, P. J. Hanson, I. C. Prentice, R. Oren, and R. J. Norby
- 2206 (2014). Evaluation of 11 terrestrial carbon-nitrogen cycle models against

- 2207** observations from two temperate Free-Air CO₂ Enrichment studies. *New*
2208 *Phytologist* 202(3), 803–822.
- 2209** Zaehle, S., S. Sitch, B. Smith, and F. Hatterman (2005). Effects of parame-
2210 ter uncertainties on the modeling of terrestrial biosphere dynamics. *Global*
2211 *Biogeochemical Cycles* 19(3), GB3020.
- 2212** Zhu, Q., W. J. Riley, J. Tang, N. Collier, F. M. Hoffman, X. Yang, and G. Bisht
2213 (2019). Representing nitrogen, phosphorus, and carbon interactions in the
2214 E3SM land model: development and global benchmarking. *Journal of Ad-*
2215 *vances in Modeling Earth Systems* 11(7), 2238–2258.
- 2216** Ziegler, C., M. E. Dusenge, B. Nyirambangutse, E. Zibera, G. Wallin, and
2217 J. Uddling (2020). Contrasting Dependencies of Photosynthetic Capacity
2218 on Leaf Nitrogen in Early- and Late-Successional Tropical Montane Tree
2219 Species. *Frontiers in Plant Science* 11, 1–12.
- 2220** Ziehn, T., J. Kattge, W. Knorr, and M. Scholze (2011). Improving the pre-
2221 dictability of global CO₂ assimilation rates under climate change. *Geophys-*
2222 *ical Research Letters* 38(10), L10404.